TU/e EINDHOVEN UNIVERSITY OF TECHNOLOGY

Stability of immersed liquid threads

Citation for published version (APA):
Gunawan, A. Y. (2004). *Stability of immersed liquid threads*. [Phd Thesis 1 (Research TU/e / Graduation TU/e), Mathematics and Computer Science]. Technische Universiteit Eindhoven. https://doi.org/10.6100/IR570022

DOI:
10.6100/IR570022

Document status and date:
Published: 01/01/2004

Document Version:
Publisher's PDF, also known as Version of Record (includes final page, issue and volume numbers)

Please check the document version of this publication:

• A submitted manuscript is the version of the article upon submission and before peer-review. There can be important differences between the submitted version and the official published version of record. People interested in the research are advised to contact the author for the final version of the publication, or visit the DOI to the publisher's website.
• The final author version and the galley proof are versions of the publication after peer review.
• The final published version features the final layout of the paper including the volume, issue and page numbers.

Link to publication

General rights
Copyright and moral rights for the publications made accessible in the public portal are retained by the authors and/or other copyright owners and it is a condition of accessing publications that users recognise and abide by the legal requirements associated with these rights.

• Users may download and print one copy of any publication from the public portal for the purpose of private study or research.
• You may not further distribute the material or use it for any profit-making activity or commercial gain
• You may freely distribute the URL identifying the publication in the public portal.

If the publication is distributed under the terms of Article 25fa of the Dutch Copyright Act, indicated by the "Taverne" license above, please follow below link for the End User Agreement:

www.tue.nl/taverne

Take down policy
If you believe that this document breaches copyright please contact us at:

openaccess@tue.nl

providing details and we will investigate your claim.

Download date: 09. Feb. 2025

Stability of Immersed Liquid Threads

Stability of Immersed Liquid Threads

PROEFSCHRIFT

ter verkrijging van de graad van doctor aan de
Technische Universiteit Eindhoven, op gezag van de
Rector Magnificus, prof.dr. R.A. van Santen, voor een
commissie aangewezen door het College voor
Promoties in het openbaar te verdedigen
op woensdag 21 januari 2004 om 16.00 uur

door

Agus Yodi Gunawan

geboren te Sumedang, Indonesië

Dit proefschrift is goedgekeurd door de promotoren:

prof.dr. J. Molenaar
en
prof.dr.ir. C.J. van Duijn

Copromotor:
dr.ir. A.A.F. van de Ven

CIP-DATA LIBRARY TECHNISCHE UNIVERSITEIT EINDHOVEN

Gunawan, Agus Y.

Stability of immersed liquid threads / by Agus Y. Gunawan. -
Eindhoven: Technische Universiteit Eindhoven, 2004.
Proefschrift. - ISBN 90-386-0752-0
NUR 919
Subject headings: hydrodynamic stability / break-up of liquid threads
2000 Mathematics Subject Classification: 76E17, 76D45, 76D07

Copyright © 2004 by Agus Yodi Gunawan

Gedrukt door: Universiteitsdrukkerij, Technische Universiteit Eindhoven

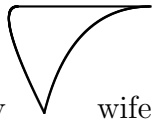

To my wife
Anne Kurniasari Nawawi
and my daughter *Najmina Maryam Gunawan*
for their love, patience and understanding
♡

Preface

In the name of Allaah, Most Gracious, Most Merciful. All the praises and thanks are to Allaah, the Lord of the 'Aalamiin (mankind, jinn and all that exists).

In this thesis, the dynamical behaviour of liquid threads immersed in a fluid is studied as a function of surface tension, viscous forces, presence of a wall (confinement) and prescribed flow. The goal of the thesis is to provide a theoretical explanation for the stability or instability of the immersed liquid threads. More specifically, phenomena such as in-phase and out-of-phase break-up for parallel polymeric liquid threads, and a droplet-string formation in concentrated polymer blend, are two of the main interests of this thesis. From the point of view of blending, the present results may provide important insights for control of the production process, such as insights into characteristic drop formation times, spatial distributions of the droplets and droplets or strings (liquid threads) formation. The thesis is just one example of the large variety of applications of mathematics known. Hopefully, the practical use of the mathematical tools illuminated here, encourages more people to apply mathematics to real life problems.

This thesis is an outcome of the author's research during his Ph.D. study at Eindhoven University of Technology (February 2000-January 2004). Most of the material in the thesis is based on the following reports and papers:

① Gunawan, A.Y., Molenaar, J. & van de Ven, A.A.F. 2001 Dynamics of a polymer blend driven by surface tension. *RANA 01-04, ISSN:0926-4507*, Eindhoven University of Technology.

② Gunawan, A.Y., Molenaar, J. & van de Ven, A.A.F. 2001 Dynamics of a polymer blend driven by surface tension. Part 2: The zero-order solution. *RANA 01-20, ISSN:0926-4507*, Eindhoven University of Technology.

③ Gunawan, A.Y., Molenaar, J. & van de Ven, A.A.F. 2001 Dynamics of a polymer blend driven by surface tension. Part 3: The first-order solution. *RANA 01-21, ISSN:0926-4507*, Eindhoven University of Technology.

④ Gunawan, A.Y., Molenaar, J. & van de Ven, A.A.F. 2002 Break-up of a row of equally spaced immersed threads. *RANA 02-08, ISSN:0926-4507*, Eindhoven University of Technology.

⑤ Gunawan, A.Y., Molenaar, J. & van de Ven, A.A.F. 2002 Note on the breakup of immersed threads in the absence of viscosity differences. *RANA 02-23, ISSN:0926-4507*, Eindhoven University of Technology.

⑥ Gunawan, A.Y., Molenaar, J. & van de Ven, A.A.F. 2002 In-phase and out-of-phase break-up of two immersed liquid threads under influence of surface tension. *European Journal of Mechanics B/Fluids* **21**, 399.

⑦ Gunawan, A.Y., Molenaar, J. & van de Ven, A.A.F. 2003 Break-up of a set of liquid threads under influence of surface tension. *[accepted for publication by the Journal of Engineering Mathematics].*

⑧ Gunawan, A.Y., Molenaar, J. & van de Ven, A.A.F. 2003 Stability of a viscoelastic thread immersed in a confined region. *RANA 03-23, ISSN:0926-4507*, Eindhoven University of Technology.

⑨ Gunawan, A.Y., Molenaar, J. & van de Ven, A.A.F. 2003 Does shear flow stabilize an immersed thread? *RANA 03-25, ISSN:0926-4507*, Eindhoven University of Technology.

Although only my name appears on the cover of this thesis, I am indebted to many people who made this work possible. Therefore, I would like to express my gratitude towards them.

First of all, I would like to thank prof.dr. J. Molenaar and dr.ir. A.A.F van de Ven, who gave me the opportunity to carry out my doctorate research in the Applied Analysis group at the Department of Mathematics and Computer Science of the Eindhoven University of Technology, for their stimulating support, the pleasant collaboration, their patience and helpful discussions during this research. Their positive encouragement helped me to get on very well in my research. Furthermore, their enthusiasm served me to experience the many interesting aspects of hydrodynamic stability.

Secondly, I would like to express my gratitude to prof.dr.ir. C.J. van Duijn, prof.dr. J.J.M. Slot, and prof.dr. F. Verhulst for invaluable comments in improving my thesis. Their constructive criticisms resulted in many improvements. I would also like to thank prof.dr.ir. A.A. van Steenhoven, dr.ir. W.T. van Horssen, and dr. Y.M.M. Knops, for helpful discussions and their enthusiasm in reading my thesis.

Next, I would like to thank the QUE-project of the Departemen Matematika Institut Teknologi Bandung (ITB), Indonesia, for their funding support during my Ph.D. study, and the chair of the Departemen Matematika ITB for allowing me to study abroad. I would also like to thank the Delta project of the Eindhoven University of Technology for helpful funding at the end of my third-year study. I am also indebted to the staff of the Indonesian Embassy at The Hague for helping me during my stay in The Netherlands.

I am also thankful to the members of Applied Analysis group, especially Marese and Enna, for providing a pleasant working environment. I also thank Sandra, Heike, Johan, Gert-Jan "Mr. Everything" Pieters, Dragan "Kezman" Bezanovic and Sorin "Dr. Analysis" Pop for the pleasant company and "leuke tijd" during my four-years study.

I am also grateful to family van Boxtel for providing a pleasant stay at t'Hofke. *Ik hoop dat jullie het nog lang goed zullen maken en dat jullie nog lang van een goede gezondheid mogen genieten.*

Naturally, I thank all Indonesian friends (Musihoven, Parakanca, Eindhoven-merdeka, IAMS-N) for their kindly friendship and spending time together in "buitenland". *Terimakasih atas bantuan dan dukungannya.*

Finally, I am indebted to my parents, my sister and my parents in law for their prayers and continuing support. Last but not least, my special thanks to my wife Anne Kurniasari Nawawi and my lovely daughter Najmina Maryam Gunawan for their love, support, patience and understanding throughout the many long years during study. *InsyaAllaah, bakal kèmpèl deui sakulawargi.*

Di akhir lembar kitab ini
Tinta penamu perlahan pergi
Tetes air matamu 'kan berhenti
Doa dan harapanmu kian pasti
Sujud bersimpuh tundukkanlah hati
Kepada Ilaahi

Eindhoven, January 2004

Agus Yodi Gunawan

Contents

List of figures

Chapter 1

Introduction

1.1 Problem definition

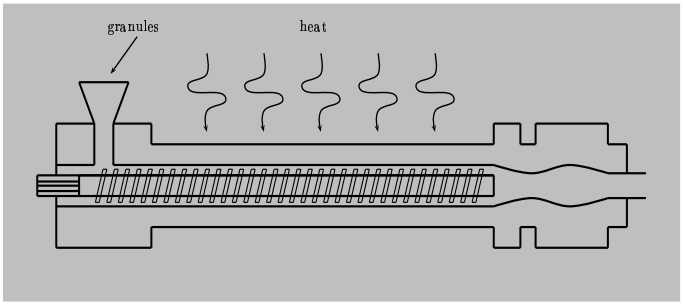

Figure 1.1: *Cross-section of an extruder.*

Nowadays, the demand for new synthetic materials increases and becomes more specific. New synthetic materials may be produced by blending different types of polymers. The material properties of a polymer blend are strongly related to its morphology determined by the blending process in an extruder. Therefore, the eventual material properties can be predicted only if a thorough understanding of this blending process is available.

In the extruder (see Figure 1.1), dry granules of two types of polymers are supplied into the hopper. Due to heating, by external heat sources and internal friction, the granules melt. In the melt, we discern between the dispersed phase and the continuous phase (or matrix phase). The polymer with the lowest volume fraction is called the dispersed phase. Subsequently, the blending takes place by the shear flow caused by the screw. In this stage, relatively big drops of one material are immersed into the shear flow of a second material. The mixing process depends on the magnitude of the capillary number Ca, which is defined as the ratio between the local shear stress Π and the interfacial stress σ/a,

$$\mathrm{Ca} = \frac{a\Pi}{\sigma}, \tag{1.1.1}$$

where σ is the surface tension and a is a characteristic radius of the drops in the dispersed phase. Due to dominant shear stresses, long threads are formed. So, the effect of the

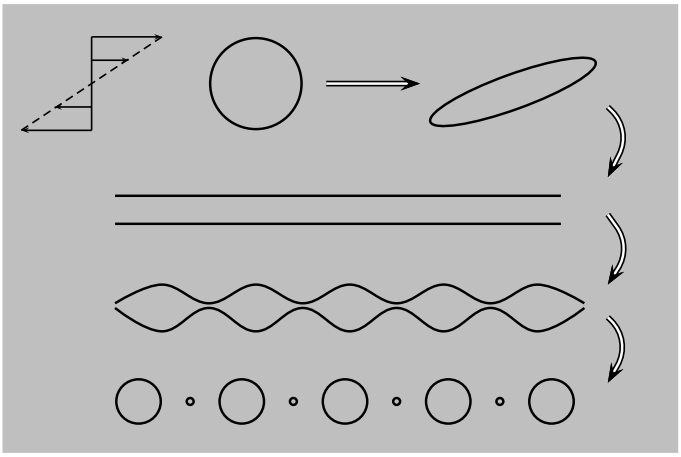

Figure 1.2: *Break-up process of a thread. The velocity field of the shear flow is indicated top left.*

shear stress is to deform and to elongate a big drop into a thread. At some moment a thread may become so thin, and thus its radius so small, that the interfacial stress becomes important. The effect of the latter is a tendency to attain the drop-shape (state of lowest surface energy). Initiated by perturbations, wavy perturbations may develop along the thread. Driven by surface tension, these waves may grow in amplitude or attenuate, depending on the stability of the system. In an unstable state, the thread will eventually break up into an array of small spherical droplets. The scheme of this process is shown in Figure 1.2.

In the blending process under consideration, the blend contains a large volume fraction of the threads. Under practical conditions, the interactions between the threads are of essential importance for the way they break up. In the experiments reported in Knops (1997) and Elemans et al. (1997), it is observed that adjacent threads may break up in-phase or out-of-phase. Both possibilities of break-up are shown in Figure 1.3. Part (a) shows the process of the breaking up of an array of parallel threads, in case the threads are less viscous than the matrix phase. The results show that the threads break up out-of-phase: at the position where one thread is expanding the adjacent thread is constricting. Part (b) shows the process of the breaking up of the parallel threads, in case the threads are more viscous than the matrix phase. The results show that the threads break up in-phase: adjacent threads expand and shrink at the same positions.

Another important phenomenon observed in blending is a droplet-string formation. Figure 1.2 shows that in the shear field a drop will deform into a long thread (string). Migler (2001) performed experiments by placing a sample (with dispersed drops) between two parallel quartz disks and rotating the upper one at a controlled rate. The shear rate was defined as the ratio between the upper plate velocity at the radial point of measurement and the gap width between two disks. Results showed that a droplet-string transition in concentrated polymer blend occurs when the size of the dispersed droplets becomes comparable to the gap width between the shearing surfaces. Upon reduction of the shear, the transition proceeded via the coalescence of droplets in four

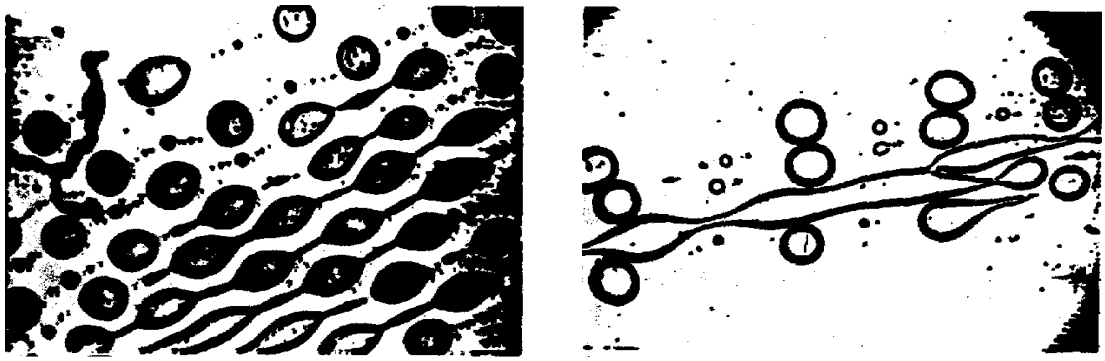

(a) Out-of-phase break-up of PA-6 (polyamide) threads in a matrix of PS-N7000 (polystyrene).

(b) In-phase break-up of PA-6 (polyamide) threads in a matrix of PS-N1000 (polystyrene).

Figure 1.3: *Experimental break-up behaviour reported in Knops (1997).*

stages. First, droplets coalescence with each others and so increase the average droplet size. Second, the large droplets self-organize into pearl necklace structures (chaining). Third, the aligned droplets coalescence with each other to form strings. And fourth, the strings then coalescence with each other to form ribbons. In the string structures regime, Migler found an unexpected phenomenon, in which the structures were still stable after the shear was stopped. Typically, at rest (after cessation of shear) the strings will break up (Tomotika (1935)). Migler proposed two stability mechanisms for the string structures. First, the wall effect, and second, the shear flow. The wider string, i.e. the string which its size is comparable to to the gap width of the shearing surfaces, is stabilized by a suppression of the instability due to finite size effects (confinement), while the narrower one is stabilized by shear flow.

From the point of view of blend production, a mathematical model simulating the phenomena described in this section may provide important insights for control of the production process. As for the spatial distribution of the droplets, it is highly important to know whether in-phase or out-of-phase break-up will occur. As for the droplet size, it is important to know that one can control the product by adjusting parameters arising from the fluid properties or the type of driving flow.

1.2 Aim of this thesis

The aim of this thesis is to analytically study the origin of the phenomena described in Section 1.1. We investigate how the break-up of threads and the droplet-string formation can be controlled by adjusting the properties of the fluids, the geometrical properties of the system and the type of imposed flow. To that end, the dynamical behaviour of immersed liquid threads is considered as a function of surface tension, viscous forces, presence of a wall and prescribed flow. We first deal with Newtonian fluids, and even-

tually we extend this work to non-Newtonian fluids. The fluids are assumed to be incompressible and so viscous that the creeping flow approximation is applicable. So, the dynamics is governed by Stokes equations. These equations are solved by means of separation of variables. The dependence on the azimuthal direction is written in terms of (complex) Fourier expansions. Substitution of the general solution into the boundary conditions yields an infinite set of linear equations for the unknown coefficients. This set is solved using the method of moments (this method is a basic mathematical technique for reducing functional equations to matrix equations (see Harrington (1993))). From this solution the so-called growth rate is calculated, a measure for the growth (or decay) of random perturbations. According to linear stability theory, a positive growth rate indicates that the system is unstable and that the threads will break up into an array of small droplets, whereas a negative growth rate indicates stability.

1.3 Survey of the literature

The study of the break-up of liquid threads has a distinguished history, starting with the work of Savart (1833) in the early nineteenth century. By illuminating the liquid thread (or: jet) carefully, Savart observed tiny undulations on a jet of water and showed that break-up always occurs, independently from the direction of gravity, the type of fluid, and the jet velocity and radius. Savart then concluded that there must be an intrinsic property of the fluid motion stimulating the break-up. Some years later, Plateau (1849) discovered that the source of the break-up is surface tension. Plateau studied the instability of an infinitely long cylindrical fluid thread produced by a jet emanating from a nozzle at high speed, and found that the system is unstable if the wave length of a perturbation is greater than π times the diameter of the jet.

The dynamical description of the problem, in terms of linear stability theory, was first introduced by Rayleigh (1878). Rayleigh considered the stability of a long cylindrical column of an incompressible inviscid fluid under the action of capillary forces, neglecting the effect of the surrounding fluid. Rayleigh's result was in accordance with the previous result of Plateau. Rayleigh then developed the important concept of the mode of maximum instability, and showed that, from an initially small disturbance, a number of unstable waves may form on the jet surface; the wave that causes the jet to break up is the one which has the maximum growth rate in amplitude. The growth rate depends upon the wave length λ of the disturbances, which is related to the wave number k by $\lambda = 2\pi/k$. It reaches a maximum when λ equals 4.51 times the diameter of the cylinder. The case of an incompressible long cylindrical column of viscous liquid has also been discussed by Rayleigh (1892). Assuming the viscosity to be paramount compared with the inertia and again neglecting the effect of the surrounding fluid, Rayleigh obtained only a limiting solution. The maximum instability occurs when the wave length of the disturbances is very large in comparison with the radius of the initial cylinder, i.e. when $\lambda = \infty$, theoretically. The case of a viscous jet issuing into gas has been discussed by Weber (1931). Weber found that for a viscous liquid jet, the most unstable wave length is greater than that predicted by Rayleigh (1878) for the perfect fluid-gas system.

Following Rayleigh's approach, Tomotika (1935) generalized the analysis to include viscosity for both the fluid column and the surrounding fluid. Tomotika found that the instability of the jet is strongly influenced by the ratios of the viscosities and densities of the jet and the surrounding fluid, and by the Ohnesorge number, a dimensionless parameter representing the ratio of viscous and interfacial-tension forces. If the ratio of viscosities of the two fluids is neither zero nor infinity, the maximum instability always occurs at a definite wave length. Moreover, Tomotika concluded that the formation of droplets of definite size is to be expected. The case of an arbitrary ratio of viscosities was also discussed by Chandrasekhar (1961). Generalized solutions of Tomotika stability analysis for several limiting cases such as low viscosity liquid jet in a gas, gas jet in a low viscosity liquid, etc., were discussed by Meister & Scheele (1967). Kinoshita et al. (1994) studied the break-up of jets and derived the equation describing the instability by an integro-differential approach. They showed that the explicit form of the derived equation enables a much easier prediction of the most unstable wave number and disturbance growth rate than Tomotika's equation.

For the case in which the fluids were not at rest, Tomotika (1936) considered the growth of disturbances when the fluids are elongated at a uniform rate. Tomotika tested the theory using a few of the experimental results given by Taylor (1934), but the data were too limited to afford a conclusive test. Mikami et al. (1975) improved Tomotika's theory by studying this phenomenon theoretically and experimentally. They showed that the disturbances which are initiated as the thread is formed, in general first damp, then amplify and finally damp again. Assuming that the break-up occurs when the amplitude of the disturbance is equal to the cylinder radius, they evaluated the time to break up and the final drop size in terms of fluid properties, extension rate, and the amplitude of the disturbance. They confirmed the results by examining, with the aid of cinematography, the break-up of a liquid thread in hyperbolic flow. Some experimental and theoretical works on viscous drop deformation in linear flows prior to 1984 were reviewed by Rallison (1984). A theoretical study of the break-up of a liquid thread in hyperbolic extensional flow and simple shear flow was also analyzed by Khakhar & Ottino (1987). They found that, under similar conditions, the drops produced in simple shear flow are larger than those produced in hyperbolic extensional flow. The dynamics of drop deformation and break-up in viscous flow, at low Reynolds number, under influences of surfactant and complex flows, prior to 1994, has been reviewed by Stone (1994).

The nonlinear dynamics of one thread when surface tension drives the motion also attracted much attention. Eggers (1993) considered a singularity, as the height of the fluid neck goes to zero, in the viscous motion of an axisymmetric liquid thread with a free surface. Eggers found that, close to pinch-off, the solution has a scaling form characterized by a set of universal exponents. Papageorgiou (1995) and Eggers (1995) derived a similarity solution that describes the asymptotic behaviour of a thinning viscous thread suspended in vacuum, near the critical time and around the location of break-up. A wide-ranging review of theoretical and experimental investigations of nonlinear dynamics of one liquid thread was given by Eggers (1997).

The stability of liquid threads and of droplets due to surface tension and external

flow has recently been studied both theoretically and experimentally to some extent. Knops (1997), Elemans et al. (1997) and Knops et al. (2001) investigated the break-up of multiple viscous threads surrounded by viscous liquid (for a detailed description see Section 1.1). Frischknecht (1998) considered the stability of a long cylindrical domain in a phase-separating binary fluid under influence of shear flow. Frischknecht explored the competition between the shear flow and the coarsening process. Using the coupled Cahn-Hilliard and Stokes equations, Frischknecht derived analytically the eigenvalues determining the stability for long-wavelength perturbations, and showed that the shear flow suppresses and sometimes completely stabilizes both the hydrodynamic Rayleigh instability and the thermodynamic instability of the cylinder. The results were consistent with a 'string phase' behaviour in phase-separating fluids in shear observed by Hashimoto et al. (1995). Navot (1999) studied the behaviour of a liquid droplet immersed in a host fluid under shear flow. At a critical value of the shear rate, Navot found that the deformation in steady state approaches a critical value as a power law of the critical shear rate. Guido et al. (2000) studied theoretically and experimentally the evolution of a liquid drop immersed in a fluid under transient shear flows; the agreement between experimental results and the theory was good. As for immersed threads in a confined region, e.g. flow between two plates or through a narrow tube, Migler (2001) reported experiments on immersed droplets sheared between two plates. Due to shear, threads are formed. Migler observed that confinement can stabilize the thread when the size of the thread becomes comparable to the gap width (see also Section 1.1). Assuming that strings can be simply viewed as droplets with a large aspect ratio, Pathak & Migler (2003) found that for confined strings deformation is a very strong function of shear; the aspect of a string scales nearly as Ca^3 with Ca the capillary number. Confinement not only promoted deformation, but also allowed larger stable droplets (strings) to exist under flow. They concluded that strings may be stabilized by a combination of shear flow and confinement. The effect of confinement on the stability of a liquid thread has also been studied by Son et al. (2003) and Hagedorn et al. (2003) via numerical simulations using a Lattice Boltzmann model.

The stability of liquid threads and of jets has also been studied for non-Newtonian fluids. Chin & Han (1979, 1980) considered the deformation of a viscoelastic droplet suspended in a viscoelastic medium in a channel consisting of a conical section and a straight cylindrical tube. A droplet of known volume was injected in the conical section at the centerline of the flow channel, through which a viscoelastic fluid was flowing at a constant flow rate. Along the axis of the channel, the flow in the conical was extensional. They observed that the droplet, initially spherical, was slightly deformed in the upper section of the cone and greatly elongated at the entrance region of the cylindrical tube. The deformability was investigated based on the flow conditions and the rheological properties of the fluids. Stability of a viscoelastic jet driven by surface tension has been numerically studied by Bousfield et al. (1986). Using finite element methods, they found the initial growth rate of the perturbation to be in agreement with linear stability theory, whereas at longer time scales, the growth rate decreased dramatically, due to the build-up of extensional stresses, and the filament evolved to a bead-on-string configuration. Palierne & Lequeux (1991) considered the relation between the wavelength and the

growth rate of the sausage instability of a thread embedded in a matrix, in the limit of vanishing Reynolds number and for incompressible fluids. The theory applied to general viscoelastic fluids, and took into account the dynamic properties of the interfacial tension due to adsorbed contaminants or interfacial agents, as well as the capability of the interface to resist a shear deformation. Brenn et al. (2000) investigated the break-up of non-Newtonian jets (Jeffreys model) moving in an inviscid gaseous environment by means of linear stability theory. They found that non-Newtonian jets are more unstable than Newtonian ones. In a comparison of theoretical and experimental results, Brenn et al. observed that the linearized theory fails to describe the nonlinear phenomena involved in viscoelastic jet break-up correctly. The linearized theory only yielded good results for the growth rate of perturbations in a regime of a low Weber number and small deformation. Stability of viscoelastic jets, drop deformation for non-Newtonian fluids, and bead-on-string formation have been recently studied by Christanti & Walker (2001), Greco (2002) and Li & Fontelos (2003).

1.4 Contents of this thesis

The structure of this thesis is as follows: in Chapters 2, 3, and 4, we discuss the stability of Newtonian systems of one, two, or more threads, respectively. Chapter 5 deals with the stability of a non-Newtonian thread immersed in Newtonian fluid in a confined region. In the latter chapter, the effects of fluid elasticity, the confinement and the Poiseuille flow on the stability of the system are investigated. The conclusions and recommendations are given in Chapter 6.

The detailed contents of the chapters is as follows. In Chapter 2, the stability of a Newtonian thread immersed in another Newtonian fluid is considered. In Section 2.1, the mathematical model and the boundary conditions are developed. The fluids are assumed to be incompressible and so viscous that the creeping flow approximation is applicable. In Section 2.2, the model is evaluated with the dynamics of the thread driven by surface tension only. The equations are solved by means of separation of variables, and the dependence on the azimuthal directions is written in the form of Fourier expansion. This simple basic situation is already known in literature. In Section 2.3, we study the effect of a shear flow; this is based on work of Frischknecht (1998). The important dimensionless parameter in this system is the capillary number Ca. By the use of *Hurwitz's criterion*, the stability of the thread is determined. It turns out that above a critical value of Ca, related to the fluid properties, the thread is always stable. The results explain the stability of the narrower string observed by Migler (2001) mentioned in Section 1.1. We also derive an analytical formula for the critical capillary number for fluids having equal viscosities .

In Chapter 3, the stability of two parallel Newtonian threads immersed in a Newtonian fluid is considered. The analysis follows the same lines as in Section 2.2, but now two systems of cylindrical coordinates, each one connected to one of the threads, are involved. Substitution of the general solution into the boundary conditions yields an infinite set of linear equations for the unknown coefficients. This set is solved us-

ing the method of moments. The stability of the threads is examined based on both a zero-order and a first-order Fourier expansion; the improvement due to a higher order expansion turns out to be rather small. Thus, we show that the zero-order approach is a reliable solution. We here find two new parameters (besides the viscosity ratio) that play an important role in the (in)stability of the threads. They are the phase difference α and the distance b between the centers of the threads. It turns out that the values of α are either 0 or π. For $\alpha = 0$, the threads show an in-phase behaviour, whereas for $\alpha = \pi$, they show an out-of-phase behaviour. We find a critical distance b_{cr} in which the behaviour changes. The results perfectly describe the experimental results reported by Knops (1997) and Elemans et al. (1997).

In Chapter 4, we extend the analysis derived in Chapter 3 to consider the stability of an arbitrary number of immersed parallel threads. We investigate the stability of systems for two types of configurations, i.e. a system of threads on a row in one plane (Section 4.1), and a system of threads at triangular vertices (Section 4.2). It turns out that the threads break up in specific phase patterns in which adjacent threads are either in-phase or out-of-phase. For L threads, in principle 2^L phase patterns are possible. However, we show that the stability of the system directly follows from L so-called *basic phase patterns*. In Section 4.3, attention is paid to the special case of threads and fluid having equal viscosity. Then, the growth rate can be calculated analytically using Hankel transformations. For this special case, we only work out the stability for the row configuration, since the triangular configuration case is very similar.

In Chapter 5, we consider the stability of an infinitely long viscoelastic thread, using the Jeffreys model, immersed in a tube filled with a Newtonian fluid. The thread moves due to a constant pressure gradient (Poiseuille flow), but so slowly that the quasi-static creeping flow approximation is applicable. Here, we study the effects of fluid elasticity, the confinement and the flow onto its stability. It turns out that a viscoelastic thread breaks up faster than a Newtonian one. The confinement does not make the thread stable, but it only makes the break-up slower. This result may explain the stability of the wider string observed by Migler (2001) mentioned in Section 1.1. As for the effect of Poiseuille flow, we obtain noticeable results. In case the immersed thread is Newtonian, the flow causes the growth rate to become imaginary, but it does not affect its real part. This implies that the Newtonian immersed thread will be oscillatory unstable and will break up as fast as the one within a quiescent fluid. In case the thread is viscoelastic, the flow causes the growth rate to increase and to become imaginary. This implies that the viscoelastic thread will be oscillatory unstable and will break up faster than the one within a quiescent fluid.

In Chapter 6, we present the general conclusions and some related topics for future research.

Chapter 2

Stability of one Newtonian thread

In this chapter, we study the stability of one liquid thread immersed in an unconfined region filled with another fluid. We apply linear stability analysis and focus on the stability of the system for two types of driving forces: first, pure surface tension, and second, surface tension together with shear flow. The fluids are assumed to be Newtonian and incompressible, the Reynolds number to be small. So, the creeping flow approximation is used.

2.1 Mathematical formulation and boundary conditions

2.1.1 Mathematical formulation

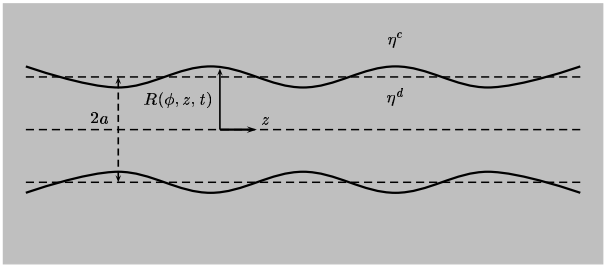

Figure 2.1: *A perturbed thread surface.*

We consider a single thread with viscosity η^d, immersed in an infinite region filled with a fluid with viscosity η^c. We define

$$\mu = \frac{\eta^d}{\eta^c} \quad , \tag{2.1.1}$$

to be the ratio of viscosities of both fluids. The indices c and d stand for the continuous phase (the surrounding fluid) and the dispersed phase (the thread), respectively. A cylindrical coordinate system (r, ϕ, z) is used, with z along the axis of the thread. As

unperturbed state we take the perfect cylinder with radius a. Its stability is tested by applying a small perturbation. The perturbed thread surface is represented by

$$R(\phi, z, t) = a\Big[1 + \epsilon f(\phi, z, t)\Big]. \tag{2.1.2}$$

Here, ϵ is a small parameter ($0 < \epsilon \ll 1$) and $f(\phi, z, t)$ is the radial displacement (the perturbation) of the thread surface. The form of the function f will be described later on. A sketch of the perturbed thread is shown in Figure 2.1.

The fluids are assumed to be Newtonian, incompressible and so viscous that inertial effects are negligible. Then, the system is governed by

$$\text{div } \mathbf{u} = 0 \ , \tag{2.1.3a}$$

$$\text{div } \boldsymbol{\tau} = \mathbf{0} \ , \tag{2.1.3b}$$

where $\mathbf{u}$ is the velocity field and $\boldsymbol{\tau}$ the total stress tensor. Since we are interested in the dynamical evolution of perturbations, we write the solution in the form

$$\begin{aligned} &\mathbf{u} = \mathbf{V} + \epsilon\mathbf{v} \ , \quad \boldsymbol{\tau} = \boldsymbol{\Pi} + \epsilon\boldsymbol{\pi} \ , \\ &\boldsymbol{\Pi} = -P\boldsymbol{\delta} + \boldsymbol{\Gamma} \ , \quad \boldsymbol{\pi} = -p\boldsymbol{\delta} + \boldsymbol{\tau} \ , \end{aligned} \tag{2.1.4}$$

where $\mathbf{V} = (U, V, W)$ is the unperturbed velocity, with U, V and W the velocity components in radial, azimuthal and axial directions, respectively, $\boldsymbol{\Pi}$ the unperturbed total stress tensor, P the unperturbed pressure, $\boldsymbol{\delta}$ the unit tensor and $\boldsymbol{\Gamma}$ the unperturbed extra stress tensor. Variables $\mathbf{v} = (u, v, w), \boldsymbol{\pi}$ and $\boldsymbol{\tau}$ are the perturbations of $\mathbf{V}, \boldsymbol{\Pi}$ and $\boldsymbol{\Gamma}$. For Newtonian fluids, we have (T indicates the transpose)

$$\boldsymbol{\tau} = \widehat{\eta}\ [\mathbf{L} + \mathbf{L}^T] \ . \tag{2.1.5}$$

Here, $\mathbf{L}$ is the gradient of the velocity, i.e.

$$\mathbf{L} = \text{grad } \mathbf{v} \ (\equiv (\nabla\mathbf{v})^T) \ , \ L_{ij} = \frac{\partial v_i}{\partial x_j} \ , \tag{2.1.6}$$

and the viscosity $\widehat{\eta}$ is given by $\widehat{\eta} = \eta^d$ for the thread and $\widehat{\eta} = \eta^c$ for the surrounding fluid. The unperturbed state depends on the problem considered. For instance, when an external flow due to a constant pressure gradient is present, the unperturbed state is the Poiseuille flow problem. For the perturbed state, we find from (2.1.3) and (2.1.4) that the perturbations $\mathbf{v}$ and $\boldsymbol{\pi}$ satisfy

$$\text{div } \mathbf{v} = 0 \ , \tag{2.1.7a}$$

$$\text{div } \boldsymbol{\pi} = \mathbf{0} \ . \tag{2.1.7b}$$

Note that formulation (2.1.7) is a coordinate-free notation, holding for every coordinate system. To make this work self-contained, we mention some notes of tensor notation in Appendix A.

2.1.2 Boundary conditions

As for the boundary conditions, at the interface we apply continuity of velocity, the dynamical conditions for the stresses, and kinematic condition expressing that the thread surface is a material surface.

The detailed evaluation of the boundary conditions is as follows. The continuity of the velocity is written as

$$[\![\mathbf{u}]\!] = 0. \tag{2.1.8}$$

Here, $[\![g]\!] = g^d - g^c$ denotes the jump of an arbitrary function g across the interface. Evaluating $\mathbf{u} = \mathbf{u}(r, \phi, z, t)$ at the interface $r = a + \epsilon a f$, we find (suppressing the dependence on ϕ, z and t for convenience)

$$\begin{aligned} \mathbf{u}(a + \epsilon a f) &= (\mathbf{V} + \epsilon \mathbf{v})(a + \epsilon a f) \\ &= (\mathbf{V} + \epsilon \mathbf{v})(a) + \epsilon a f \frac{\partial}{\partial r}\Big[\mathbf{V} + \epsilon \mathbf{v}\Big](a) + O(\epsilon^2) \\ &= \mathbf{V}(a) + \epsilon\Big[\mathbf{v}(a) + a f \frac{\partial \mathbf{V}}{\partial r}(a)\Big] + O(\epsilon^2). \end{aligned} \tag{2.1.9}$$

Substitution of (2.1.9) into (2.1.8) yields for the unperturbed ($\mathrm{O}(\epsilon^0)$) and the perturbed ($\mathrm{O}(\epsilon^1)$) terms,

$$\epsilon^0: \quad [\![\mathbf{V}(a)]\!] = 0, \tag{2.1.10a}$$

$$\epsilon^1: \quad \Big[\!\Big[\mathbf{v}(a) + a f \frac{\partial \mathbf{V}}{\partial r}(a)\Big]\!\Big] = 0. \tag{2.1.10b}$$

Next, we formulate conditions for the stresses. The outward unit normal $\mathbf{n} = \mathrm{n}_r \mathbf{e}_r + \mathrm{n}_\phi \mathbf{e}_\phi + \mathrm{n}_z \mathbf{e}_z$ at the interface is given by

$$\begin{aligned} \mathbf{n} &= \frac{1}{\sqrt{1 + \left(\epsilon \frac{a}{R}\frac{\partial f}{\partial \phi}\right)^2 + \left(\epsilon a \frac{\partial f}{\partial z}\right)^2}}\left[\mathbf{e}_r - \epsilon \frac{a}{R}\frac{\partial f}{\partial \phi}\mathbf{e}_\phi - \epsilon a \frac{\partial f}{\partial z}\mathbf{e}_z\right] \\ &= \mathbf{e}_r - \epsilon \frac{\partial f}{\partial \phi}\mathbf{e}_\phi - \epsilon a \frac{\partial f}{\partial z}\mathbf{e}_z + \boldsymbol{O}(\epsilon^2). \end{aligned} \tag{2.1.11}$$

Here, $\mathbf{e}_r$, $\mathbf{e}_\phi$ and $\mathbf{e}_z$ are the unit base vectors in radial, azimuthal and axial direction, respectively. Two unit tangent vectors on the perturbed interface, orthogonal to $\mathbf{n}$ and to each other (up to $O(\epsilon^2)$), are

$$\mathbf{t}_1 = \epsilon \frac{\partial f}{\partial \phi}\mathbf{e}_r + \mathbf{e}_\phi + \boldsymbol{O}(\epsilon^2), \tag{2.1.12a}$$

$$\mathbf{t}_2 = \epsilon a \frac{\partial f}{\partial z}\mathbf{e}_r + \mathbf{e}_z + \boldsymbol{O}(\epsilon^2). \tag{2.1.12b}$$

The stress vector $\mathbf{g}$ at the interface is given by

$$\mathbf{g} = \boldsymbol{\tau}\mathbf{n} = (\boldsymbol{\Pi} + \epsilon\boldsymbol{\pi})\mathbf{n}. \tag{2.1.13}$$

Substituting (2.1.11) into (2.1.13), we find the $r-$, $\phi-$ and $z-$ components of $\mathbf{g}$ at the interface:

$$\mathrm{g}_r = \Pi_{rr}(a) + \epsilon\left[\pi_{rr}(a) + af\frac{\partial \Pi_{rr}}{\partial r}(a) - \Pi_{r\phi}(a)\frac{\partial f}{\partial \phi} - a\Pi_{rz}(a)\frac{\partial f}{\partial z}\right] + O(\epsilon^2), \tag{2.1.14a}$$

$$\mathrm{g}_\phi = \Pi_{r\phi}(a) + \epsilon\left[\pi_{r\phi}(a) + af\frac{\partial \Pi_{r\phi}}{\partial r}(a) - \Pi_{\phi\phi}(a)\frac{\partial f}{\partial \phi} - a\Pi_{z\phi}(a)\frac{\partial f}{\partial z}\right] + O(\epsilon^2), \tag{2.1.14b}$$

$$\mathrm{g}_z = \Pi_{rz}(a) + \epsilon\left[\pi_{rz}(a) + af\frac{\partial \Pi_{rz}}{\partial r}(a) - \Pi_{z\phi}(a)\frac{\partial f}{\partial \phi} - a\Pi_{zz}(a)\frac{\partial f}{\partial z}\right] + O(\epsilon^2). \tag{2.1.14c}$$

The dynamical boundary conditions require that

$$[\![\mathbf{g}\cdot\mathbf{t}]\!] = 0, \tag{2.1.15a}$$

$$[\![\mathbf{g}\cdot\mathbf{n}]\!] = -\sigma\left(\frac{1}{R_1} + \frac{1}{R_2}\right). \tag{2.1.15b}$$

Here, σ is the surface tension (in Newton/meter), and R_1 and R_2 are the principle radii of curvature, defined as

$$\begin{aligned}
\frac{1}{R_1} &= -\frac{\dfrac{\partial^2 R}{\partial z^2}}{\left[1 + \left(\dfrac{\partial R}{\partial z}\right)^2\right]^{3/2}} = -\epsilon a\frac{\partial^2 f}{\partial z^2} + O(\epsilon^2),\\
\frac{1}{R_2} &= \frac{R^2 + 2\left(\dfrac{\partial R}{\partial \phi}\right)^2 - R\dfrac{\partial^2 R}{\partial \phi^2}}{\left[R^2 + \left(\dfrac{\partial R}{\partial \phi}\right)^2\right]^{3/2}} = \frac{1}{a}\left[1 - \epsilon\left(f + \frac{\partial^2 f}{\partial \phi^2}\right)\right] + O(\epsilon^2).
\end{aligned} \tag{2.1.16}$$

So, (2.1.15a) represents continuity of the tangential component of the stress vector $\mathbf{g}$, and (2.1.15b) discontinuity of its normal component. Note that the jump in the normal stress is balanced by the surface tension. The minus sign at the right-hand side of (2.1.15b) follows the convention in Chandrasekhar (1961). Substituting (2.1.12a) and (2.1.12b) into (2.1.15a), we obtain

$$\epsilon^0: \quad [\![\Pi_{r\phi}]\!] = 0, \quad [\![\Pi_{rz}]\!] = 0, \tag{2.1.17a}$$

$$\epsilon^1: \quad \left[\!\!\left[\pi_{r\phi} + af\frac{\partial \Pi_{r\phi}}{\partial r} + \left[\Pi_{rr} - \Pi_{\phi\phi}\right]\frac{\partial f}{\partial \phi} - a\Pi_{z\phi}\frac{\partial f}{\partial z}\right]\!\!\right] = 0, \tag{2.1.17b}$$

$$\epsilon^1: \quad \left[\!\!\left[\pi_{rz} + af\frac{\partial \Pi_{rz}}{\partial r} - \Pi_{z\phi}\frac{\partial f}{\partial \phi} + a\left[\Pi_{rr} - \Pi_{zz}\right]\frac{\partial f}{\partial z}\right]\!\!\right] = 0. \tag{2.1.17c}$$

From (2.1.15b), we find

$$\epsilon^0: \quad [\![\Pi_{rr}]\!] = -\frac{\sigma}{a}, \tag{2.1.18a}$$

$$\epsilon^1: \quad \left[\!\!\left[\pi_{rr} + af\frac{\partial \Pi_{rr}}{\partial r} - 2\Pi_{r\phi}\frac{\partial f}{\partial \phi} - 2a\Pi_{rz}\frac{\partial f}{\partial z}\right]\!\!\right] = \frac{\sigma}{a}\left[f + a^2\frac{\partial^2 f}{\partial z^2} + \frac{\partial^2 f}{\partial \phi^2}\right]. \tag{2.1.18b}$$

Note that from now on the jump $[\![\cdot]\!]$ is evaluated at $r = a$, since we have developed the perturbed boundary conditions with respect to the unperturbed state. In doing this, we only maintained first-order terms in the perturbations. Hence, we apply linear stability theory. Using (2.1.4) and (2.1.5), we can rewrite (2.1.17) and (2.1.18) in terms of the pressure and the velocities, as will be done in the next section.

The kinematic condition requires that at the perturbed interface $R(\phi, z, t)$, being a material surface, the radial velocity is given by the material derivative (DR/Dt) following a thread particle:

$$\mathbf{u}^d \cdot \mathbf{e}_r = \frac{DR}{Dt} = \frac{\partial R}{\partial t} + (\mathbf{u}^d \cdot \mathbf{e}_\phi)\frac{1}{R}\frac{\partial R}{\partial \phi} + (\mathbf{u}^d \cdot \mathbf{e}_z)\frac{\partial R}{\partial z}. \tag{2.1.19}$$

2.2 Stability due to surface tension

2.2.1 Solution methodology

Here, we investigate the stability of one Newtonian immersed thread, when the dynamics of the system is due to surface tension only. Treatment of this case is mainly included to introduce the reader to techniques and notations. Our (numerical) results can be checked, since data are available in the literature.

We represent the radial displacement $f(\phi, z, t)$ in (2.1.2) by the expansion

$$f(\phi, z, t) = \sum_{m=0}^{\infty} \varepsilon_m(t) \cos m\phi \cos kz. \tag{2.2.1}$$

So, $f(\phi, z, t)$ is a sum of modes with amplitudes $\varepsilon_m(t)$. The modes are periodic in z with wave number k and contain a Fourier expansion in ϕ. Note that since the thread has cylindrical symmetry it is sufficient to consider only an axisymmetric perturbation. However, we shall solve the equations for arbitrary modes because the solution will serve as a benchmark. Since the dynamics is only due to surface tension, the unperturbed state has a trivial solution for the velocities, i.e. $\mathbf{V} = \mathbf{0}$, and a constant pressure satisfying $[\![P]\!] = -\sigma/a$, with σ the surface tension. Using (2.1.5) and (2.1.7a), we find that the perturbed equations satisfy (see also Appendix A)

$$0 = \text{div } \mathbf{v} \ , \tag{2.2.2a}$$

$$\text{grad } p = \widehat{\eta} \ \text{div } (\text{grad } \mathbf{v})^T \ . \tag{2.2.2b}$$

Written out in components in cylindrical coordinates, (2.2.2) reads

$$0 = \frac{1}{r}\frac{\partial\,[ru]}{\partial r} + \frac{1}{r}\frac{\partial v}{\partial \phi} + \frac{\partial w}{\partial z}, \tag{2.2.3a}$$

$$\frac{\partial p}{\partial r} = \widehat{\eta}\left[\frac{1}{r}\frac{\partial}{\partial r}\left[r\frac{\partial u}{\partial r}\right] + \frac{1}{r^2}\frac{\partial^2 u}{\partial \phi^2} + \frac{\partial^2 u}{\partial z^2} - \frac{2}{r^2}\frac{\partial v}{\partial \phi} - \frac{u}{r^2}\right], \tag{2.2.3b}$$

$$\frac{1}{r}\frac{\partial p}{\partial \phi} = \widehat{\eta}\left[\frac{1}{r}\frac{\partial}{\partial r}\left[r\frac{\partial v}{\partial r}\right] + \frac{1}{r^2}\frac{\partial^2 v}{\partial \phi^2} + \frac{\partial^2 v}{\partial z^2} + \frac{2}{r^2}\frac{\partial u}{\partial \phi} - \frac{v}{r^2}\right], \tag{2.2.3c}$$

$$\frac{\partial p}{\partial z} = \widehat{\eta}\left[\frac{1}{r}\frac{\partial}{\partial r}\left[r\frac{\partial w}{\partial r}\right] + \frac{1}{r^2}\frac{\partial^2 w}{\partial \phi^2} + \frac{\partial^2 w}{\partial z^2}\right]. \tag{2.2.3d}$$

For convenience, the equations will be brought into dimensionless form. The distance, velocity, and stress components are made dimensionless with respect to a, σ/η^c, and σ/a, respectively. For instance, we obtain

$$r = ar^*,\ \mathbf{u} = \frac{\sigma}{\eta^c}\mathbf{u}^*,\ \boldsymbol{\tau} = \frac{\sigma}{a}\boldsymbol{\tau}^*,\quad \text{and}\quad ka = k^*. \tag{2.2.4}$$

In the sequel, we shall omit the stars, since confusion is not possible. In accordance with (2.2.1), we propose as general expressions for the pressure and the velocity components u, v and w in (2.2.3) the expansions

$$p = \sum_{m=0}^{\infty} p_m(r,t)\cos m\phi \cos kz, \tag{2.2.5a}$$

$$u = \sum_{m=0}^{\infty} u_m(r,t)\cos m\phi \cos kz, \tag{2.2.5b}$$

$$v = \sum_{m=1}^{\infty} v_m(r,t)\sin m\phi \cos kz, \tag{2.2.5c}$$

$$w = \sum_{m=0}^{\infty} w_m(r,t)\cos m\phi \sin kz. \tag{2.2.5d}$$

Here, we assumed that separation of variables is applicable. So, the dependence on ϕ is written in terms of Fourier modes. We used that the azimuthal velocity v is an odd function of ϕ, whereas the other velocities are even functions in ϕ. We note that there is no contribution of the zeroth order mode in v, hence without loss of generality we may take $v_0 = 0$. Substitution of (2.2.5) into (2.2.3) yields equations for the amplitudes. For

$m = 0, 1, 2, \cdots$, we arrive at

$$0 = \frac{1}{r}\frac{\partial\left[ru_m\right]}{\partial r} + \frac{m}{r}v_m + kw_m, \tag{2.2.6a}$$

$$\frac{\partial p_m}{\partial r} = \widehat{\eta}\left[\frac{1}{r}\frac{\partial}{\partial r}\left[r\frac{\partial u_m}{\partial r}\right] - \frac{m^2+1+(kr)^2}{r^2}u_m - \frac{2m}{r^2}v_m\right], \tag{2.2.6b}$$

$$-\frac{m}{r}p_m = \widehat{\eta}\left[\frac{1}{r}\frac{\partial}{\partial r}\left[r\frac{\partial v_m}{\partial r}\right] - \frac{m^2+1+(kr)^2}{r^2}v_m - \frac{2m}{r^2}u_m\right], \tag{2.2.6c}$$

$$-kp_m = \widehat{\eta}\left[\frac{1}{r}\frac{\partial}{\partial r}\left[r\frac{\partial w_m}{\partial r}\right] - \frac{m^2+(kr)^2}{r^2}w_m\right]. \tag{2.2.6d}$$

Here, $\widehat{\eta} = \mu$ for $r < 1$ and $\widehat{\eta} = 1$ for $r > 1$. To solve (2.2.6) we proceed as follows. Taking the divergence of both sides of (2.2.2b), we obtain for the pressure

$$\Delta p = 0, \tag{2.2.7}$$

with Δ the Laplace operator in cylindrical coordinates. Substitution of (2.2.5a) into (2.2.7) leads to

$$\frac{1}{r}\frac{\partial}{\partial r}\left[r\frac{\partial p_m}{\partial r}\right] - \frac{m^2+(kr)^2}{r^2}p_m = 0. \tag{2.2.8}$$

The general solution of (2.2.8) is

$$p_m(r,t) = 2\widehat{\eta}\left[A_m I_m(kr) + D_m K_m(kr)\right], \quad m \geq 0, \tag{2.2.9}$$

where I_m and K_m are modified Bessel functions of order m, and A_m and D_m are unknown time dependent coefficients; the factor $2\widehat{\eta}$ is added for convenience. Substitution of (2.2.9) into (2.2.6d) leads to the general solution for $w_m(r,t), m \geq 0$:

$$w_m(r,t) = -A_m r I_{m+1}(kr) + B_m I_m(kr) + D_m r K_{m+1}(kr) + E_m K_m(kr). \tag{2.2.10}$$

Since there is no zeroth order mode in v present, we find from substituting (2.2.9) into (2.2.6b), that the solution for u_0 is given by

$$u_0(r,t) = A_0 r I_0(kr) + C_0 I_1(kr) + D_0 r K_0(kr) + F_0 K_1(kr). \tag{2.2.11}$$

Substituting this expression into (2.2.6a), we find the relations

$$C_0 = -\left(B_0 + \frac{2}{k}A_0\right) \quad \text{and} \quad F_0 = E_0 + \frac{2}{k}D_0. \tag{2.2.12}$$

So, we obtain

$$u_0(r,t) = A_0 r I_0(kr) - \left[B_0 + \frac{2}{k}A_0\right]I_1(kr) + D_0 r K_0(kr) + \left[E_0 + \frac{2}{k}D_0\right]K_1(kr). \tag{2.2.13}$$

Next, we calculate the solution for $m > 0$. We substitute (2.2.9) and (2.2.10) into (2.2.6a) and (2.2.6b) and eliminate v_m from these two equations, to obtain the following equation for u_m:

$$u_m'' + \frac{3}{r}u_m' - \frac{m^2 + (kr)^2 - 1}{r^2}u_m = \frac{G(r,t)}{\widehat{\eta}} \ , \tag{2.2.14}$$

where $G(r,t)$ is defined as

$$\begin{aligned} G(r,t) \ &= \ 2\widehat{\eta}\left[2kA_mI_{m+1}(kr) + \frac{mA_m - kB_m}{r}I_m(kr) - 2kD_mK_{m+1}(kr)\right. \\ &\qquad \left. + \frac{mD_m - kE_m}{r}K_m(kr)\right]. \end{aligned}$$

Here, the prime denotes the derivative with respect to r. From (2.2.14) we find as general solution

$$\begin{aligned} u_m(r,t) = A_mrI_m(kr) - \left[B_m + \frac{1}{k}(m+2)A_m\right]I_{m+1}(kr) + \frac{C_m}{r}I_m(kr) \\ + D_mrK_m(kr) + \left[E_m + \frac{1}{k}(m+2)D_m\right]K_{m+1}(kr) + \frac{F_m}{r}K_m(kr) \ . \end{aligned} \tag{2.2.15}$$

Substitution of (2.2.10) and (2.2.15) into (2.2.6a) yields that

$$\begin{aligned} v_m(r,t) = -\left[(B_m + \frac{1}{k}(m+2)A_m + \frac{k}{m}C_m\right]I_{m+1}(kr) - \frac{1}{r}C_mI_m(kr) \\ + \left[E_m + \frac{1}{k}(m+2)D_m + \frac{k}{m}F_m\right]K_{m+1}(kr) - \frac{1}{r}F_mK_m(kr) \ . \end{aligned} \tag{2.2.16}$$

Next, we discern between the solution inside the thread ($r < 1$) and outside the thread ($r > 1$). Since the solution for $r < 1$ should remain finite for $r \to 0$, we find

$$p_m^d(r,t) = 2\mu A_mI_m(kr) \ , \tag{2.2.17a}$$

$$u_0^d(r,t) = A_0rI_0(kr) - \left[B_0 + \frac{2}{k}A_0\right]I_1(kr) \ , \tag{2.2.17b}$$

$$u_m^d(r,t) = A_mrI_m(kr) - \left[B_m + \frac{1}{k}(m+2)A_m\right]I_{m+1}(kr) + \frac{C_m}{r}I_m(kr) \ , \tag{2.2.17c}$$

$$v_0^d(r,t) = 0 \ , \tag{2.2.17d}$$

$$v_m^d(r,t) = -\left[B_m + \frac{1}{k}(m+2)A_m + \frac{k}{m}C_m\right]I_{m+1}(kr) - \frac{1}{r}C_mI_m(kr) \ , \tag{2.2.17e}$$

$$w_m^d(r,t) = -A_mrI_{m+1}(kr) + B_mI_m(kr) \ . \tag{2.2.17f}$$

For $r > 1$ the solution should be bounded at infinity. We obtain

$$p_m^c(r,t) = 2D_m K_m(kr) \ , \tag{2.2.18a}$$

$$u_0^c(r,t) = D_0 r K_0(kr) + \left[E_0 + \frac{2}{k}D_0\right] K_1(kr) \ , \tag{2.2.18b}$$

$$u_m^c(r,t) = D_m r K_m(kr) + \left[E_m + \frac{1}{k}(m+2)D_m\right] K_{m+1}(kr) + \frac{F_m}{r}K_m(kr) \ , \tag{2.2.18c}$$

$$v_0^c(r,t) = 0 \ , \tag{2.2.18d}$$

$$v_m^c(r,t) = \left[E_m + \frac{1}{k}(m+2)D_m + \frac{k}{m}F_m\right] K_{m+1}(kr) - \frac{1}{r}F_m K_m(kr) \ , \tag{2.2.18e}$$

$$w_m^c(r,t) = D_m r K_{m+1}(kr) + E_m K_m(kr) \ . \tag{2.2.18f}$$

Up to here, we did not write explicitly the dependence of the field variables on time t; however, at this point, it must be noted that A_m, B_m, etc. are functions of t. These coefficients follows from the boundary conditions. From Section 2.1.2, we obtain the boundary conditions for components of the perturbed quantities ($O(\epsilon^1)$), in non-dimensional form,

$$[\![u_m]\!] = 0, \tag{2.2.19a}$$

$$[\![v_m]\!] = 0, \tag{2.2.19b}$$

$$[\![w_m]\!] = 0, \tag{2.2.19c}$$

$$[\![\pi_{r\phi}]\!] = \left[\!\!\left[\widehat{\eta}\left(mu_m - \frac{\partial v_m}{\partial r} + v_m\right)\right]\!\!\right] = 0, \tag{2.2.19d}$$

$$[\![\pi_{rz}]\!] = \left[\!\!\left[\widehat{\eta}\left(ku_m - \frac{\partial w_m}{\partial r}\right)\right]\!\!\right] = 0, \tag{2.2.19e}$$

$$[\![\pi_{rr}]\!] = \left[\!\!\left[- p_m + 2\widehat{\eta}\frac{\partial u_m}{\partial r}\right]\!\!\right] = (1 - k^2 - m^2)\varepsilon_m. \tag{2.2.19f}$$

From the kinematic condition we find

$$u_m^d = \frac{d}{dt}\varepsilon_m(t). \tag{2.2.20}$$

In practice, the expansions (2.2.5) are cut off at $m = M$. Thus, we obtain (4+6M) unknowns and equations (note that for $M = 0$ we have $v_0 = 0$, so (2.2.19b) and (2.2.19d) will be obviously satisfied). In this section, we shall deal with the cases $M = 0, 1$ and $M = 2$. Note that in (2.2.1) the $m = 0$ mode corresponds to an axisymmetric mode perturbation, and the $m > 0$ modes to non-axisymmetric mode perturbations.

2.2.2 Stability analysis

2.2.2.1 The axisymmetric mode perturbation

Evaluating boundary conditions (2.2.19) for $m = 0$, we obtain the linear system

$$\mathbf{M}_0\mathbf{z}_0 = \mathbf{e}_0, \tag{2.2.21}$$

where $\mathbf{M}_0$ is a 4 by 4 matrix, $\mathbf{z}_0 = (A_0, B_0, D_0, E_0)^T$, and $\mathbf{e}_0 = (0, 0, 0, (1-k^2)\varepsilon_0)^T$. The expression for $\mathbf{M}_0$ is given in Appendix B.1.

According to Cramer's rule, the solution of (2.2.21) is given by

$$(\mathbf{z}_0)_j = \left[(-1)^{4+j}(1-k^2)|\mathbf{M_0}^{4,j}|\right]\frac{\varepsilon_0(t)}{|\mathbf{M}_0|}, \tag{2.2.22}$$

where $|\cdot|$ denotes the determinant and $\mathbf{M}_0^{i,j}$ is the 3×3 sub-matrix of $\mathbf{M}_0$, which can be found by omitting the i-th row and the j-th column of $\mathbf{M}_0$. From (2.2.17b), (2.2.20) and (2.2.22), we obtain

$$\frac{d}{dt}\varepsilon_0(t) = q_0(k,\mu)\varepsilon_0(t), \tag{2.2.23}$$

where

$$q_0(k,\mu) = \frac{(k^2-1)}{|\mathbf{M}_0|}\left[\left(I_0(k) - \frac{2}{k}I_1(k)\right)|\mathbf{M}_0^{4,1}| + I_1(k)|\mathbf{M}_0^{4,2}|\right]. \tag{2.2.24}$$

Since $\mathbf{M}_0$ is a real matrix, q_0 is also real. The behaviour of the solution of (2.2.23) depends on the sign of q_0. The real parameter q_0 is the so-called growth rate of the axisymmetric disturbance mode. It acts as *the degree of instability* mentioned in Tomotika (1935). If $q_0 > 0$, then the mode grows in time, indicating instability. If $q_0 < 0$, then the mode decays in time, indicating stability.

Let us briefly discuss some limiting cases. First, we consider the case when the thread is much less viscous than the surrounding fluid ($\mu \to 0$). Putting $\mu = 0$ in $\mathbf{M}_0$ and evaluating (2.2.24), we find (in dimensional form)

$$q_0(k,\mu) = \frac{\sigma(1-(ka)^2)}{2\eta^c}\frac{1}{1+(ka)^2-(ka)^2K_0^2(ka)/K_1^2(ka)}\ . \tag{2.2.25}$$

This result is in agreement with the work of Tomotika (1935). Second, we consider the case when the thread is much more viscous than the surrounding fluid ($\mu \to \infty$). We multiply the third and fourth rows of $\mathbf{M}_0$ in (2.2.21) by a factor of $1/\mu$ to obtain a new matrix, $\mathbf{M}_0'$ say. Now, $\mathbf{e}_0$ becomes $\mathbf{e}_0' = (0, 0, 0, (1-k^2)\varepsilon_0/\mu)^T$. Equation (2.2.24) also holds for this case, with $\mathbf{M}_0$ replaced by $\mathbf{M}_0'$ and (k^2-1) by $(k^2-1)/\mu$. Taking $1/\mu \to 0$ and evaluating $|\mathbf{M}_0'|$, etc., we find (in dimensional form)

$$q_0(k,\mu) = \frac{\sigma((ka)^2-1)}{2\eta^d}\frac{1}{1+(ka)^2-(ka)^2I_0^2(ka)/I_1^2(ka)}\ , \tag{2.2.26}$$

a result that is identical with the work of Rayleigh (1892).

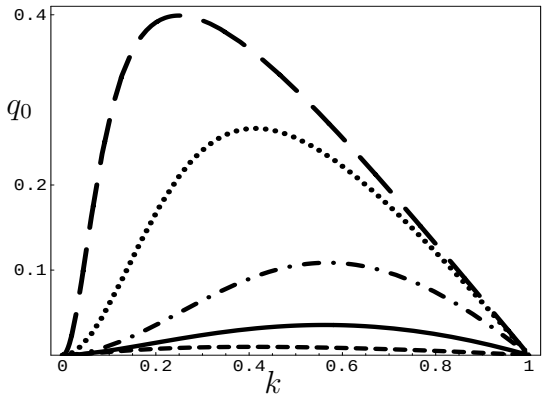

Figure 2.2: *Curves of q_0 as functions of the wave number k for different μ values: $\mu = 10$ (dashed curve), $\mu = 1$ (solid curve), $\mu = 0.1$ (dash-dot curve), $\mu = 0.01$ (dotted curve), and $\mu = 0.001$ (long dashed curve).*

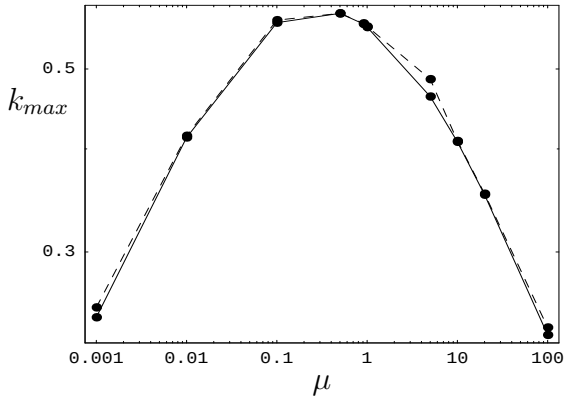

Figure 2.3: *Wave number k_{max} as a function of the ratio of viscosities μ. Present approach (solid line) and Tomotika's results (1935) (dashed line).*

When the ratio μ is neither infinite nor zero, the value of q_0 follows from (2.2.24). Figure 2.2 shows the curves of q_0 versus the wave number k for various values of μ. Note that for $k > 1$, always $q_0 < 0$. From this figure, we see that $q_0 > 0$ for all μ and this indicates instability. If μ increases, the values of q_0 decrease. Thus, the more viscous the thread, the longer it takes to disintegrate. If the thread is very viscous, it will remain undeformed for a long time before finally breaking up into droplets of very small size. Similar results were reported earlier by Tomotika (1935) and Mikami et al. (1975).

According to Rayleigh (1892), the disturbance that causes the thread to break up is the one which has the maximum growth rate. From Figure 2.2, we see that there is one wave number, k_{max}, for which q_0 attains its maximum value. Thus, k_{max} is the wave number for which the disturbance grows fastest. The curve of k_{max} as a function of μ is shown in Figure 2.3. From this Figure, we see that the present results are in perfect agreement with the results of Tomotika (1935).

2.2.2.2 The non-axisymmetric mode perturbation

The results in this case will be used as a comparison with the results for the shear flow problem, to be presented in Section 2.3.

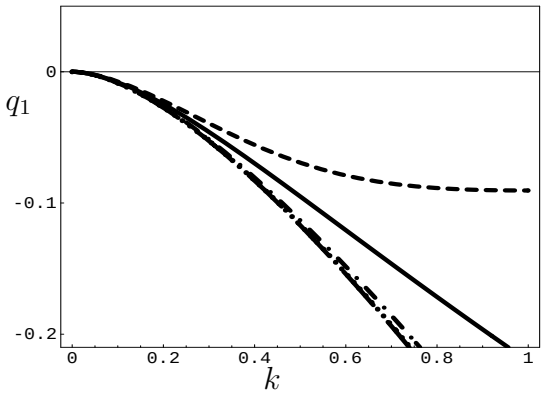

Figure 2.4: *Same information as in Figure 2.2, but now for q_1.*

Evaluating the boundary conditions for $m = 0$ and $m = 1$, we find, as counterpart of (2.2.21), the linear system

$$\mathbf{M}\mathbf{z} = \begin{pmatrix} \mathbf{M}_0 & \mathbf{0} \\ \mathbf{0} & \mathbf{M}_1 \end{pmatrix} \begin{pmatrix} \mathbf{z}_0 \\ \mathbf{z}_1 \end{pmatrix} = \begin{pmatrix} \mathbf{e}_0 \\ \mathbf{e}_1 \end{pmatrix}, \tag{2.2.27}$$

where $\mathbf{M}_1$ is a 6 by 6 matrix, $\mathbf{z}_1 = (A_1, B_1, C_1, D_1, E_1, F_1)^T$, and $\mathbf{e}_1 = (0, 0, 0, 0, 0, -k^2\varepsilon_1)^T$. Further, $\mathbf{M}_0$, $\mathbf{z}_0$ and $\mathbf{e}_0$ are the same as in (2.2.21). The expression of $\mathbf{M}_1$ is given in Appendix B.1. Since the system (2.2.27) is uncoupled, we may independently solve the equations

$$\mathbf{M}_m\mathbf{z}_m = \mathbf{e}_m, \quad \text{for} \quad m = 0, 1. \tag{2.2.28}$$

From (2.2.17c), (2.2.20) and (2.2.28), we obtain

$$\frac{d}{dt}\varepsilon_m(t) = q_m(k, \mu)\varepsilon_m(t), \quad \text{for} \quad m = 0, 1, \tag{2.2.29}$$

where q_0 is the same as in (2.2.24), and

$$q_1(k, \mu) = \frac{k^2}{|\mathbf{M}_1|}\left[\left(I_1(k) - \frac{3}{k}I_2(k)\right)|\mathbf{M}_1^{6,1}| + I_2(k)|\mathbf{M}_1^{6,2}| + I_1(k)|\mathbf{M}_1^{6,3}|\right]. \tag{2.2.30}$$

Here, q_1 is the growth rate of the first-order non-axisymmetric mode. Figure 2.4 shows curves of q_1 as functions of k for various values of μ. The growth rate q_1 is negative for all k. Thus, this mode always decays. Using the same procedure, we obtain the second-order non-axisymmetric mode q_2 as shown in Figure 2.5. Again, we see that the $m = 2$ mode is negative. Since the axisymmetric mode ($m = 0$) is unstable, we conclude that the (non-axisymmetric) higher-order modes do not affect the stability of the thread, and thus the thread is unstable.

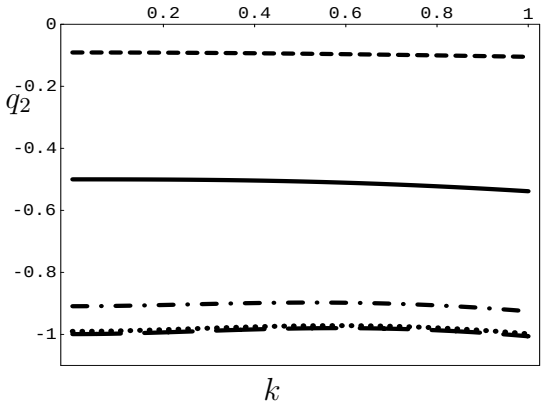

Figure 2.5: *Same information as in Figure 2.2, but now for q_2.*

We now proceed by considering the peculiar case $k = 0$, in which the perturbed thread remains uniform in z-direction and in which there is no displacement in this direction. Due to incompressibility (here requiring conservation of area for the cross-section), the cross-section can only deform in a non-axisymmetric mode with $m \geq 2$ (the mode $m = 1$ only gives a rigid-body translation). For this special case, we see from Figures 2.2 and 2.4 that indeed the growth rates vanish for $m = 0$ and $m = 1$. However, this is not the case for $m = 2$, as we can see from Figure 2.5. For $m \geq 2$, we shall analytically calculate the growth rate, providing a check on the numerical results. In this case, instead of the modified Bessel functions, we obtain r^m and r^{-m} as the solution. For $m \geq 2$, we obtain the following solutions for $r < 1$,

$$u_m^d(r,t) = A_m r^{m-1} + \frac{m}{2(m+1)} B_m r^{m+1}, \tag{2.2.31a}$$

$$v_m^d(r,t) = -A_m r^{m-1} - \frac{m+2}{2(m+1)} B_m r^{m+1}, \tag{2.2.31b}$$

$$w_m^d(r,t) = 0, \tag{2.2.31c}$$

$$p_m^d(r,t) = 2\mu B_m r^m, \tag{2.2.31d}$$

and for $r > 1$,

$$u_m^c(r,t) = C_m r^{-(m+1)} + \frac{m}{2(m-1)} D_m r^{-(m-1)} \ , \tag{2.2.32a}$$

$$v_m^c(r,t) = C_m r^{-(m+1)} + \frac{m-2}{2(m-1)} D_m r^{-(m-1)} \ , \tag{2.2.32b}$$

$$w_m^c(r,t) = 0, \tag{2.2.32c}$$

$$p_m^c(r,t) = 2D_m r^{-m} \ . \tag{2.2.32d}$$

Evaluating the boundary conditions, we obtain the linear system

$$\mathbf{M}_{m;k=0}\mathbf{z}_m = \mathbf{e}_m, \tag{2.2.33}$$

with $\mathbf{z}_m = (A_m, B_m, C_m, D_m)^T$ and $\mathbf{e}_m = (0, 0, 0, (1 - m^2)\varepsilon_m)^T$. The expression for $\mathbf{M}_{m;k=0}$ is given in Appendix B.1. From (2.2.20), (2.2.31a) and (2.2.33), we again obtain (2.2.29), but now with

$$q_m(\mu; k = 0) = -\frac{m}{2(1+\mu)}, \quad m \geq 2. \tag{2.2.34}$$

Equation (2.2.34) shows that the thread is stable towards z-independent deformations resulting in a non-circular cross section.

2.3 Stability in the presence of shear flow

In this section, we investigate the hydrodynamic stability of a Newtonian thread immersed in a shear field. The shear flow tends to deform and elongate the thread. Using *Hurwitz's criterion*, we determine the range of ratios of viscosities for which the shear stabilizes the thread.

2.3.1 Mathematical formulation and solution methodology

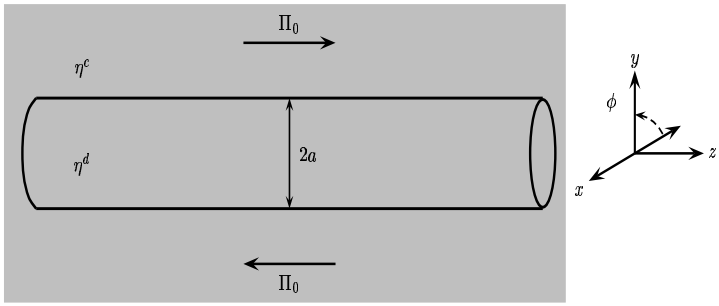

Figure 2.6: *Thread immersed in a fluid in shear flow.*

Let us consider a single thread immersed in an infinite region filled with fluid. An external flow is imposed along the z-direction by applying a constant shear stress Π_0 far away from the thread. The domain of the system is shown in Figure 2.6. The parameters, i.e. a, η^d, etc., have similar meanings as in Section 2.2. We define the ratio of viscosities of both fluids as in (2.1.1), i.e. $\mu = \eta^d/\eta^c$.

As unperturbed state, we take the thread to be a perfect cylinder. Its stability is tested by applying a small perturbation. The thread surface is represented as in (2.1.2) with a perturbed radial displacement

$$f(\phi, z, t) = \Re\left[\sum_{m=-\infty}^{\infty} \varepsilon_m(t) e^{i(m\phi + kz)}\right]. \tag{2.3.1}$$

Here, $i = \sqrt{-1}$ is the imaginary unit and $\Re$ is the real part symbol. We have expressed the perturbation as a complex Fourier series in ϕ and taken it periodic in z with wave

number k. Since the solution is periodic in the z-direction, k must be real. The ε_m are the time-dependent disturbance amplitudes and ϵ is a small parameter ($0 < \epsilon \ll 1$). Note that ε_m is assumed to be complex. In the sequel, we shall not write the '$\Re$'-symbol explicitly, as is common practice in complex calculations.

The fluids are assumed to be Newtonian, incompressible and so viscous that the creeping flow approximation is applicable. So, the system is governed by (2.1.3), (2.1.4) and (2.1.5). At the interface, we have the continuity of the velocities, the dynamical conditions and the kinematic condition. In the next section, we discuss the unperturbed and the perturbed solutions.

2.3.1.1 The unperturbed solution

We assume that there is no pressure gradient present in the unperturbed state. We only prescribe a uniform shear stress Π_0. This implies that the pressure P is constant, apart from a possible jump at the thread surface. Thus, for this state we obtain

$$\text{div } \mathbf{V} = 0 \ , \tag{2.3.2a}$$

$$\text{div } (\text{grad } \mathbf{V})^T = \mathbf{0}. \tag{2.3.2b}$$

We try $\mathbf{V} = (0, 0, W(r, \phi))$ with $W(r, \phi) = -iG(r)e^{i\phi}$ satisfying (2.3.2). For later convenience, the factor $-i$ is added. Then, we find that the general solution of (2.3.2) is given by

$$W(r, \phi) = -i \left(Ar + \frac{B}{r} \right) e^{i\phi}. \tag{2.3.3}$$

The constants A and B are to be determined from the boundary conditions, and take different values in the two phases. The boundary conditions, in $O(\epsilon^0)$, are

$$[\![W]\!] = 0, \tag{2.3.4a}$$

$$[\![\Pi_{rz}]\!] = [\![\Gamma_{rz}]\!] = 0 \tag{2.3.4b}$$

$$[\![\Pi_{rr}]\!] = [\![-P]\!] = -\frac{\sigma}{a}. \tag{2.3.4c}$$

Note that the other boundary conditions at the interface are obviously satisfied. We also have two other conditions, i.e. the solution must remain bounded at the origin, and for $r \to \infty$ we prescribe $W \to -i\Pi_0 r e^{i\phi}/\eta^c$. This latter condition implies that the shear stress at infinity goes to Π_0. Evaluating the boundary conditions, we find

$$W = \begin{cases} -i \dfrac{2\Pi_0}{\eta^c(1+\mu)} r e^{i\phi} \ \ ; \ \ 0 \le r \le a, \\ -i \dfrac{\Pi_0}{\eta^c} \left[r + \dfrac{1-\mu}{1+\mu} \dfrac{a^2}{r} \right] e^{i\phi} \ \ ; \ \ r \ge a, \end{cases} \tag{2.3.5}$$

and

$$P = \begin{cases} P_0 + \dfrac{\sigma}{a}, & 0 \le r \le a, \\ P_0, & r \ge a, \end{cases} \tag{2.3.6}$$

for some constant P_0. For convenience, the equations are brought into dimensionless form. The distance, velocity, and stress components are made dimensionless with respect to a, σ/η^c, and σ/a, respectively. For example, we have

$$\begin{aligned} &r = ar^*, \quad z = az^*, \quad R = aR^*, \quad \mathbf{u} = \frac{\sigma}{\eta^c}\mathbf{u}^*, \quad \boldsymbol{\tau} = \frac{\sigma}{a}\boldsymbol{\tau}^*, \\ &p = \frac{\sigma}{a}p^*, \quad t = \frac{a\eta^c}{\sigma}t^*, \quad \text{and} \quad k = \frac{k^*}{a}. \end{aligned} \tag{2.3.7}$$

In the sequel we omit the stars, since confusion is not possible. For the velocity W, substitution of (2.3.7) into (2.3.5) yields

$$W = \begin{cases} -i\dfrac{2\mathrm{Ca}}{1+\mu} r e^{i\phi} \quad ; \quad 0 \le r \le 1, \\ -i\mathrm{Ca}\left[r + \dfrac{1-\mu}{1+\mu}\dfrac{1}{r}\right] e^{i\phi} \quad ; \quad r \ge 1. \end{cases} \tag{2.3.8}$$

Here, we have introduced the capillary number Ca defined as

$$\mathrm{Ca} = \frac{\Pi_0 a}{\sigma}. \tag{2.3.9}$$

We also calculate the derivative of W with respect to r:

$$\frac{\partial W}{\partial r} = \begin{cases} -i\dfrac{2\mathrm{Ca}}{1+\mu} e^{i\phi} \quad ; \quad 0 \le r \le 1, \\ -i\mathrm{Ca}\left[1 - \dfrac{1-\mu}{1+\mu}\dfrac{1}{r^2}\right] e^{i\phi} \quad ; \quad r \ge 1. \end{cases} \tag{2.3.10}$$

Note that (2.3.10) has a discontinuity at $r = 1$, except for $\mu = 1$. From (2.3.8) we calculate the unperturbed stress components as

$$\begin{aligned} &\Pi_{rr} = \Pi_{\phi\phi} = \Pi_{zz} = \begin{cases} \dfrac{-P_0 a}{\sigma} - 1 \quad ; \quad 0 \le r \le 1, \\ \dfrac{-P_0 a}{\sigma} \quad ; \quad r \ge 1, \end{cases} \\ &\Gamma_{r\phi} = 0, \\ &\Gamma_{rz} = \begin{cases} -i\dfrac{2\mu\mathrm{Ca}}{1+\mu} e^{i\phi} \quad ; \quad 0 \le r \le 1, \\ -i\mathrm{Ca}\left[1 - \dfrac{1-\mu}{1+\mu}\dfrac{1}{r^2}\right] e^{i\phi} \quad ; \quad r \ge 1, \end{cases} \\ &\Gamma_{z\phi} = \begin{cases} \dfrac{2\mu\mathrm{Ca}}{1+\mu} e^{i\phi} \quad ; \quad 0 \le r \le 1, \\ \mathrm{Ca}\left[1 + \dfrac{1-\mu}{1+\mu}\dfrac{1}{r^2}\right] e^{i\phi} \quad ; \quad r \ge 1, \end{cases} \end{aligned} \tag{2.3.11}$$

We note that at the interface $r = 1$ the stress Γ_{rz} is continuous (as it should be), but this does not hold for $\Gamma_{z\phi}$, except for $\mu = 1$.

2.3.1.2 The perturbed solution

From (2.1.3), (2.1.4) and (2.1.5) with $\mathbf{v} = u\mathbf{e}_r + v\mathbf{e}_\phi + w\mathbf{e}_z$, we find that the perturbations u, v, w and p satisfy the set of four equations (2.2.3). Analogous to (2.2.5), we propose as general expressions for the solution, the expansions

$$p = \sum_{m=-\infty}^{\infty} p_m(r,t)e^{i(m\phi+kz)}, \tag{2.3.12a}$$

$$u = \sum_{m=-\infty}^{\infty} u_m(r,t)e^{i(m\phi+kz)}, \tag{2.3.12b}$$

$$v = \sum_{m=-\infty}^{\infty} -iv_m(r,t)e^{i(m\phi+kz)}, \tag{2.3.12c}$$

$$w = \sum_{m=-\infty}^{\infty} -iw_m(r,t)e^{i(m\phi+kz)}. \tag{2.3.12d}$$

Note that in contrast to (2.2.5), we have added here an extra factor $-i$ to v_m and w_m. Here, we assume that p_m, u_m, etc., are complex variables. In these formulae we should read the right-hand sides as preceded by the 'real part of'. Substitution of (2.3.12) into (2.2.3) yields the equations for the coefficients:

$$0 = \frac{1}{r}\frac{\partial\left[ru_m\right]}{\partial r} + \frac{m}{r}v_m + kw_m, \tag{2.3.13a}$$

$$\frac{\partial p_m}{\partial r} = \widehat{\eta}\left[\frac{1}{r}\frac{\partial}{\partial r}\left[r\frac{\partial u_m}{\partial r}\right] - \frac{m^2+1+(kr)^2}{r^2}u_m - \frac{2m}{r^2}v_m\right], \tag{2.3.13b}$$

$$-\frac{m}{r}p_m = \widehat{\eta}\left[\frac{1}{r}\frac{\partial}{\partial r}\left[r\frac{\partial v_m}{\partial r}\right] - \frac{m^2+1+(kr)^2}{r^2}v_m - \frac{2m}{r^2}u_m\right], \tag{2.3.13c}$$

$$-kp_m = \widehat{\eta}\left[\frac{1}{r}\frac{\partial}{\partial r}\left[r\frac{\partial w_m}{\partial r}\right] - \frac{m^2+(kr)^2}{r^2}w_m\right]. \tag{2.3.13d}$$

These equations are identical to the equations in (2.2.6). So, the solution for both phases are given by (2.2.17) and (2.2.18). However, there is one essential difference here: as the present problem is not rotationally symmetric, the assumption $v_0 = 0$ does not longer hold. Instead, (2.2.17d) and (2.2.18d) become

$$v_0^d(r) = C_0 I_1(kr), \quad \text{and} \quad v_0^c(r) = F_0 K_1(kr). \tag{2.3.14}$$

Next, we derive the boundary conditions at the interface. From Section 2.1.2, we

obtain for the $O(\epsilon^1)$-contributions,

$$[\![u]\!] = 0, \tag{2.3.15a}$$

$$[\![v]\!] = 0, \tag{2.3.15b}$$

$$[\![w]\!] = -\left[\!\!\left[f\frac{\partial W}{\partial r} \right]\!\!\right], \tag{2.3.15c}$$

$$[\![\tau_{r\phi}]\!] = \left[\!\!\left[\widehat{\eta}\left(\frac{\partial u}{\partial \phi} + \frac{\partial v}{\partial r} - v \right) \right]\!\!\right] = \left[\!\!\left[\Gamma_{z\phi}\frac{\partial f}{\partial z} \right]\!\!\right], \tag{2.3.15d}$$

$$[\![\tau_{rz}]\!] = \left[\!\!\left[\widehat{\eta}\left(\frac{\partial u}{\partial z} + \frac{\partial w}{\partial r} \right) \right]\!\!\right] = \left[\!\!\left[\Gamma_{z\phi}\frac{\partial f}{\partial \phi} \right]\!\!\right] - \left[\!\!\left[\frac{\partial \Gamma_{rz}}{\partial r} f \right]\!\!\right], \tag{2.3.15e}$$

$$[\![\tau_{rr}]\!] = \left[\!\!\left[-p + 2\widehat{\eta}\frac{\partial u}{\partial r} \right]\!\!\right] = \left[f + \frac{\partial^2 f}{\partial z^2} + \frac{\partial^2 f}{\partial \phi^2} \right]. \tag{2.3.15f}$$

Note that the jump in (2.3.15c) and the second term in the right-hand side of (2.3.15e) were forgotten to include by Frischknecht (1998). The present correction gives noticeable results for the range of ratios of viscosities above which the thread is stable, as we will discuss in the next section. In terms of the components of the expansions (2.3.12), (2.3.15) reads

$$[\![u_m]\!] = 0, \tag{2.3.16a}$$

$$[\![v_m]\!] = 0, \tag{2.3.16b}$$

$$[\![w_m]\!] = \mathrm{Ca}\frac{\mu - 1}{\mu + 1}\left(\varepsilon_{m-1} - \varepsilon_{m+1} \right), \tag{2.3.16c}$$

$$\left[\!\!\left[\widehat{\eta}\left(m u_m - \frac{\partial v_m}{\partial r} + v_m \right) \right]\!\!\right] = k\mathrm{Ca}\frac{\mu - 1}{\mu + 1}\left(\varepsilon_{m-1} + \varepsilon_{m+1} \right), \tag{2.3.16d}$$

$$\left[\!\!\left[\widehat{\eta}\left(k u_m - \frac{\partial w_m}{\partial r} \right) \right]\!\!\right] = m\mathrm{Ca}\frac{\mu - 1}{\mu + 1}\left(\varepsilon_{m-1} + \varepsilon_{m+1} \right), \tag{2.3.16e}$$

$$\left[\!\!\left[-p_m + 2\widehat{\eta}\frac{\partial u_m}{\partial r} \right]\!\!\right] = (1 - k^2 - m^2)\varepsilon_m. \tag{2.3.16f}$$

Next, we consider the evolution in time of the perturbation amplitude $\varepsilon_m(t)$. At the perturbed interface $R(\phi, z, t)$, the radial velocity is the material derivative (DR/Dt) following a thread particle (see (2.1.19)). Since at the interface $\mathbf{V}^d = (0, 0, W^d)$, we obtain from (2.1.19) (with $\mathbf{u}^d = W^d\mathbf{e}_z + \epsilon\ (u^d\mathbf{e}_r + v^d\mathbf{e}_\phi + w^d\mathbf{e}_z)$)

$$\epsilon\ u^d = \frac{\partial R}{\partial t} + \epsilon\ v^d\frac{\partial R}{\partial \phi} + (W^d + \epsilon\ w^d)\frac{\partial R}{\partial z}. \tag{2.3.17}$$

Using (2.1.2) and (2.3.1) for R and (2.3.12b) for u^d in (2.3.17), we obtain for the term linear in ϵ,

$$\sum_{m=-\infty}^{\infty} u_m^d e^{i(m\phi+kz)} = \sum_{m=-\infty}^{\infty} \frac{d\varepsilon_m}{dt} e^{i(m\phi+kz)} + ikW^d \sum_{m=-\infty}^{\infty} \varepsilon_m e^{i(m\phi+kz)} \ . \tag{2.3.18}$$

Now, W^d is given by the first equation of (2.3.8), however with the restriction that we have to take the real part of this. This yields, for $r = 1$,

$$W^d = -i\frac{\mathrm{Ca}}{\mu+1}\left(e^{i\phi} - e^{-i\phi}\right) . \tag{2.3.19}$$

Substituting this into (2.3.18), rearranging terms in the last term, and equating equal powers of $e^{i\phi}$, we arrive at

$$\frac{d}{dt}\varepsilon_m(t) = u_m^d - \frac{k\mathrm{Ca}}{\mu+1}\left(\varepsilon_{m-1} - \varepsilon_{m+1}\right), \quad \text{for } m \in (-\infty, \infty). \tag{2.3.20}$$

In practice, the series (2.3.1) is cut off at a finite length, $2M + 1$ say. So, we have terms from $m = -M$ to $m = M$. Note that in order to satisfy the boundary conditions (2.3.16c)-(2.3.16e), the solution must be cut off one order higher, i.e. at $m = M + 1$.

2.3.2 Stability analysis

Equations (2.3.20) contain the information about the time evolution of the initial perturbation. In this section, we shall work this out for several cases. First, we take the cut off value M equal to $M = 0$. This corresponds to the case that the cross-sections of the thread are always perfectly circular. This inevitably implies that this case can not incorporate the effect of the shear flow. We only report this case in order to compare the present approach with results in literature. The emphasis is on the $M = 1$ case, for which the shear flow is really relevant.

2.3.2.1 The $M = 0$ case

In this case, $\varepsilon_0 \neq 0$ and $\varepsilon_m = 0$ for $m = \pm1, \pm2, \cdots$. From (2.3.20), the amplitude $\varepsilon_0(t)$ evolves according to

$$\frac{d}{dt}\varepsilon_0(t) = u_0^d. \tag{2.3.21}$$

Evaluating (2.3.16), we arrive at

$$\mathbf{Mz} \equiv \begin{pmatrix} \mathbf{M}_{-1} & \mathbf{0} & \mathbf{0} \\ \mathbf{0} & \mathbf{M}_0 & \mathbf{0} \\ \mathbf{0} & \mathbf{0} & \mathbf{M}_1 \end{pmatrix} \begin{pmatrix} \mathbf{z}_{-1} \\ \mathbf{z}_0 \\ \mathbf{z}_1 \end{pmatrix} = \begin{pmatrix} \mathbf{e}_{-1} \\ \mathbf{e}_0 \\ \mathbf{e}_1 \end{pmatrix} . \tag{2.3.22}$$

For simplicity, we shall write $\mathbf{M}$ as a diagonal block matrix; $\mathbf{M} = \mathrm{diag}(\mathbf{M}_{-1}, \mathbf{M}_0, \mathbf{M}_1)$. Thus, we may solve the equation via

$$\mathbf{M}_m\mathbf{z}_m = \mathbf{e}_m, \ m = -1, 0, 1. \tag{2.3.23}$$

Here, $\mathbf{z}_m = (A_m, B_m, C_m, D_m, E_m, F_m)^T$, $m = -1, 0, 1$, and

$$\mathbf{e}_{-1} = \left(0, 0, -\mathrm{Ca}\frac{\mu-1}{\mu+1}\varepsilon_0, k\mathrm{Ca}\frac{\mu-1}{\mu+1}\varepsilon_0, -\mathrm{Ca}\frac{\mu-1}{\mu+1}\varepsilon_0, 0\right)^T, \tag{2.3.24a}$$

$$\mathbf{e}_0 = \left(0, 0, 0, 0, 0, (1-k^2)\varepsilon_0\right)^T, \tag{2.3.24b}$$

$$\mathbf{e}_1 = \left(0, 0, \mathrm{Ca}\frac{\mu-1}{\mu+1}\varepsilon_0, k\mathrm{Ca}\frac{\mu-1}{\mu+1}\varepsilon_0, \mathrm{Ca}\frac{\mu-1}{\mu+1}\varepsilon_0, 0\right)^T. \tag{2.3.24c}$$

Expressions for $\mathbf{M}_m$ are given in Appendix B.2. Since u_0^d only depends on A_0 and B_0 (see (2.2.17b)) we may solve these coefficients from (2.3.22) by only considering

$$\mathbf{M}_0\mathbf{z}_0 = \mathbf{e}_0. \tag{2.3.25}$$

Note that from the second and the fourth row of (2.3.25) we directly obtain $C_0 = 0 = F_0$. Thus, (2.3.25) is now the same as (2.2.24) in Section 2.2.2.1, and the results have already been shown in Figure 2.2.

2.3.2.2 The $M = 1$ case

Here, we take $\varepsilon_m \neq 0$, for $m = -1, 0, 1$. Equations (2.3.20) give

$$\frac{d}{dt}\varepsilon_{-1}(t) = u_{-1}^d + \frac{k\mathrm{Ca}}{\mu+1}\varepsilon_0(t), \tag{2.3.26a}$$

$$\frac{d}{dt}\varepsilon_0(t) = u_0^d - \frac{k\mathrm{Ca}}{\mu+1}\Big(\varepsilon_{-1}(t) - \varepsilon_1(t)\Big), \tag{2.3.26b}$$

$$\frac{d}{dt}\varepsilon_1(t) = u_1^d - \frac{k\mathrm{Ca}}{\mu+1}\varepsilon_0(t). \tag{2.3.26c}$$

Evaluation of the boundary conditions leads to (2.3.23) with $m = -2, \cdots, 2$. Expressions for u_{-1}^d, u_0^d and u_1^d are given in (2.2.17b) and (2.2.17c), while the coefficients in it follow from

$$\mathbf{M}_m\mathbf{z}_m = \mathbf{e}_m, \;\; m = -1, 0, 1, \tag{2.3.27}$$

with $\mathbf{z}_m = (A_m, B_m, C_m, D_m, E_m, F_m)^T$ and

$$\mathbf{e}_{-1} = \left(0, 0, -\mathrm{Ca}\frac{\mu-1}{\mu+1}\varepsilon_0, k\mathrm{Ca}\frac{\mu-1}{\mu+1}\varepsilon_0, -\mathrm{Ca}\frac{\mu-1}{\mu+1}\varepsilon_0, -k^2\varepsilon_{-1}\right)^T, \tag{2.3.28a}$$

$$\mathbf{e}_0 = \left(0, 0, \mathrm{Ca}(\mu-1)(\varepsilon_{-1}-\varepsilon_1)/(\mu+1), k\mathrm{Ca}(\mu-1)(\varepsilon_{-1}+\varepsilon_1)/(\mu+1), 0, (1-k^2)\varepsilon_0\right)^T, \tag{2.3.28b}$$

$$\mathbf{e}_1 = \left(0, 0, \mathrm{Ca}\frac{\mu-1}{\mu+1}\varepsilon_0, k\mathrm{Ca}\frac{\mu-1}{\mu+1}\varepsilon_0, \mathrm{Ca}\frac{\mu-1}{\mu+1}\varepsilon_0, -k^2\varepsilon_1\right)^T. \tag{2.3.28c}$$

In (2.3.27) we wrote down the equation only for $m = -1, 0$ and 1, since the evolution equation (2.3.26) only contains $\varepsilon_{-1}, \varepsilon_0$ and ε_1. The analogon of (2.2.23) reads here

$$\frac{d\mathbf{y}}{dt} = \mathbf{Q}(k, \mu, \mathrm{Ca})\mathbf{y}, \qquad \mathbf{Q} \equiv \begin{pmatrix} q_{11} & q_{12} & 0 \\ q_{21} & q_{22} & q_{23} \\ 0 & q_{32} & q_{33} \end{pmatrix} \tag{2.3.29}$$

where $\mathbf{y} \equiv (\varepsilon_{-1}(t), \varepsilon_0(t), \varepsilon_1(t))^T$, while the q_{ij}'s are given in Appendix B.2. Note that the q_{ij}'s are real. They generally depend on k, μ and Ca, but the diagonal elements of $\mathbf{Q}$ are independent of Ca. The presence of the shear flow leads to a coupling of modes via the non-diagonal elements. The behaviour of the solution of (2.3.29) depends on the sign of the real parts of the eigenvalues of the matrix $\mathbf{Q}$. If all eigenvalues have negative real parts, the unperturbed solution is stable. If at least one of the eigenvalues has a positive real part, the unperturbed solution is unstable. Let q be an eigenvalue of $\mathbf{Q}$, satisfying the equation

$$q^3 + a_1 q^2 + a_2 q + a_3 = 0, \tag{2.3.30}$$

where the coefficients a_j are real. Note that the a_j depend on k, μ and Ca. Expressions for a_j in terms of q_{ij} are written out in Appendix B.2. To find the necessary and sufficient conditions for the coefficients a_j in order for all roots of (2.3.30) to have negative real parts, we will use *Hurwitz's criterion*. This criterion says that all roots of the third-order algebraic equation (2.3.30) have negative real parts, if and only if (see Merkin (1997))

$$a_1 > 0, \quad a_2 > 0, \quad a_3 > 0, \quad a_4 = a_1 a_2 - a_3 > 0. \tag{2.3.31}$$

If one of the inequalities in (2.3.31) is reversed, then at least one of the roots of equation (2.3.30) will have positive real part, and this is an indication of instability of the system. For fixed values μ and Ca, we should realize that the inequalities (2.3.31) must hold for *all* wave numbers k.

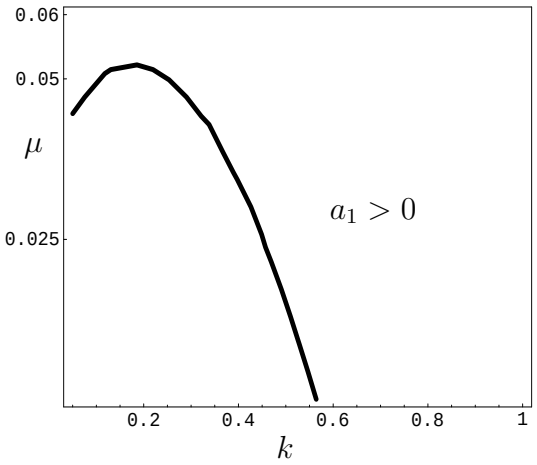

Figure 2.7: *Curve defined by the relation $a_1(k, \mu) = 0$ in the (k, μ) plane.*

Next, we shall use (2.3.31) to determine a critical value of Ca, denoted by Ca_{cr}, above which the thread is stable. Since a_1 in (2.3.30) is only determined by the diagonal

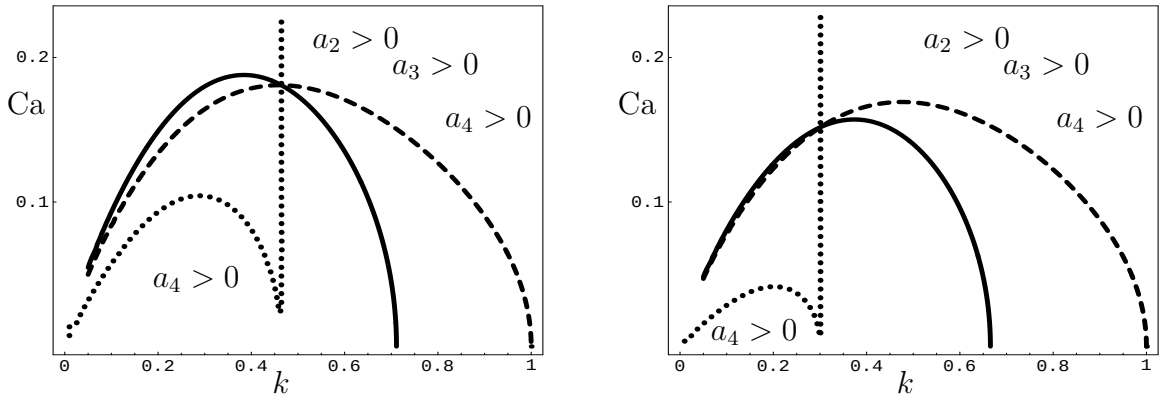

(a) $\mu = 0.1$. (b) $\mu = 0.15$.

Figure 2.8: *Curves defined by the relations* $a_2(k, \mu, \mathrm{Ca}) = 0$ *(solid line),* $a_3(k, \mu, \mathrm{Ca}) = 0$ *(dashed line), and* $a_4(k, \mu, \mathrm{Ca}) = 0$ *(dotted line) in the* (k, Ca) *plane for two values of* μ*.*

elements of the matrix $\mathbf{Q}$ (see Appendix B.2), it does not depend on Ca: $a_1 = a_1(k, \mu)$. By equating $a_1(k, \mu) = 0$, we obtain the curve of μ as a function of k shown in Figure 2.7. Below this curve, $a_1(k, \mu) < 0$, and above it $a_1(k, \mu) > 0$. Here and in the sequel, it should be understood that the curve is the border between the regions of positive and the negative values for the coefficients (here a_1). Figure 2.7 shows that the curve has a maximum value at $\mu_a \approx 0.05$. If $\mu < \mu_a$, then there exist values for k for which $a_1(k, \mu) < 0$. This indicates that the perturbed thread is unstable. If $\mu > \mu_a$, then the perturbed thread may be stabilized by the imposed shear flow. To investigate this, we should also check the other coefficients, a_2, a_3 and a_4; the results are shown in Figure 2.8. These Figures show the curves $a_i(k, \mu, \mathrm{Ca}) = 0$, for $i = 2, 3, 4$, for fixed value of μ, yielding Ca as a function of k for two different values of μ, $\mu = 0.1$ and $\mu = 0.15$. Part (a) shows that the curves $a_2 = 0$ and $a_3 = 0$ cross each other at some value of k, at $k = k_s$

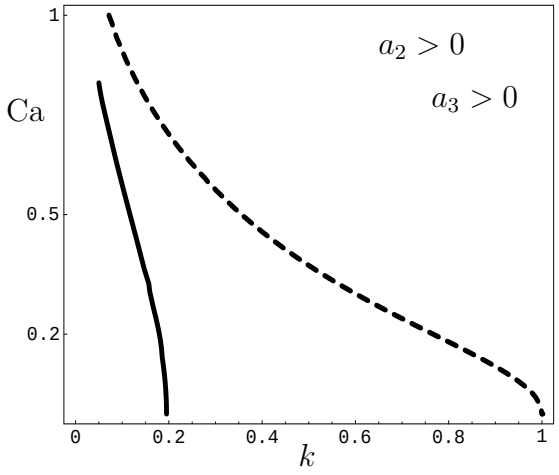

Figure 2.9: *Same information as in Figure 2.8, but now for* $\mu = 3.0$*.*

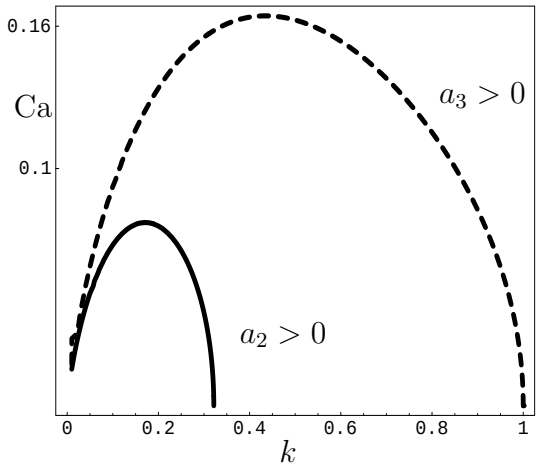

Figure 2.10: *Same information as in Figure 2.8, but now for* $\mu = 1$.

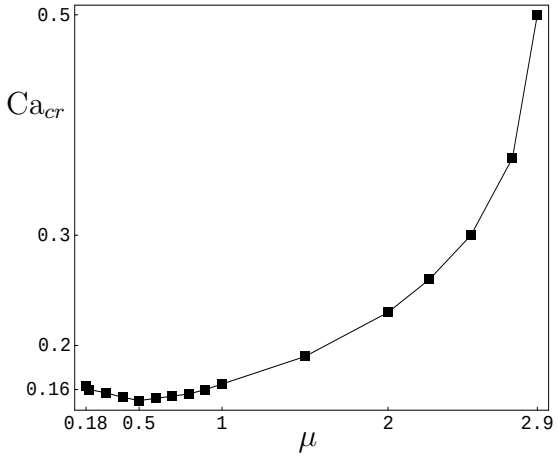

Figure 2.11: *Critical capillary number* Ca_{cr} *as a function of the ratio of viscosities* μ.

say. Thus, $a_2(k_s, 0.1, \mathrm{Ca}) = 0 = a_3(k_s, 0.1, \mathrm{Ca})$. Substituting these values into (2.3.31), we see that also $a_4(k_s, 0.1, \mathrm{Ca}) = 0$, and this curve is drawn as a vertical line in Figure 2.8. In this case, no critical value for Ca above which the thread is stable exists, since there are for every value of Ca always values of k for which one or more of the coefficients a_2, a_3 or a_4 becomes negative. If μ increases, k_s decreases; see Figure 2.8(b). Thus, the window of k on the left in the graphs of Figure 2.8, in which $a_4 < 0$ becomes narrower. However, increasing μ too far we again obtain instability as shown in Figure 2.9. From this figure, we see that at the left a small window of k is always present for which the coefficients a_2 and a_3 have negative values. From more detailed calculations we find that no instability will occur for μ such that $0.18 \leq \mu \leq 2.9$. If μ is outside this range, instability appears. This range is larger than the range found by Frischknecht (1998) ($0.8 \leq \mu \leq 1.0$), due to the correction in the derivation of the boundary conditions we found, as mentioned in Section 2.3.1.2. Hence, for $0.18 \leq \mu \leq 2.9$ we can determine a critical Capillary number Ca_{cr}, as we shall show next. Note that for this range the

values of a_4 are always positive for all k's. As an illustration, we investigate the system for which the fluids have no viscosity difference, so $\mu = 1$. Figure 2.10 shows the curves $a_2 = 0$ and $a_3 = 0$, giving Ca as a function of k for $\mu = 1$. The solid and the dashed curves depict the values of $a_2 = 0$ and $a_3 = 0$, respectively. We find a critical value of Ca, $\mathrm{Ca}_{cr} \approx 0.16$, above which the thread will be stable at all wave number k's. Figure 2.11 shows the critical capillary number Ca_{cr} as a function of the ratio of the viscosities μ. We see that Ca_{cr} has a minimum near $\mu = 0.5$. So, if the viscosity of the thread is about half the viscosity of the surrounding medium, high stresses are needed to stabilize the thread.

In general, we must include the higher-order mode perturbations into the calculations in order to ensure convergence of the truncated system. The more higher modes, the bigger the size of the matrix $\mathbf{Q}$ in (2.3.29) and calculations may become cumbersome. However, we may estimate the number of modes that gives reliable results as follows. In the absence of the external flow, the matrix $\mathbf{Q}$ becomes diagonal. The only mode that gives instability is the axisymmetric mode; see Section 2.2. From (2.3.20), we see that since the boundary conditions (2.3.16) are proportional to Ca, the off-diagonal elements of $\mathbf{Q}$ are all proportional to Ca. The presence of shear flow leads to a coupling of modes via this off-diagonal. Thus, we only need to include modes whose damping rates are less than or of the order of the applied shear rate. Formula (2.2.34) gives a description of the damping rates of high m modes.

2.3.3 Critical capillary number for $\mu = 1$

If the fluids have equal viscosities, i.e. $\mu = 1$, the only non-vanishing interfacial condition is the condition for the normal stress (2.3.16f). The jump in the normal stress across the interface can now be incorporated by introducing it as a discrete hoop force S,

$$S = \sum_{m=-\infty}^{\infty} (1 - k^2 - m^2)\varepsilon_m(t)e^{i(m\phi+kz)}, \tag{2.3.32}$$

acting only on the interfacial surface $r = 1$. This way, the governing equations can be declared to hold in the whole space (for every $r \in [0, \infty)$), where S is introduced as a body force characterized by a Dirac delta function $\delta(r-a)$. The perturbed state is then governed by, for $r \geq 0$,

$$0 = \text{div } \mathbf{v} \ , \tag{2.3.33a}$$

$$\text{grad } p = \widehat{\eta} \text{ div } (\text{grad } \mathbf{v})^T + \mathbf{e}_r\delta(r-a)S \ . \tag{2.3.33b}$$

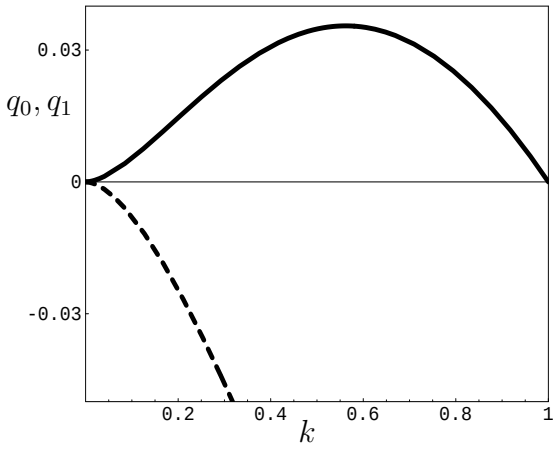

Figure 2.12: *Curves of q_0 (solid line) and q_1 (dashed line) as functions of k, for $\mu = 1$.*

The detailed derivation of the solution of (2.3.33) is postponed to Section 4.3; here we only present the result. The solution for the radial velocity reads

$$\begin{aligned} u_m &= \frac{(1-k^2-m^2)\varepsilon_m}{4}\left[\int_0^\infty \frac{s^3+2k^2s}{(s^2+k^2)^2}\Big(J_{m+1}(s)J_{m+1}(sr)+J_{m-1}(s)J_{m-1}(sr)\Big)ds\right. \\ &\quad \left. + \int_0^\infty \frac{s^3}{(s^2+k^2)^2}\Big(J_{m-1}(s)J_{m+1}(sr)+J_{m+1}(s)J_{m-1}(sr)\Big)ds\right], \end{aligned} \tag{2.3.34}$$

and we obtain for $r > 1$

$$\begin{aligned} u_m &= \frac{(1-k^2-m^2)}{4}\varepsilon_m\left[\frac{1}{2k}\frac{d}{dk}\left[k^2\Big(I_{m+1}(k)K_{m+1}(kr)+I_{m-1}(k)K_{m-1}(kr)\Big)\right]\right. \\ &\quad -k\frac{d}{dk}\Big[I_{m+1}(k)K_{m+1}(kr)+I_{m-1}(k)K_{m-1}(kr)\Big] \\ &\quad \left.-\frac{1}{2k}\frac{d}{dk}\left[k^2\Big(I_{m-1}(k)K_{m+1}(kr)+I_{m+1}(k)K_{m-1}(kr)\Big)\right]\right]. \end{aligned} \tag{2.3.35}$$

Let us consider the evolution equation (2.3.29). For $\mu = 1$, the matrix $\mathbf{Q}$ becomes

$$\mathbf{Q} \equiv \begin{pmatrix} q_1 & \frac{k\mathrm{Ca}}{2} & 0 \\ -\frac{k\mathrm{Ca}}{2} & q_0 & \frac{k\mathrm{Ca}}{2} \\ 0 & -\frac{k\mathrm{Ca}}{2} & q_1 \end{pmatrix}, \tag{2.3.36}$$

where $q_m = u_m(r=1)/\varepsilon_m$, as given by (2.3.35). In (2.3.36), we have used that $q_{-1} = q_1$. Figure 2.12 shows the curves of q_0 and q_1 as functions of k, for $0 \le k \le 1$. Note that the values of q_0 are positive, while the values of q_1 are negative.

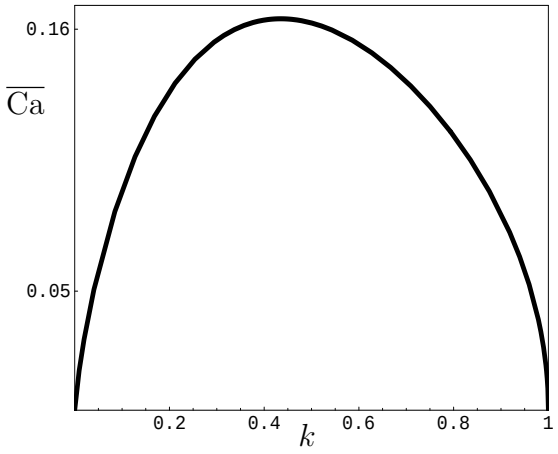

Figure 2.13: *Curve of* $\overline{\mathrm{Ca}}$ *as a function of* k*, for* $\mu = 1$*. The maximum value of* $\overline{\mathrm{Ca}}$ *indicates the critical capillary number* Ca_{cr}*.*

Let us denote the modulus of q_m by $|q_m|$, $m = 0, 1$. The eigenvalues of (2.3.36) satisfy equation (2.3.30), where the constants are given by

$$a_1 = 2|q_1| - |q_0|, \tag{2.3.37a}$$

$$a_2 = |q_1|^2 - |q_0 q_1| + \left(\frac{k^2\mathrm{Ca}^2}{2} - |q_0 q_1|\right), \tag{2.3.37b}$$

$$a_3 = |q_1|\left(\frac{k^2\mathrm{Ca}^2}{2} - |q_0 q_1|\right). \tag{2.3.37c}$$

From Figure 2.12, we see that $|q_1| > |q_0|$. So, the coefficients a_m $(m = 1, 2, 3)$ will be positive if and only if the term inside the brackets is positive, that is if

$$\frac{k^2\mathrm{Ca}^2}{2} - |q_0 q_1| > 0. \tag{2.3.38}$$

Using that $a_4 = a_1 a_2 - a_3$, we find with (2.3.37) that

$$a_4 = \left(2|q_1| - |q_0|\right)\left(|q_1|^2 - |q_0 q_1|\right) + \left(|q_1| - |q_0|\right)\left(\frac{k^2\mathrm{Ca}^2}{2} - |q_0 q_1|\right) > 0, \tag{2.3.39}$$

provided that (2.3.38) holds. Thus, we may define the critical capillary number Ca_{cr} as,

$$\mathrm{Ca}_{cr} = \max_{0<k<1}\left\{\frac{\sqrt{2|q_0 q_1|}}{k}\right\}. \tag{2.3.40}$$

Let us define $\overline{\mathrm{Ca}}(k) = \sqrt{2|q_0 q_1|}/k$. Figure 2.13 shows the curve of $\overline{\mathrm{Ca}}$ as a function of k. The maximum value of $\overline{\mathrm{Ca}}$ gives the critical capillary number Ca_{cr}. For this special case, we find $\mathrm{Ca}_{cr} \approx 0.164$.

To conclude, we remark that the three coefficients a_m, $m = 1, 2, 3$, are all positive if $\mathrm{Ca} > \mathrm{Ca}_{cr}$, i.e. for sufficiently large shear rate. This means that a thread immersed in a fluid with the same viscosity, that is loaded by a constant shear rate at infinity, is stable for shear rates such that $\mathrm{Ca} > \mathrm{Ca}_{cr}$.

2.4 Conclusions

In this chapter, we have investigated the stability of one Newtonian thread immersed in a Newtonian fluid. First, we have derived the mathematical model including the boundary conditions. The fluids were assumed to be incompressible and so viscous, that the system is governed by the Stokes equations. The thread was perturbed by small random perturbations. The stability of the system was characterized by its growth rate, i.e. the rate at which the most unstable perturbation mode grows. Next, we studied the stability of the system for two types of driving forces: first, pure surface tension, and second, surface tension together with shear flow.

For the stability due to surface tension only, it turned out that the thread is always unstable since the axisymmetric mode grows in time. We found that the maximum instability, i.e. the maximum value of the growth rate, always occurs at a definite value of the wave number k of the perturbation mode, indicating that drops of definite size will be formed. The wave number of the perturbation mode corresponding to the maximum instability decreases as the viscosity ratio tends to zero or to infinity. For the special case that the thread deforms uniformly in the axial direction, i.e. $k = 0$, we have analytically calculated the growth rates of the higher modes ($m \geq 2$). The higher the mode, the greater the damping rate.

For the stability in the presence of shear flow, we have solved the equations for the unperturbed and perturbed state. The unperturbed state was described by a Couette-like problem. Here, an important parameter called the capillary number Ca has been introduced. This number indicates the magnitude of the applied shear. The perturbed state was governed by the Stokes equations. We have solved the equations by means of complex Fourier expansions and shown how the equation for the growth rate leads to an eigenvalue problem. The stability was investigated by use of *Hurwitz's* criterion. We found that the shear flow stabilizes the thread only for $0.18 \leq \mu \leq 2.9$, and only if the applied shear stress is high enough.

The results for the stability in the presence of the shear flow presented here may also shed light on the stability of the "narrower string" observed by Migler (2001), who proposed that the string is stabilized by shear flow, as mentioned in Section 1.1.

Chapter 3

Stability of two Newtonian threads

In this Chapter, we extend the analysis derived in Section 2 and consider the stability of two adjacent parallel immersed threads, under the action of both surface tension and viscous forces. The system is governed by the Stokes equations which are solved by means of separation of variables in two systems of cylindrical coordinates, each one connected to one of the threads. In this, the dependence on the azimuthal directions is written in the form of Fourier expansions. Substitution of the general solution into the boundary conditions yields an infinite set of linear equations for the unknown coefficients. This set is solved using the method of moments. Next, the instability (the growth rate) of initial disturbances is investigated. If an initial disturbance increases in time, the initial state is unstable resulting in breaking-up. Here, the instability of the threads is examined based on both a zero-order and a first-order Fourier expansion. The zero-order analysis follows the lines presented in Knops (1997), but avoids some unreliable assumptions. This refinement leads to expressions that are simpler to evaluate. The model confirms that the break-up can indeed occur in-phase as well as out-of-phase. This depends on the viscosity ratio of the two fluids and on the distance between the threads. All this is in correspondence with experimental observations. In an analogous way the first-order expansion is evaluated. The results show that the zero-order solution is already quite reliable to describe the essential features.

3.1 Mathematical formulation

Consider two infinitely long parallel threads, both with radius a and viscosity η^d, which are surrounded by a viscous fluid with viscosity η^c. We denote the ratio of the viscosities by $\mu = \eta^d/\eta^c$, as in (2.1.1). Let b be the distance between the two centers of the threads. In Figure 3.1 an axial cross-section is sketched. The indices 1 and 2 refer to thread 1 and thread 2, respectively. Two cylindrical coordinate systems will be used, (r_1, ϕ_1, z_1) centered along the axis of thread 1, (r_2, ϕ_2, z_2) centered along the axis of thread 2. If thread J $(J = 1, 2)$ is taken as frame of reference, we have the relations, for $j, J \in \{1, 2\}$,

$$\begin{aligned} r_J \cos\phi_J &= (j - J)b + r_j \cos\phi_j, \\ r_J \sin\phi_J &= r_j \sin\phi_j, \\ z_J &= z_j. \end{aligned} \tag{3.1.1}$$

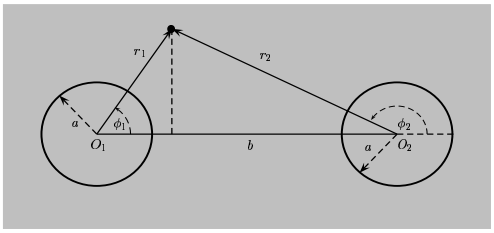

Figure 3.1: *Axial cross-section of the two threads and the corresponding two cylindrical coordinate systems.*

Next, let us consider the thread surfaces. If the perturbations are still small, the threads are close to cylinders. The disturbed radii are written as a sum of modes, that are periodic in z with wave number k, and periodic in ϕ. The dependence on ϕ is written as a Fourier expansion. Thus, the perturbed surface R_j of thread j ($j = 1, 2$) is represented by

$$R_j(\phi_j, z, t) = a\left[1 + \epsilon\left(\sum_{m=0}^{\infty} \varepsilon_{j,m}(t) \cos m\phi_j\right) \cos(k_j z - \alpha_j)\right]. \tag{3.1.2}$$

Since z_1 and z_2 are identical, we dropped the index in the z-coordinates. Here, ϵ is a small parameter ($0 < \epsilon \ll 1$), $\varepsilon_{j,m}$ is the time dependent amplitude of mode m at thread j, and α_j is the phase of the mode. Since only phase differences are important, we may take $\alpha_1 = 0$ and $\alpha_2 = \alpha$. The parameter α is unknown in advance.

The fluids are assumed to be Newtonian, incompressible and so viscous that the system is governed by Stokes equations (2.2.2). The equations are brought into dimensionless form by use of (2.2.4), i.e. the distance, velocity, and stress components are made dimensionless by means of a, σ/η^c, and σ/a, respectively, where σ is the surface tension. Let us first consider the solution if only one thread J ($J = 1$ or 2) is present. We propose as general expressions for the solution the expansions as in (2.2.5), for instance, we have

$$p_J(r_J, \phi_J, z, t) = \sum_{m=0}^{\infty} p_{J,m}(r_J, t) \cos m\phi_J \cos(k_J z - \alpha_J). \tag{3.1.3}$$

Substitution of the expansions into the equations yields similar coefficients as in (2.2.17) and (2.2.18). For example, for $r_J < 1$ we obtain,

$$p^d_{J,m}(r_J, t) = 2\mu A_{J,m} I_m(k_J r_J), \tag{3.1.4}$$

and for $r_J > 1$,

$$p^c_{J,m}(r, t) = 2D_{J,m} K_m(k_J r_J). \tag{3.1.5}$$

Next, we consider the solution for the continuous phase when the two threads are present. The solution for the continuous phase is influenced by both threads. As an ansatz, we represent the solution outside the threads by a linear combination of expansions like the one in (3.1.3) written with respect to both threads. This linear combination automatically satisfies the Stokes equations. Its coefficients follow from the application

of the boundary conditions around each thread. The addition of the velocities (u_j, v_j, w_j) is done vectorially, while the scalar quantities p_j are simply added. The resulting sums could be represented in any of the cylindrical coordinate systems of the two threads. Taking for this thread J and indicating this with subscript (J), we obtain the representations

$$p^c_{(J)} = \sum_{j=1}^{2} p^c_j, \tag{3.1.6a}$$

$$u^c_{(J)} = \sum_{j=1}^{2} \Big[u^c_j \cos(\phi_J - \phi_j) + v^c_j \sin(\phi_J - \phi_j) \Big], \tag{3.1.6b}$$

$$v^c_{(J)} = \sum_{j=1}^{2} \Big[-u^c_j \sin(\phi_J - \phi_j) + v^c_j \cos(\phi_J - \phi_j) \Big], \tag{3.1.6c}$$

$$w^c_{(J)} = \sum_{j=1}^{2} w^c_j. \tag{3.1.6d}$$

Now, let us consider the boundary conditions at the interface of thread J. We apply the boundary conditions derived in Section 2.1.2, but now we add an index J to indicate that the evaluation is applied at the surface of thread J, for example,

$$[\![u]\!]_1 = u^d_1 - u^c_{(1)} = 0, \tag{3.1.7}$$

to denote the continuity of the radial velocity around thread 1. Evaluating the boundary conditions, we obtain an infinite set of equations for the unknown coefficients. We shall obtain approximate solutions by using the method of moments (see Harrington (1993)). Let us outline the procedure:

- First, we truncate the expansions (in (3.1.3), etc.) at some cut-off value M, i.e. we take into account
$$2 \times (4 + 6M) = 8 + 12M \tag{3.1.8}$$
unknowns and ignore the other ones. Except for $M = 0$ each order contains 12 unknowns (the expressions for $M = 0$ do not contain $C_{j,0}$ and $F_{j,0}$, and therefore for $M = 0$ we only have 8 unknowns).

- Second, we solve the unknowns by means of the boundary conditions at the two interfaces. Using a linear theory, the boundary conditions ((3.1.7), etc.) have to be evaluated at the interface S_J given by $r_J = 1$ for $J = 1, 2$. In these conditions, we have to evaluate all quantities at S_J in terms of ϕ_J: at the interface between thread 1 and the continuous phase, the quantities of the continuous phase should be expressed in a Fourier expansion of ϕ_1 only, whereas at the interface between thread 2 and the continuous phase it is the other way around. This implies that the product of a Bessel function and a Fourier expansion with respect to thread

2 should be expressed as a product of Bessel functions and a Fourier expansion with respect to thread 1 or the other way around. To handle this, we use the geometrical relations (3.1.1), and Graf's addition theorem of Bessel functions (see, for example, Watson (1966)). This theorem states that for $r_1 < b$,

$$K_n(kr_2)\cos n\phi_2 = (-1)^n \sum_{m=-\infty}^{\infty} K_{n+m}(kb) I_m(kr_1)\cos m\phi_1. \tag{3.1.9}$$

This relation also holds with cos replaced by sin and at the same time $(-1)^n$ replaced by $(-1)^{n+1}$. Applying (3.1.1) and (3.1.9), we find that the boundary conditions at S_1 are now functions of r_1 and ϕ_1 containing terms with $\cos m\phi_1$ or $\sin m\phi_1$. The jump $[\![G]\!]_1$, with G representing one of the quantities $u, v, w, \pi_{\phi r}, \pi_{zr}$, and π_{rr}, now takes the form

$$[\![G]\!]_1 = \sum_{m=0}^{\infty} [\![G_m]\!]_1 f_m(\phi_1), \tag{3.1.10}$$

where $f_m(\phi_1)$ is either $\cos m\phi_1$ or $\sin m\phi_1$, depending on whether G is odd (e.g. in case of $v, \pi_{\phi r}$) or even in ϕ_1. In principle, boundary conditions (3.1.7), etc., must be satisfied *for every value of* ϕ_1, which results in an infinite number of equations. To make the problem tractable, we will not require point-wise satisfaction of the boundary conditions, but instead we require that the m-th order moments, with $m \in [0, 1, \cdots, M]$, of the boundary conditions are satisfied. Here, the m-th order moment of $[\![G]\!]_1$ is defined as

$$\mathcal{M}_m\{[\![G]\!]_1\} = \int_0^{2\pi} [\![G]\!]_1 f_m(\phi_1) d\phi_1. \tag{3.1.11}$$

By taking the first $M+1$ moments of the boundary conditions (8 conditions for $M = 0$ and 12 conditions for every m with $1 \le m \le M$), we thus obtain $(8+12M)$ equations and unknowns. Hence, in this way we obtain a finite set of equations for the unknown coefficients.

To illustrate and clarify the procedure, we work it out for two cases in the next section.

3.2 Solutions for $M = 0$ and $M = 1$

In this section, we address the evaluation of the boundary conditions for the cases $M = 0$, the so-called zero-order solution, and $M = 1$, the so-called first-order solution. From this, the generalization of the procedure to higher orders will become clear. Throughout this section, thread 1 will be taken as the frame of reference.

In the case $M = 0$ we have 8 unknowns. Then, we do not need boundary conditions for v and $\pi_{r\phi}$. From (2.2.5c) we see that v_1 is identically zero. This is not so for $v^c_{(1)}$, as follows from (3.1.6c). However, $v^c_{(1)}$ is an odd function in ϕ_1, and consequently the zero-moment is zero. The same holds for $\pi_{r\phi}$.

The evaluation of boundary conditions at the interface S_1 requires that all quantities are expressed in terms of (r_1, ϕ_1). As an example, we will work this out for the continuity of radial velocity. From $[\![u]\!]_1 = u_1^d - u_{(1)}^c = 0$, we obtain the condition

$$X(t)\cos(k_1 z) - \Big[Y(r_2, \phi_1, \phi_2, t)\Big]_{r_1=1} \cos(k_2 z - \alpha) = 0, \tag{3.2.1}$$

where

$$\begin{aligned} X(t) \;=\; & \left(I_0(k_1) - \frac{2}{k_1} I_1(k_1)\right) A_{1,0}(t) - I_1(k_1) B_{1,0}(t) \\ & - \left(K_0(k_1) + \frac{2}{k_1} K_1(k_1)\right) D_{1,0}(t) - K_1(k_1) E_{1,0}(t), \end{aligned} \tag{3.2.2}$$

and

$$\begin{aligned} Y(r_2, \phi_1, \phi_2, t) = \Bigg[& \left(r_2 K_0(k_2 r_2) + \frac{2}{k_2} K_1(k_2 r_2)\right) D_{2,0}(t) \\ & + E_{2,0}(t) K_1(k_2 r_2) \Bigg] \cos(\phi_1 - \phi_2) \ , \end{aligned} \tag{3.2.3}$$

while the $A.$, $B.$, $D.$ and $E.$ are still unknown coefficients. We remind that for convenience we have taken $\alpha_1 = 0$ and $\alpha_2 = \alpha$. In (3.2.1), the important point is that neither X nor Y depends on z. Since (3.2.1) must be satisfied for all $z \in \mathbb{R}$, we conclude that the wave numbers k_1 and k_2 must be the same, so $k_1 = k_2 = k$. Moreover, the phase α may attain only the values 0 or π. If $\alpha = 0$, thread 2 breaks up in-phase with thread 1, whereas for $\alpha = \pi$ thread 2 breaks up out-of-phase with thread 1. We remark that varying the values of α leads to various *phase patterns*. We code a pattern by the vector

$$\mathbf{s}_n = (s_{n,1}, s_{n,2})^T, \text{ with } s_{n,j} = \pm 1 \text{ for } \begin{cases} j = 1, 2 \\ n = 1, 2, 3, 4 \end{cases} . \tag{3.2.4}$$

Since we have 2 threads which may take binary values, the number of patterns is $2^2 = 4$. However, because of symmetry, many patterns will have identical break-up behaviour, e.g. $(-1, 1)^T$ has the same behaviour as $(1, -1)^T$. Without loss of generality, we may take $s_{n,1} = 1$. Hence, we only meet with the two cases:

1. $\alpha = 0$, which is coded by $\mathbf{s}_1 = (1, 1)^T$: the threads will break up in-phase.
2. $\alpha = \pi$, which is coded by $\mathbf{s}_2 = (1, -1)^T$: the threads will break up out-of-phase.

For a given phase pattern $\mathbf{s}_n$, (3.2.1) reduces to

$$X(t) - s_{n,2}\Big[Y(r_2, \phi_1, \phi_2, t)\Big]_{r_1=1} = 0. \tag{3.2.5}$$

Here, Y is still written in terms of (r_2, ϕ_1, ϕ_2). With the help of (3.1.1) and (3.1.9), we may evaluate r_2 and ϕ_2 as functions of ϕ_1 only. As an example, we show this for the

first term of Y in (3.2.3):

$$\begin{aligned} r_2 K_0(kr_2)\cos(\phi_1-\phi_2)\Big|_{r_1=1} &= K_0(kr_2)[r_2\cos\phi_1\cos\phi_2 + r_2\sin\phi_1\sin\phi_2]\Big|_{r_1=1} \\ &= K_0(kr_2)[(\cos\phi_1 - b)\cos\phi_1 + \sin^2\phi_1] \\ &= K_0(kr_2)[1 - b\cos\phi_1] \\ &= \sum_{m=-\infty}^{\infty} K_m(kb)I_m(k)\cos m\phi_1[1-b\cos\phi_1] \\ &= \sum_{m=-\infty}^{\infty} K_m(kb)I_m(k)\left[\cos m\phi_1 - \frac{b}{2}\Big(\cos(m\phi_1+\phi_1)+\cos(m\phi_1-\phi_1)\Big)\right] \\ &= \sum_{m=-\infty}^{\infty}\left[K_m(kb)I_m(k) - \frac{b}{2}\Big(K_{m-1}(kb)I_{m-1}(k)+K_{m+1}(kb)I_{m+1}(k)\Big)\right]\cos m\phi_1. \end{aligned} \tag{3.2.6}$$

The calculation above is a correction on the calculation by Knops (1997). Knops assumed that $\phi_2 \ll \phi_1$, and, for example, took $\cos(\phi_1-\phi_2)\approx\cos\phi_1$. Along the same lines, we finally obtain that (3.2.5) can be written as

$$[\![u]\!]_1 = [\![u_0]\!]_1 + \sum_{m=1}^{\infty}[\![u_m]\!]_1\cos m\phi_1 = 0. \tag{3.2.7}$$

Basically, we obtain an infinite set of equations namely $[\![u_m]\!]_1 = 0$, for $m = 0, 1, 2, \cdots$.

3.2.1 The $M = 0$ case

For the zero-order mode, we approximate the expansion (3.2.7) by taking the zero-moment of it, yielding $[\![u_0]\!]_1 = 0$, only. Evaluating the zero-moment of all boundary conditions and choosing an appropriate ordering of the unknowns, we arrive for given $\mathbf{s}_n$ at a matrix equation for the unknown coefficients ($n = 1, 2$):

$$(\mathbf{H}\mathbf{D}_n)\mathbf{z}_n = \mathbf{D}_n\mathbf{e}, \tag{3.2.8}$$

where the matrices $\mathbf{H}$ and $\mathbf{D}_n$ are defined as

$$\mathbf{H} = \begin{pmatrix} \mathbf{H}_0 & \mathbf{H}_1 \\ \mathbf{H}_1 & \mathbf{H}_0 \end{pmatrix}, \quad \mathbf{D}_n = \begin{pmatrix} s_{n,1}\mathbf{I}_4 & \mathbf{0} \\ \mathbf{0} & s_{n,2}\mathbf{I}_4 \end{pmatrix}, \tag{3.2.9}$$

with 4×4 submatrices $\mathbf{H}_0$ and $\mathbf{H}_1$, and identity matrix $\mathbf{I}_4$. Explicit expressions for $\mathbf{H}_0$ and $\mathbf{H}_1$ are given in Appendix B.3. The vectors $\mathbf{z}_n$ and $\mathbf{e}$ are given by $\mathbf{z}_n = \left(\mathbf{z}_{n,1}^T, \mathbf{z}_{n,2}^T\right)^T$ and $\mathbf{e} = \left(\mathbf{e}_1^T, \mathbf{e}_2^T\right)^T$ with (for $j = 1, 2$)

$$\mathbf{z}_{n,j}(t) = (A_{j,0}^{(n)}(t), B_{j,0}^{(n)}(t), D_{j,0}^{(n)}(t), E_{j,0}^{(n)}(t))^T \text{ and } \mathbf{e}_j = (0,0,0,(1-k^2)\varepsilon_{j,0}(t))^T. \tag{3.2.10}$$

So, $\mathbf{z}_n$ and $\mathbf{e}$ have length 8. To obtain the lower part of the matrix $\mathbf{H}$, we simply may replace coordinates referring to thread 1 by coordinates referring to thread 2. In view

of the symmetry as shown in Figure 3.1, we may assume that $\varepsilon_{1,0} = \varepsilon_{2,0}$, so we have $\mathbf{e}_1 = \mathbf{e}_2$. Thus, we can simplify the calculation as follows. We rewrite (3.2.8) as

$$\mathbf{H}_0\mathbf{z}_{n,1} + s_{n,2}\mathbf{H}_1\mathbf{z}_{n,2} = \mathbf{e}_1, \tag{3.2.11a}$$

$$\mathbf{H}_1\mathbf{z}_{n,1} + s_{n,2}\mathbf{H}_0\mathbf{z}_{n,2} = s_{n,2}\mathbf{e}_1. \tag{3.2.11b}$$

In (3.2.11), we have substituted $s_{n,1} = 1$ and $\mathbf{e}_1 = \mathbf{e}_2$. Combining (3.2.11a) and (3.2.11b), we find

$$(\mathbf{H}_0 + \mathbf{H}_1)(\mathbf{z}_{n,1} + s_{n,2}\mathbf{z}_{n,2}) = (1 + s_{n,2})\mathbf{e}_1, \tag{3.2.12a}$$

$$(\mathbf{H}_0 - \mathbf{H}_1)(\mathbf{z}_{n,1} - s_{n,2}\mathbf{z}_{n,2}) = (1 - s_{n,2})\mathbf{e}_1. \tag{3.2.12b}$$

From (3.2.12), for $\mathbf{s}_1 = (1, 1)^T$, when the two threads break up in-phase, we obtain

$$(\mathbf{H}_0 + \mathbf{H}_1)\mathbf{z}_{n,1} = \mathbf{e}_1, \quad \text{and} \quad \mathbf{z}_{n,2} = \mathbf{z}_{n,1}, \tag{3.2.13}$$

and for $\mathbf{s}_2 = (1, -1)^T$, when the two threads break up out-of-phase,

$$(\mathbf{H}_0 - \mathbf{H}_1)\mathbf{z}_{n,1} = \mathbf{e}_1, \quad \text{and} \quad \mathbf{z}_{n,2} = \mathbf{z}_{n,1}, \tag{3.2.14}$$

For convenience, we denote the components of $\mathbf{z}_{n,1}$ by $(\mathbf{z}_{n,1})_l$, $l = 1, \cdots, 4$, $\mathbf{H}_+ \equiv \mathbf{H}_0 + \mathbf{H}_1$ and $\mathbf{H}_- \equiv \mathbf{H}_0 - \mathbf{H}_1$. The solution of (3.2.13) is given by

$$(\mathbf{z}_{n,1})_l = (-1)^l \frac{(1 - k^2)|\mathbf{H}_+^{4,l}|}{|\mathbf{H}_+|}\varepsilon_{1,0}(t). \tag{3.2.15}$$

We note that the coefficients are proportional to the amplitude of the disturbance. The same expression applies for the solution of (3.2.14) with the sign (+) replaced by the sign (−).

3.2.2 The $M = 1$ case

For the first-order approach, i.e. the $M = 1$ case, we have twenty unknowns and six boundary conditions, two more than in the zero-order approach ($M = 0$). The latter stem from the jump in velocity and shear stress in azimuthal direction. After application of transformations (3.1.1, 3.1.9) and calculation of the zero- and first-moments, these six boundary conditions give rise to twenty relations, i.e. 2×4 relations from the zero-moment and 2×6 relations from the first moment. Similar as in the zero-order approach, we arrive at a matrix equation like the one in (3.2.8). The properties of the matrix $\mathbf{H}$ are the same as in the previous case, except that the size of the block matrices $\mathbf{H}_0$ and $\mathbf{H}_1$ are now 10 by 10, the vectors $\mathbf{z}_{n,j}(t)$ $(j, n = 1, 2)$ are defined as

$$\mathbf{z}_{n,j}(t) = (A_{j,0}^{(n)}, B_{j,0}^{(n)}, D_{j,0}^{(n)}, E_{j,0}^{(n)}, A_{j,1}^{(n)}, B_{j,1}^{(n)}, C_{j,1}^{(n)}, D_{j,1}^{(n)}, E_{j,1}^{(n)}, F_{j,1}^{(n)})^T, \tag{3.2.16}$$

and the right-hand side vectors are given by

$$\mathbf{e}_j = (0, 0, 0, (1 - k^2)\varepsilon_{j,0}, 0, 0, 0, -k^2\varepsilon_{j,1}, 0, 0)^T. \tag{3.2.17}$$

Explicit expression for $\mathbf{H}$ is given in Appendix B.3. The same procedure as in the zero-order approach can be followed to solve the unknown coefficients. Now, (3.2.15) becomes ($l = 1, 2, \cdots, 10$)

$$(\mathbf{z}_{n,1})_l = (-1)^l \frac{1}{|\mathbf{H}_+|}\left[(1-k^2)\,|\mathbf{H}_+^{4,l}|\varepsilon_{1,0}(t) - k^2\,|\mathbf{H}_+^{8,l}|\varepsilon_{1,1}(t)\right]. \tag{3.2.18}$$

3.3 Stability analysis

To analyze the stability of the system we apply the kinematic condition (2.1.19). We first deal with the $M = 0$ case. As an illustration, we work out the evaluation for the phase pattern $\mathbf{s}_1 = (1, 1)^T$. Since the dynamics is only driven by surface tension, we obtain from (2.1.19) and (2.2.17b)

$$\frac{d\varepsilon_{1,0}(t)}{dt} = u_{1,0}^d = \left(I_0(k) - \frac{2}{k}I_1(k)\right)A_{1,0}(t) - I_1(k)B_{1,0}(t), \tag{3.3.1}$$

where

$$\begin{aligned} A_{1,0}(t) &= -\frac{(1-k^2)|\mathbf{H}_+^{4,1}|}{|\mathbf{H}_+|}\varepsilon_{1,0}(t), \\ B_{1,0}(t) &= \frac{(1-k^2)|\mathbf{H}_+^{4,2}|}{|\mathbf{H}_+|}\varepsilon_{1,0}(t). \end{aligned} \tag{3.3.2}$$

For convenience, we omitted the superscript (1) in the coefficients, i.e. $A_{1,0}(t) \equiv A_{1,0}^{(1)}(t)$ (see (3.2.10)). Substitution of (3.3.2) into (3.3.1) yields

$$\frac{d\varepsilon_{1,0}(t)}{dt} = q^+(k, \mu, b)\varepsilon_{1,0}(t), \tag{3.3.3}$$

where

$$q^+(k, \mu, b) = \frac{(k^2-1)}{|\mathbf{H}_+|}\left[\left(I_0(k) - \frac{2}{k}I_1(k)\right)|\mathbf{H}_+^{4,1}| + I_1(k)|\mathbf{H}_+^{4,2}|\right]. \tag{3.3.4}$$

A similar expression holds for the case $\mathbf{s}_2 = (1, -1)^T$ with the sign $(+)$ replaced by $(-)$.

In general, the stability problem up to and including the M-th Fourier mode reduces to the matrix differential equation

$$\frac{d\mathbf{y}}{dt} = \mathbf{Q}(k, \mu, b)\mathbf{y}, \tag{3.3.5}$$

where $\mathbf{y}$ is the vector of the perturbation amplitudes and $\mathbf{Q}(k, \mu, b)$ is an $(M + 1)$ by $(M + 1)$ matrix depending on the distance b, the ratio of viscosities μ, and the wave number k. The instability of the threads is determined by the eigenvalue of $\mathbf{Q}$ with the largest real part. For instance, for the $M = 1$ case we have $\mathbf{y} = (\varepsilon_{1,0}(t), \varepsilon_{1,1}(t))^T$, and

the elements q_{ij} of the matrix $\mathbf{Q}$ are given by

$$\begin{aligned} q_{11} &= \frac{(k^2-1)}{|\mathbf{H}_s|}\left[(I_0(k)-\frac{2}{k}I_1(k))|\mathbf{H}_s^{4,1}|+I_1(k)|\mathbf{H}_s^{4,2}|\right], \\ q_{12} &= \frac{k^2}{|\mathbf{H}_s|}\left[(I_0(k)-\frac{2}{k}I_1(k))|\mathbf{H}_s^{8,1}|+I_1(k)|\mathbf{H}_s^{8,2}|\right], \\ q_{21} &= \frac{(k^2-1)}{|\mathbf{H}_s|}\left[(I_1(k)-\frac{3}{k}I_2(k))|\mathbf{H}_s^{4,5}|+I_2(k)|\mathbf{H}_s^{4,6}|+I_1(k)|\mathbf{H}_s^{4,7}|\right], \\ q_{22} &= \frac{k^2}{|\mathbf{H}_s|}\left[(I_1(k)-\frac{3}{k}I_2(k))|\mathbf{H}_s^{8,5}|+I_2(k)|\mathbf{H}_s^{8,6}|+I_1(k)|\mathbf{H}_s^{8,7}|\right], \end{aligned} \tag{3.3.6}$$

where s can be either $+$ or $-$. As before we denote these dimensionless eigenvalues for the in-phase and out-of phase cases by q^+ and q^-, respectively.

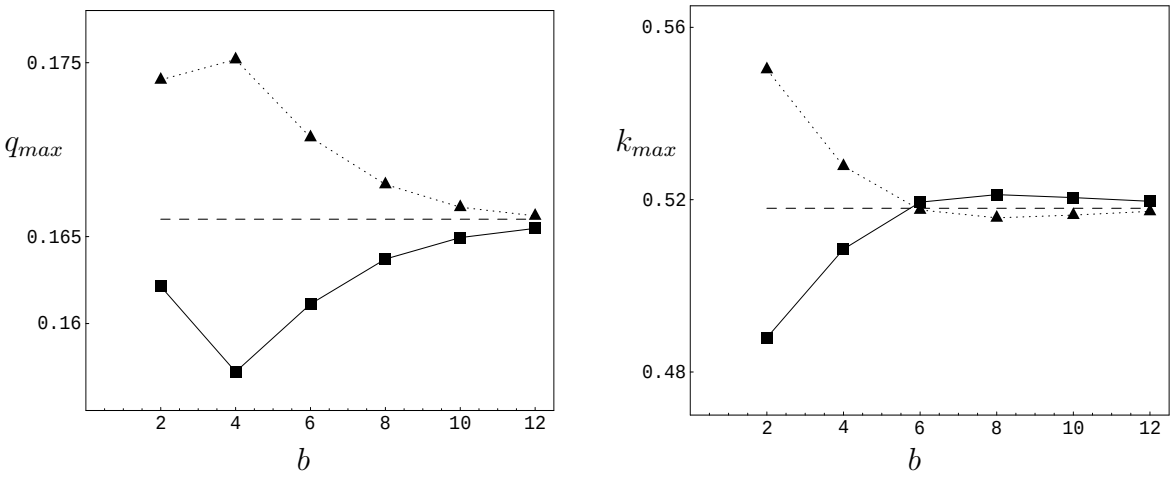

(a) q_{max} vs b. (b) k_{max} vs b.

Figure 3.2: *Plots of $q^{\pm}_{max}$ and $k^{\pm}_{max}$ as functions of the distance b, for $\mu = 0.04$ and $M = 0$. The solid and dotted lines correspond to the in-phase and out-of-phase cases, respectively. The dashed horizontal lines indicate the limiting values for $b \to \infty$.*

To get insight in the break-up behaviour of the two threads system, we calculate the factor $q(k, \mu, b)$ for both $M = 0$ and $M = 1$. Fixing the geometrical parameter b and the material parameter μ, we determine the values q^+ and q^- by optimizing over k, since the (in)stability of the system is determined by the mode corresponding with the highest $q^{\pm}$-value. We denote this highest value of $q^{\pm}$ by

$$q^{\pm}_{max} = \max\{q^{\pm}(k; \mu, b)\}. \tag{3.3.7}$$

In Figures 3.2-3.5 the values of q^+_{max} and q^-_{max}, calculated this way, are given as functions of the distance b of the threads, for two values of μ. The case $\mu = 0.04$ corresponds to a situation in which the threads are less viscous than the surrounding fluid, whereas

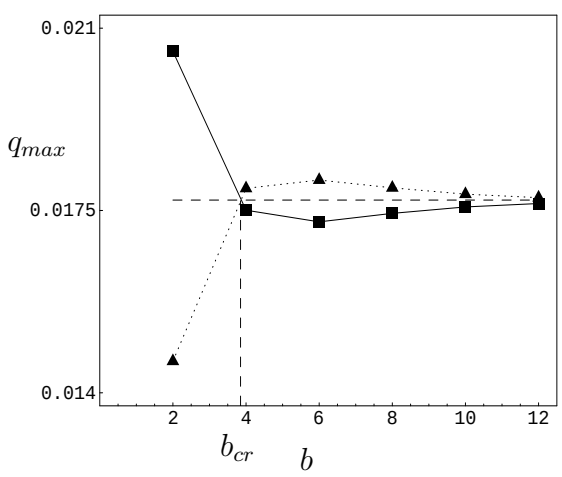

(a) q_{max} vs b.

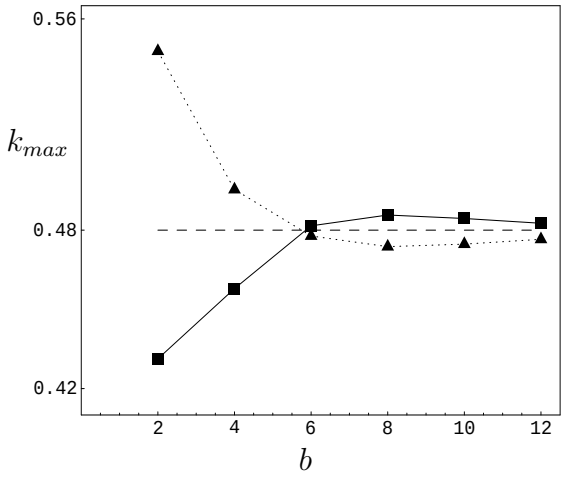

(b) k_{max} vs b.

Figure 3.3: *Same information as in Figure 3.2 but now for $\mu = 4$.*

for $\mu = 4$ it is the other way around. The graph of k_{max}, defined as the value of the wave number k corresponding to the highest q-value, is also presented in part (b) of these figures as a function of the distance b. For $\mu = 0.04$, q^-_{max} is always greater than q^+_{max}. This implies that the threads will break up out-of-phase. However, for $\mu = 4$, the curves cross at a critical distance b_{cr}. If $b < b_{cr}$ the threads will break up in-phase, whereas if $b > b_{cr}$ the threads will break up out-of-phase. The discovery of the existence of this critical parameter b_{cr} is a new result in this field. In the limiting case $b \to \infty$, when the problem tends to the simple case of one thread, q^+_{max} and q^-_{max} become equal to $\hat{q}_{max}$, say; this is approximately the case if the distance b becomes 12 times, or more,

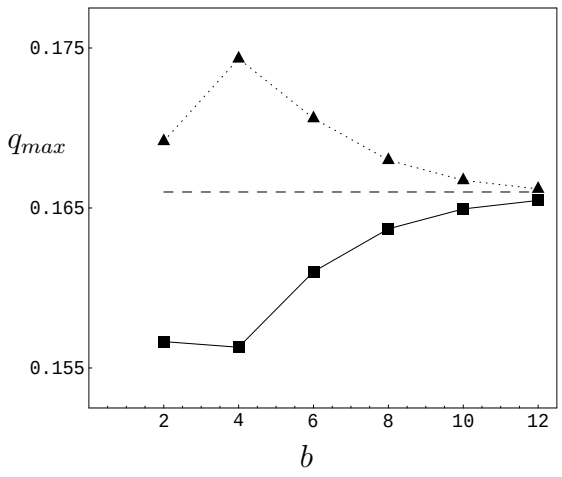

(a) q_{max} vs b.

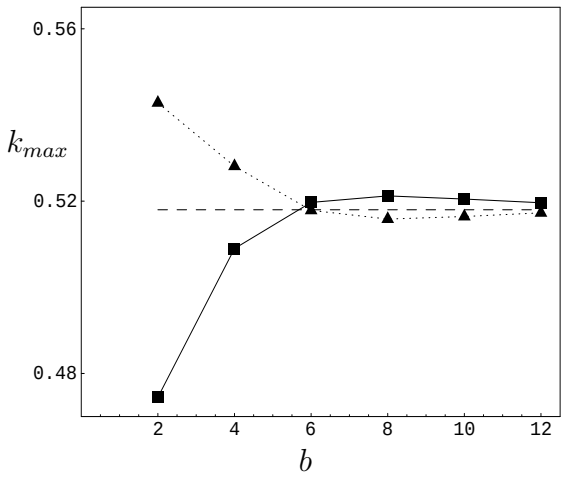

(b) k_{max} vs b.

Figure 3.4: *Same information as in Figure 3.2 but now for $M = 1$.*

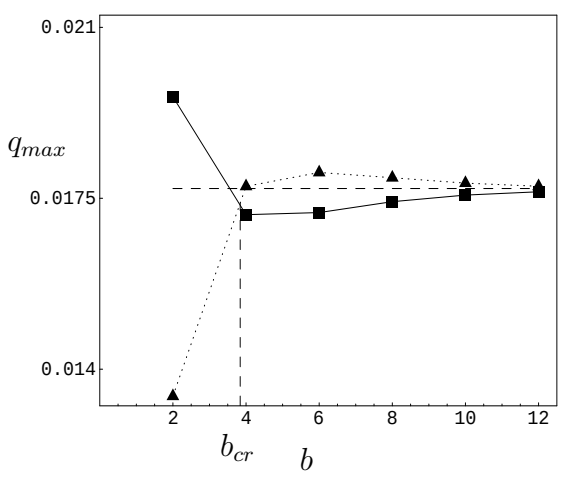

(a) q_{max} vs b.

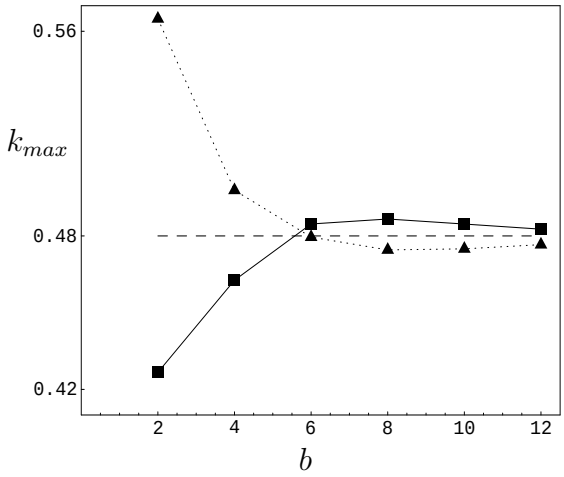

(b) k_{max} vs b.

Figure 3.5: *Same information as in Figure 3.2 but now for $\mu = 4$ and $M = 1$.*

the radius a of the thread. This indicates that in that case the threads will break up independently of each other, and then none of the phase differences are preferable. The limiting value $\hat{q}_{max}$ for the single thread case is denoted by the dashed horizontal line in part (a) of Figures 3.2-3.5. Comparing the results in Figures 3.2-3.5, we observe that the instability behaviour hardly differs for the $M = 0$ and the $M = 1$ cases, so the $M = 0$ results are reliable to draw conclusions from.

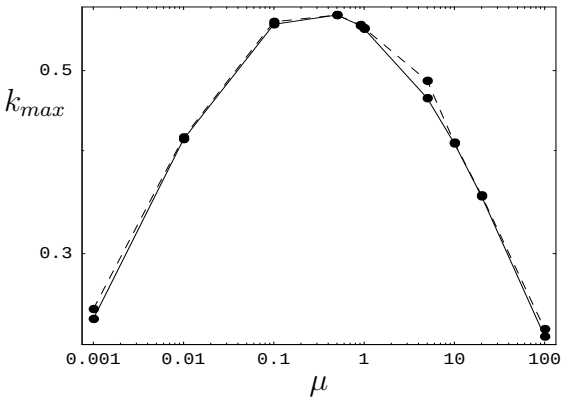

Figure 3.6: *Curve of k_{max} as a function of the ratio of viscosities μ (on a logarithmic scale) for the single thread case. The dashed line represents the results from Tomotika (1935), and the solid line represents results based on the present work in the zero-order approach ($M = 0$). The only significant deviation is for the data point $\mu = 5$. This clearly stems from a typing error in Tomotika's work.*

For the limiting case of one thread ($b \to \infty$), we numerically calculated the maximum value k_{max} of the wave number, for different values of the ratio of viscosities μ. Fixing the value of μ and taking the value of b quite large, we determined k_{max} and the results

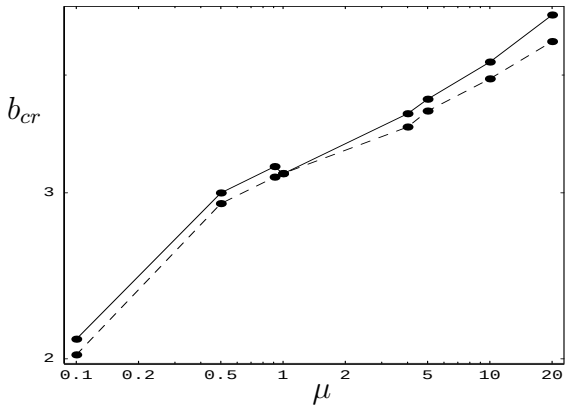

Figure 3.7: *Graph of the critical distance b_{cr} as a function of the ratio of viscosities μ (on a logarithmic scale) for $M = 0$ (solid line) and $M = 1$ (dashed line).*

are plotted in Figure 3.6 (solid line). In this Figure we also represent (dashed line) Tomotika's result (1935). We see from this figure that the present results confirm the previous results of Tomotika for nearly all μ-values.

For the critical distance b_{cr}, we also present in Figure 3.7 the graph as a function of the ratio of viscosities μ. If $b_{cr} \to 2$ the two threads touch each other. For the investigated range of μ-values, we find that the greater μ is, the greater is b_{cr}. The extension from $M = 0$ to $M = 1$ leads to very small corrections only.

The case $\mu = 1$ deserves special attention. In experiments, it is perfectly possible to find two fluids with matching viscosities that are immiscible. Stone & Brenner (1996) considered this case analytically for the one-thread system. In the next Chapter, we analytically study this case for the many-threads system.

3.4 Conclusions

In this chapter, we have described a general method to determine the degree of instability for a set of two parallel viscous threads immersed in a viscous liquid. The general solution of the underlying Stokes problem was decomposed into Fourier modes, and the boundary conditions then led to an infinite set of equations for the unknown coefficients. This set was truncated at finite M, and the truncated set was solved by use of the method of moments.

The method was evaluated for the zero-order ($M = 0$) and first-order ($M = 1$) solutions. As an illustration, the zero-order solution was worked out. The zero-order approximation leads to relatively simple equations for the unknown coefficients. No infinite series are involved in the entries of the matrix of coefficients as was found in Knops (1997) due to redundant simplifications. The behaviour of the break-up process of the threads is characterized by the degree of instability q, which depends on the viscosity ratio μ, the wave number of the perturbations k and the distance between the two threads b. For large viscosity ratio, when the threads are more viscous than the matrix, we found a critical relative distance b_{cr}. For $b < b_{cr}$, the threads will break up

in-phase, for $b > b_{cr}$ out-of-phase. The smaller the viscosity ratio, the more the out-of-phase break up is preferred. This is in accordance with experimental results reported in Knops (1997), Elemans et al. (1997) and Knops et al. (2001). However, the results in Figure 3 of Knops et al. (2001) based on minimization of energy dissipation arguments disagree with the present findings. Not only the value of the critical b_{cr} is different, but also the qualitative behaviour, since we find that out-of-phase break-up takes place for $b > b_{cr}$, whereas in Knops et al. (2001) this is found for $b < b_{cr}$.

We have also performed the instability analysis for $M = 1$ which led to a large amount of arithmetical work. We found that the extension from $M = 0$ to $M = 1$ leads only to minor quantitative corrections in the results.

From the point of view of blend production the present results may provide important insights for control of the production process. Two aspects deserve mentioning: characteristic drop formation times and spatial distributions of the droplets. As for formation time, the time scale of the dynamical process is governed by the value of the q-factor, plotted in Figures 3.2-3.5. In most extrusion devices the blend is only a restricted time in the molten state. As soon as it is cooled down, the spatial droplet distribution at that moment will freeze in. For economical reasons, from industry there is a need for fast formation processes. From the results summarized in the Figures mentioned above it is clear that high values for μ and small values for b are highly favourable for speeding up the break-up process.

As for the spatial distribution of the droplets, it is highly important to know that either in-phase or out-of-phase break-up may occur. As if the present results also apply to systems with many threads (see next chapter), it must be possible to produce blends with the droplets either on a cubic grid, resulting from in-phase break-up, or on a body centered cubic grid, resulting from out-of-phase break-up, just by controlling the two parameters μ and b in an appropriate way. So, this implies in practice that important properties of the blends can be adjusted quite easily, since both μ and b, the latter of which is essentially determined by the volume fraction of the big drops in the initial situation, are simply controlled in production conditions. These considerations are based on our findings that the present results for two threads may be transferred to many-threads systems. This is the topic of the next chapter.

Chapter 4

Stability of a set of Newtonian threads

In this chapter, we show how the description of the break-up of a cylindrical thread due to surface tension can be generalized to an arbitrary number of interacting threads in an arbitrary configuration. We study a system of immersed threads starting with two types of configurations, i.e. a system of threads on a row and a system of threads at triangular vertices. From these cases, which are worked out in detail, it becomes clear how the stability of an arbitrary configuration can be determined. The (in)stability of the configuration is discussed in terms of the so-called perturbation growth rate. It turns out that the threads break up in specific phase patterns in which neighbouring threads are either in-phase or out-of-phase. For L threads, in principle 2^L phase patterns are possible. However, we show that the stability of the system directly follows from L so-called basic phase patterns. Special attention is paid to the special case of threads and fluid having equal viscosity. Then, the growth rate can be calculated analytically using Hankel transformations. We derive an estimate for the growth rate in this case, which turns out to be quite sharp.

4.1 Row configuration

Consider a sequence of L infinitely long parallel threads, equally spaced with distances b. All threads have viscosity η^d and radius a. They are surrounded by a fluid with viscosity η^c. We denote the ratio of the viscosities as in (2.1.1), i.e. $\mu = \eta^d/\eta^c$. For thread j ($j = 1, \cdots, L$), a cylindrical coordinate system (r_j, ϕ_j, z_j) will be used with z measured along the axis of the thread. In Figure 4.1, the coordinates r_j and ϕ_j are indicated for a system with $L = 3$. In general, if thread J is taken as frame of reference, we have the relations ($j, J = 1, \cdots, L$):

$$\begin{aligned} r_J \cos\phi_J &= (j-J)b + r_j \cos\phi_j, \\ r_J \sin\phi_J &= r_j \sin\phi_j, \\ z_J &= z_j \equiv z. \end{aligned} \tag{4.1.1}$$

Let us consider a perturbation of thread j, that is periodic in z with wave number k_j. Because the problem is not axisymmetric, the perturbation of thread j will also depend on ϕ_j. This dependence is represented by a Fourier expansion. The radius R_j of thread

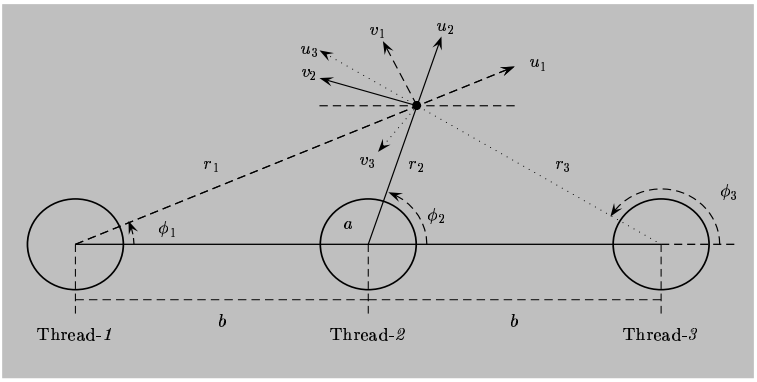

Figure 4.1: *Cylindrical coordinate systems for $L = 3$.*

j is then written as

$$R_j(\phi_j, z, t) \quad = \quad a\left[1 + \sum_{m=0}^{\infty} \varepsilon_{j,m}(t) \cos m\phi_j \cos(k_j z - \alpha_j)\right]. \tag{4.1.2}$$

Since the z-axes of all threads are parallel, we dropped the index j from the z-coordinates. Here, $\varepsilon_{j,m}$ is the time-dependent amplitude of the m-th mode, and α_j is the phase of this mode. The $\varepsilon_{j,m}$ and α_j are unknown in advance.

The dynamics of the disintegrating threads under this perturbation is known if we calculate the velocity field $\mathbf{v} = (u, v, w)$ and the pressure p. Since all motions are slow due to the high viscosity, we use the creeping flow approximation and assume the system to satisfy the Stokes equation. The fluids are incompressible, so the incompressibility condition holds. Thus, we model the system by (2.1.3). Since the dynamics is due to surface tension only, the unperturbed velocity is zero and the unperturbed pressure is constant. For the perturbed system, the equations are given by (2.2.2). The equations are brought into dimensionless form by use of (2.2.4), i.e. as units of the distance, velocity, and stress components we take a, σ/η^c, and σ/a, respectively, where σ is the surface tension. Separating variables and expressing the dependence on ϕ in terms of Fourier modes, we obtain expressions for the solution inside thread j similar to (2.2.5). For example, the radial component u_j^d of the velocity is given by

$$u_j^d(r_j, \phi_j, z, t) = \sum_{m=0}^{\infty} u_{j,m}^d(r_j, t) \cos m\phi_j \cos(k_j z - \alpha_j). \tag{4.1.3}$$

The same holds for the continuous phase with the index d replaced by c. For example, the radial velocity of the continuous phase with respect to thread j for $j = 1, \cdots, L$ is written as

$$u_j^c = \sum_{m=0}^{\infty} u_{j,m}^c(r_j, t) \cos m\phi_j \cos(k_j z - \alpha_j). \tag{4.1.4}$$

Substituting (4.1.3), etc., and (4.1.4), etc., into (2.2.2), we find the solutions as in (2.2.17) and (2.2.18).

The solution for the continuous phase is influenced by all threads. As an ansatz, we represent the solution outside the threads by the linear combination of expansions like the one in (4.1.4) with respect to all the different threads; $j = 1, \cdots, L$. As a counterpart of (3.1.6), we obtain

$$p^c_{(J)} = \sum_{j=1}^{L} p^c_j, \tag{4.1.5a}$$

$$u^c_{(J)} = \sum_{j=1}^{L} \Big[u^c_j \cos(\phi_J - \phi_j) + v^c_j \sin(\phi_J - \phi_j) \Big], \tag{4.1.5b}$$

$$v^c_{(J)} = \sum_{j=1}^{L} \Big[-u^c_j \sin(\phi_J - \phi_j) + v^c_j \cos(\phi_J - \phi_j) \Big], \tag{4.1.5c}$$

$$w^c_{(J)} = \sum_{j=1}^{L} w^c_j. \tag{4.1.5d}$$

As for the conditions at the interfaces, we apply the same conditions as in the two-threads system (see (3.1.7)). The evaluation of the boundary conditions at thread J requires expansion of the product of a Bessel function and a Fourier expansion with respect to thread j, $j \neq J$, around thread J. To handle this, we use the geometrical relations (4.1.1) and Graf's addition theorem of Bessel function (see Watson (1966)). We finally obtain solutions by applying the method of moments to the truncated system.

4.1.1 Evaluation of boundary conditions

For clarity, we restrict ourselves in this section to the zero-order Fourier expansion, since this lowest mode already yields a reliable solution as shown in Chapter 3.

Let thread J, $1 \leq J \leq L$, be taken as frame of reference. The evaluation of boundary conditions at its interface requires that we express all quantities in terms of (r_J, ϕ_J). As an example, we will describe this for the continuity of the radial velocity. Since only phase differences are relevant, we may take $\alpha_J = 0$. Requiring $[\![u]\!]_J = u^d_J - u^c_{(J)} = 0$ and using (4.1.3) and (4.1.5b), we obtain the condition:

$$X(t)\cos(k_J z) - \sum_{j \neq J} [Y(r_j, \phi_J, \phi_j, t)] \cos(k_j z - \alpha_j) = 0. \tag{4.1.6}$$

In general, X and Y are given by long expressions which provide little information. They will be made explicit below for $L = 3$. Here, the important point is that neither X nor Y depends on z. Since (4.1.6) must be satisfied for all $z \in \mathbb{R}$, we conclude that the wave numbers k_J and k_j must be the same, so $k_j = k$ for all j. Moreover, the phases α_j may take only the values 0 and π. If $\alpha_j = 0$, thread j breaks up in-phase with thread J, whereas for $\alpha_j = \pi$ thread j is out-of-phase with thread J. We remark that varying the

values of α_j leads to various *phase patterns*. Since we have L positions which may take binary values the number of patterns is 2^L. We code a pattern by the vector

$$\mathbf{s}_n = (s_{n,1}, s_{n,2}, \cdots, s_{n,L})^T, \text{ with } s_{n,j} = \pm 1 \text{ for } \begin{cases} j = 1, \cdots, L \\ n = 1, \cdots, 2^L \end{cases} . \tag{4.1.7}$$

However, because of symmetry, many patterns will have identical break-up behaviour. For a given phase pattern $\mathbf{s}_n$, (4.1.6) reduces to

$$X(t) - \sum_{j \neq J} s_{n,j}[Y(r_j, \phi_J, \phi_j, t)] = 0. \tag{4.1.8}$$

Here, Y is still written in terms of (r_j, ϕ_J, ϕ_j), but we can rewrite the r_j and ϕ_j dependences in terms of ϕ_J only. Then, we can expand Y in a Fourier series in ϕ_J. After changing the order of summations, we obtain

$$X(t) - \sum_{m=-\infty}^{\infty} \left(\sum_{j \neq J} s_{n,j} \hat{Y}_m(t; |j-J|kb) \right) \cos m\phi_J = 0. \tag{4.1.9}$$

Here, $\hat{Y}_m$ results from expressing Y in terms of r_J and ϕ_J and expanding this in a Fourier series. Note that $\hat{Y}_m$ contains $|j-J|b$, the distance between thread J and j. Taking the zero-moment of (4.1.9), i.e. integrating over ϕ_J, we obtain

$$X(t) - \sum_{j \neq J} s_{n,j} \hat{Y}_0(t; |j-J|kb) = 0 \ . \tag{4.1.10}$$

For the zero-order Fourier approach, we remark that we have $L \times 4$ unknown coefficients (see (2.2.17) and (2.2.18) for $m = 0$). As an illustration, we evaluate the solution for $L = 3$ explicitly.

4.1.2 The $L = 3$ case

To illustrate the theory of the preceding section, we apply it to a system of three threads on a row as shown in Figure 4.1. Here, thread $J = 1$ is taken as reference system. For the zero-order Fourier mode, the azimuthal velocity v_1^d inside the thread is vanishing. However, $v_{(1)}^c$ does not vanish in general, as follows from (4.1.5c), but since $v_{(1)}^c$ is, after applying Graf's addition theorem, an odd function in ϕ_1, and thus its zero-moment is zero. The same holds for $\tau_{r_1\phi_1}$. For the $m = 0$ mode, we have for $j = 1, 2, 3$,

$$\begin{aligned} p_j^d(r_j, \phi_j, z, t) &= p_{j,0}^d(r_j, t)\cos(kz - \alpha_j), \\ u_j^d(r_j, \phi_j, z, t) &= u_{j,0}^d(r_j, t)\cos(kz - \alpha_j), \\ w_j^d(r_j, \phi_j, z, t) &= w_{j,0}^d(r_j, t)\sin(kz - \alpha_j), \end{aligned} \tag{4.1.11}$$

while (4.1.5) reads in this case

$$\begin{aligned} p^c_{(1)} &= p^c_1 + p^c_2 + p^c_3, \\ u^c_{(1)} &= u^c_1 + u^c_2 \cos(\phi_1 - \phi_2) + u^c_3 \cos(\phi_1 - \phi_3), \\ w^c_{(1)} &= w^c_1 + w^c_2 + w^c_3. \end{aligned} \tag{4.1.12}$$

The evaluation of boundary conditions at the interface S_1 requires expressing all quantities in terms of (r_1, ϕ_1). As an example, we will work this out for the continuity of the radial velocity. From $[\![u]\!]_1 = u^d_1 - u^c_{(1)} = 0$, we obtain the condition

$$X(t)\cos(kz) - \sum_{j=2}^{3} [Y(r_j, \phi_1, \phi_j, t)] \cos(kz - \alpha_j) = 0, \tag{4.1.13}$$

where

$$\begin{aligned} X(t) &= \left(I_0(k) - \frac{2}{k} I_1(k)\right) A_{1,0}(t) - I_1(k) B_{1,0}(t) \\ &\quad - \left(K_0(k) + \frac{2}{k} K_1(k)\right) D_{1,0}(t) - K_1(k) E_{1,0}(t), \end{aligned} \tag{4.1.14}$$

and

$$Y(r_j, \phi_1, \phi_j, t) = \left[\left(r_j K_0(k r_j) + \frac{2}{k} K_1(k r_j)\right) D_{j,0}(t) + E_{j,0}(t) K_1(k r_j)\right] \cos(\phi_1 - \phi_j). \tag{4.1.15}$$

We remind that for convenience we have taken $\alpha_1 = 0$. As argued above with respect to (4.1.6), equation (4.1.13) implies that α_2 and α_3 can only attain the values 0 or π. This leads to the following phase patterns:

1. $\alpha_1 = 0,\ \alpha_2 = 0$, and $\alpha_3 = 0$, coded by $\mathbf{s}_1 = (1, 1, 1)^T$; all adjacent threads break up in-phase.

2. $\alpha_1 = 0,\ \alpha_2 = \pi$, and $\alpha_3 = 0$, coded by $\mathbf{s}_2 = (1, -1, 1)^T$; all adjacent threads break up out-of-phase.

3. $\alpha_1 = 0,\ \alpha_2 = 0$, and $\alpha_3 = \pi$, coded by $\mathbf{s}_3 = (1, 1, -1)^T$; thread 3 breaks up out-of-phase with respect to thread 1 and 2.

4. $\alpha_1 = 0,\ \alpha_2 = \pi$, and $\alpha_3 = \pi$, coded by $\mathbf{s}_4 = (1, -1, -1)^T$; both threads 2 and 3 break up out-of-phase with respect to thread 1.

We remark that cases 3 and 4 are identical in view of the symmetry of the system. In Figure 4.2 one of the possible phase patterns for $L = 3$ is sketched. For given $\mathbf{s}_n$, condition (4.1.13) reduces to

$$X(t) - \sum_{j=2}^{3} s_{n,j} [Y(r_j, \phi_1, \phi_j, t)] = 0. \tag{4.1.16}$$

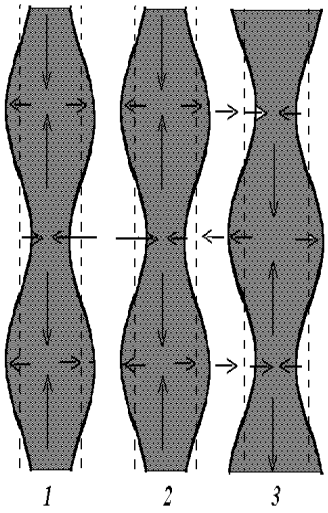

Figure 4.2: *Top view of one of the possible phase patterns if $L = 3$. Thread 1 and 2 are in-phase and thread 2 and 3 are out-of-phase.*

Expressing all terms with respect to ϕ_1 and taking the zero-moment, we obtain (compare to (4.1.10); here, $\hat{Y} \equiv \hat{Y}_0$)

$$X(t) - \Big(s_{n,2}\hat{Y}(t; kb) + s_{n,3}\hat{Y}(t; 2kb) \Big) = 0. \tag{4.1.17}$$

The contribution of both thread 2 and 3 is given by the same expression $\hat{Y}$, but with different arguments kb and $2kb$, respectively. Evaluating the zero-moment of all boundary conditions and choosing an appropriate ordering of the unknowns, for a given $\mathbf{s}_n$ $(n = 1, \cdots, 8)$, we arrive at a matrix equation for the unknown coefficients:

$$(\mathbf{H}\mathbf{D}_n)\mathbf{z}_n = \mathbf{D}_n\mathbf{e}, \tag{4.1.18}$$

where the matrices $\mathbf{H}$ and $\mathbf{D}_n$ are defined as

$$\mathbf{H} = \begin{pmatrix} \mathbf{H}_0 & \mathbf{H}_1 & \mathbf{H}_2 \\ \mathbf{H}_1 & \mathbf{H}_0 & \mathbf{H}_1 \\ \mathbf{H}_2 & \mathbf{H}_1 & \mathbf{H}_0 \end{pmatrix}, \quad \mathbf{D}_n = \begin{pmatrix} s_{n,1}\mathbf{I}_4 & \mathbf{0} & \mathbf{0} \\ \mathbf{0} & s_{n,2}\mathbf{I}_4 & \mathbf{0} \\ \mathbf{0} & \mathbf{0} & s_{n,3}\mathbf{I}_4 \end{pmatrix}, \tag{4.1.19}$$

with 4×4 submatrices $\mathbf{H}_j$ and identity matrix $\mathbf{I}_4$. The vectors $\mathbf{z}_n$ and $\mathbf{e}$ are given by $\mathbf{z}_n = \left(\mathbf{z}_{n,1}^T, \mathbf{z}_{n,2}^T, \mathbf{z}_{n,3}^T\right)^T$ and $\mathbf{e} = \left(\mathbf{e}_1^T, \mathbf{e}_2^T, \mathbf{e}_3^T\right)^T$ with

$$\mathbf{z}_{n,j}(t) = (A_{j,0}^{(n)}(t), B_{j,0}^{(n)}(t), D_{j,0}^{(n)}(t), E_{j,0}^{(n)}(t))^T \text{ and } \mathbf{e}_j = (0, 0, 0, (1 - k^2)\varepsilon_{j,0}(t))^T. \tag{4.1.20}$$

So, $\mathbf{z}_n$ and $\mathbf{e}$ have length 12. For convenience, we denote the components of $\mathbf{z}_n$ by $(\mathbf{z}_n)_l$. Explicit expressions for $\mathbf{H}_j$, $j = 0, 1, 2$, are given in Appendix B.4. The matrix $\mathbf{H}$

depends on the numbering of the threads. However, this is just a matter of permutation. The solution of (4.1.18) is given by

$$(\mathbf{z}_n)_l = (-1)^l s_{n,[l/4]} \frac{1-k^2}{|\mathbf{H}|} \left(\sum_{j=1}^{3} \left(s_{n,j} \, |\mathbf{H}^{4j,l}| \right) \varepsilon_{j,0}(t) \right), \tag{4.1.21}$$

where $[x]$ in $s_{n,[x]}$ is defined as the ceiling of x, i.e. the smallest integer greater than or equal to x. Here, $|\cdot|$ denotes the determinant and $\mathbf{H}^{4j,l}$ is the 11×11 sub-matrix of $\mathbf{H}$, which can be found by omitting the $(4j)$-th row and the l-th column of $\mathbf{H}$. For example, we obtain

$$(\mathbf{z}_n)_1 \equiv A_{1,0}^{(n)}(t) = -s_{n,1} \frac{1-k^2}{|\mathbf{H}|} \left(s_{n,1} \, |\mathbf{H}^{4,1}| \varepsilon_{1,0}(t) + s_{n,2} \, |\mathbf{H}^{8,1}| \varepsilon_{2,0}(t) + s_{n,3} \, |\mathbf{H}^{12,1}| \varepsilon_{3,0}(t) \right). \tag{4.1.22}$$

We note that this coefficient is linearly proportional to the amplitudes of the perturbations.

The extension from $L = 3$ to $L > 3$ is straightforward. For a given phase pattern $\mathbf{s}_n$, we then have $L \times 4$ unknown coefficients and

$$\mathbf{H} = \begin{pmatrix} \mathbf{H}_0 & \mathbf{H}_1 & \cdots & \mathbf{H}_{L-1} \\ \mathbf{H}_1 & \mathbf{H}_0 & \cdots & \mathbf{H}_{L-2} \\ \vdots & \vdots & & \vdots \\ \mathbf{H}_{L-1} & \mathbf{H}_{L-2} & \cdots & \mathbf{H}_0 \end{pmatrix}. \tag{4.1.23}$$

Equation (4.1.21) still holds with 3 replaced by L.

4.1.3 Stability analysis

To analyze the stability of the system we use the kinematic condition (2.1.19). For $j = 1, \cdots, L$, and a given phase pattern $\mathbf{s}_n$ $(n = 1, \cdots, 2^L)$ we obtain

$$\frac{d\varepsilon_{j,0}(t)}{dt} = u_{j,0}^d = \left(I_0(k) - \frac{2}{k} I_1(k) \right) A_{j,0}^{(n)}(t) - I_1(k) B_{j,0}^{(n)}(t), \tag{4.1.24}$$

where

$$\begin{aligned} A_{j,0}^{(n)}(t) &= -s_{n,j} \frac{1-k^2}{|\mathbf{H}|} \left(\sum_{l=1}^{L} \left(s_{n,l} \, |\mathbf{H}^{4l,4j-3}| \right) \varepsilon_{l,0}(t) \right), \\ B_{j,0}^{(n)}(t) &= s_{n,j} \frac{1-k^2}{|\mathbf{H}|} \left(\sum_{l=1}^{L} \left(s_{n,l} \, |\mathbf{H}^{4l,4j-2}| \right) \varepsilon_{l,0}(t) \right). \end{aligned} \tag{4.1.25}$$

Since $A_{j,0}^{(n)}(t)$ and $B_{j,0}^{(n)}(t)$ are linear combinations of the amplitudes, we may write

$$\frac{d}{dt}(s_{n,j}\varepsilon_{j,0}(t)) = \sum_{l=1}^{L} Q_{j,l} s_{n,l} \varepsilon_{l,0}(t), \tag{4.1.26}$$

with

$$Q_{j,l} = -\frac{1-k^2}{|\mathbf{H}|}\left([I_0(k) - \frac{2}{k}I_1(k)]|\mathbf{H}^{4l,4j-3}| + I_1(k)|\mathbf{H}^{4l,4j-2}|\right). \tag{4.1.27}$$

In (4.1.26), we have multiplied both sides of (4.1.24) by $s_{n,j}$. In matrix notation, we obtain

$$\frac{d\mathbf{y}}{dt} = \mathbf{Q}(b,\mu,k)\mathbf{y}, \tag{4.1.28}$$

where $\mathbf{y}$, with elements $y_j \equiv s_{n,j}\varepsilon_{j,0}(t)$, is the vector of the perturbation amplitudes multiplied by the phase pattern component $s_{n,j}$, and $\mathbf{Q}$, with elements $Q_{j,l}$, is an L by L matrix depending on the distance b, the ratio of viscosities μ, and the wave number k. The stability of the L-threads system is determined by analyzing the structure of the solutions of (4.1.28). Since the dependence on phase pattern $\mathbf{s}_n$ is now included in $\mathbf{y}$ and the time dependence of any $\mathbf{y}$ is determined by the eigenvalues of $\mathbf{Q}$, we may draw conclusions about the (in)stability of all phase patterns at the same time from only calculating the L eigenvalues $q_j, j = 1, \cdots, L$. The eigenvectors $\mathbf{x}_j$ of $\mathbf{Q}$ play an important role. These eigenvectors form a basis for the space of possible initial perturbations $\mathbf{y}(0)$. It should be realized that each $\mathbf{x}_j$ corresponds in a unique way to a phase pattern via the definition

$$\mathbf{s}_j = (\text{sign}(\mathbf{x}_j)_1, \text{sign}(\mathbf{x}_j)_2, \cdots, \text{sign}(\mathbf{x}_j)_L)^T. \tag{4.1.29}$$

We call such a pattern $\mathbf{s}_j$ a *basic phase pattern* and we have L of them. The time evolution of the j-th basic phase pattern is determined by the real part of q_j. Since a general phase pattern is a linear combination of the basic phase patterns, the (in)stability of the system follows from the (in)stability of the basic phase patterns, so from the q_j. The important conclusion is that, instead of optimizing over 2^L phase patterns, it suffices to calculate the L eigenvalues q_j of $\mathbf{Q}$. Per basic phase pattern we can calculate the growth rate $q_{j_{max}}$ by optimizing the real part of q_j over all k. The growth rate q_{max} of the system as

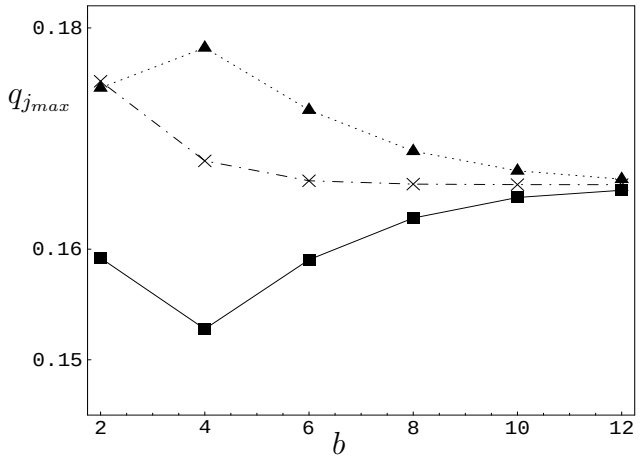

Figure 4.3: *Curves of $q_{j_{max}}$ as functions of b for $\mu = 0.04$. The patterns corresponding to $j = 1, 2$ and 3 are denoted by box, triangle and cross symbols, respectively.*

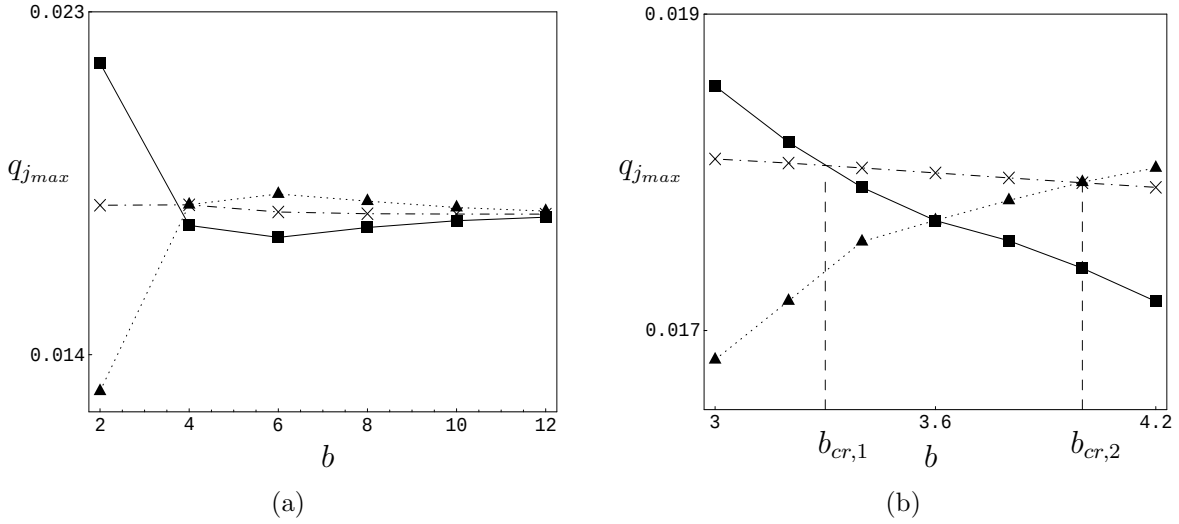

Figure 4.4: *Same information as in Figure 4.3, but now for $\mu = 4$. Part (b) shows the details of the plot in the vicinity of the critical distances.*

a whole is then obtained by taking the maximum of the $q_{j_{max}}$ over $j = 1, \cdots, L$.

As an illustration, let us apply the theory for $L = 3$; this illustrates the general cases satisfactorily. Fixing the geometrical parameter b and the material parameter μ, we calculate the eigenvalues q_j and eigenvectors $\mathbf{x}_j$ of $\mathbf{Q}$ defined by (4.1.27) and (4.1.28). We find that the eigenvectors $\mathbf{x}_1, \mathbf{x}_2$ and $\mathbf{x}_3$ give rise, via (4.1.29), to the basic phase patterns $(1,1,1)^T, (1,-1,1)^T$ and $(1,1,-1)^T$, respectively. In view of symmetry, the pattern $(1,-1,-1)^T$ has the same behaviour as $(1,1,-1)^T$. We calculate the growth rates $q_{1_{max}}$, $q_{2_{max}}$ and $q_{3_{max}}$ by optimizing the eigenvalues q_1, q_2 and q_3 over all wave numbers k. In Figures 4.3 and 4.4 we have plotted $q_{1_{max}}, q_{2_{max}}$ and $q_{3_{max}}$ as functions of b, for two values of μ. The case $\mu = 0.04$ corresponds to a situation in which the threads are less viscous than the surrounding fluid, whereas for $\mu = 4$ it is the other way around. The growth rate q_{max} of the system as a whole is determined by the envelope of the three curves. The figure provides the information in which pattern the break-up will occur. The figures show that this strongly depends on μ and b. For $\mu = 0.04$, $q_{2_{max}}$ is dominant for all b (see Figure 4.3). This implies that the threads will disintegrate out-of-phase. However, for $\mu = 4$, the curves cross at two critical distances $b_{cr,1}$ and $b_{cr,2}$ (see Figure 4.4b). If $b < b_{cr,1}$ the threads will break up in $(1,1,1)^T$ (in-phase) pattern. If $b_{cr,1} < b < b_{cr,2}$ the threads will break up in the $(1,1,-1)^T$ (mixed) pattern, whereas for $b > b_{cr,2}$ the threads will break up $(1,-1,1)^T$ (out-of-phase) pattern.

4.2 Triangular and arbitrary configurations

Here, we show how the method presented above can easily be applied to more intricate configurations. For illustrative purposes we deal with the triangular configuration $\triangle O_1O_2O_3$ shown in Figure 4.5. Take the base line ℓ as the horizontal axis of a system of

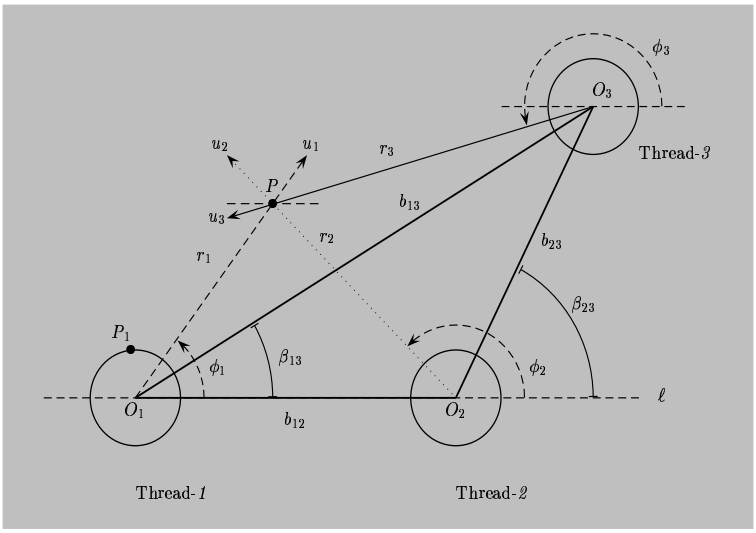

Figure 4.5: *Coordinate system used for the triangular configuration. Extension to arbitrary configurations of L threads directly follows from this figure.*

cylindrical coordinates (r_i, ϕ_i, z) at thread i with ϕ_i measured counterclockwise with respect to ℓ. Moreover, let $b_{ij} = b_{ji}$ be the distance between threads i and j, and $\beta_{ij} = \beta_{ji}$ be the angle between the line from O_i to O_j and the axis ℓ, so, $\beta_{12} = 0$. Scaling the radial direction r_i and the distance $b_{ij} \equiv b_{i,j}$ by a as in (2.2.4), and then omitting the stars notation in the sequel, we obtain the following geometrical relations for $j \neq J$ with $j, J = 1, 2, 3$:

$$r_J \cos\phi_J = r_j \cos\phi_j + \mathrm{sgn}(j-J)\left(\sum_{l=l_m}^{l_M-1} b_{l,l+1}\cos\beta_{l,l+1}\right), \tag{4.2.1a}$$

$$r_J \sin\phi_J = r_j \sin\phi_j + \mathrm{sgn}(j-J)\left(\sum_{l=l_m}^{l_M-1} b_{l,l+1}\sin\beta_{l,l+1}\right), \tag{4.2.1b}$$

where $l_m = \min\{j, J\}$ and $l_M = \max\{j, J\}$, and $\mathrm{sgn}(j-J)$ is the sign function defined as

$$\mathrm{sgn}(j-J) = \begin{cases} -1, & j < J, \\ 0, & j = J, \\ 1, & j > J. \end{cases} \tag{4.2.2}$$

From Figure 4.5, we also obtain the relations:

$$r_J \cos(\phi_J - \beta_{Jj}) = r_j \cos(\phi_j - \beta_{Jj}) + \mathrm{sgn}(j-J) b_{Jj}, \tag{4.2.3a}$$

$$r_J \sin(\phi_J - \beta_{Jj}) = r_j \sin(\phi_j - \beta_{Jj}). \tag{4.2.3b}$$

These relations are needed when evaluating the boundary conditions at the interfaces.

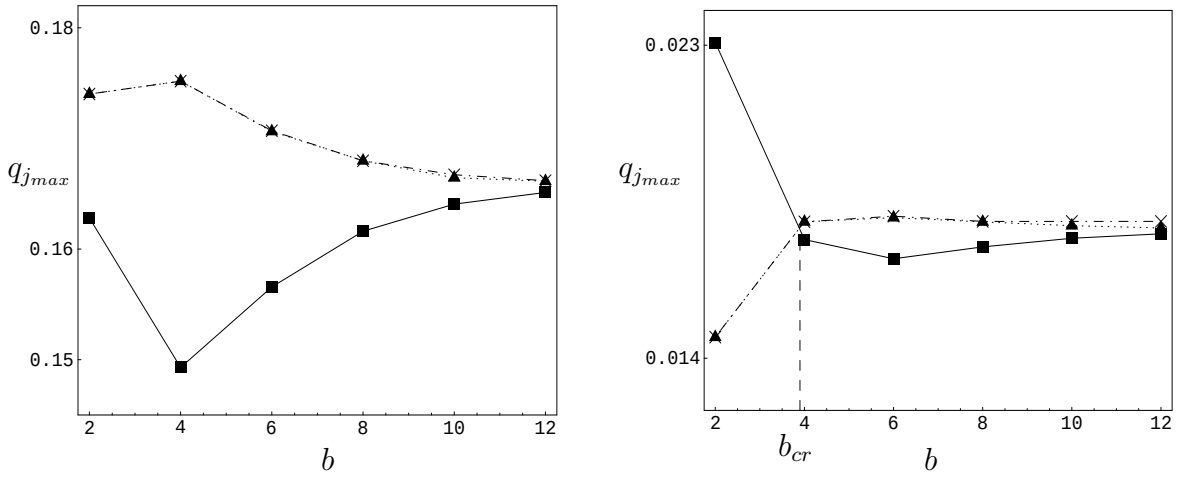

(a) $\mu = 0.04$. (b) $\mu = 4$.

Figure 4.6: *Same information as in Figure 4.3, but now for the equilateral triangle configuration.*

The ideas for solving the creeping flow approximation are similar to those in previous section. Let us outline the method:

- Take (r_J, ϕ_J, z) as frame of reference and take as general expressions for the solutions for the radial velocity, for $j \neq J$ with $j, J = 1, 2, 3$:

$$u_j(r_j, \phi_j, z, t) = \left(\sum_{m=0}^{\infty} u_{j,m}(r_j, t) \cos m(\phi_j - \beta_{Jj}) \right) \cos(k_j z - \alpha_j), \tag{4.2.4}$$

  and analogous for v_j, w_j and p_j. As above, the solutions for the Fourier coefficients are given by (2.2.17) and (2.2.18).

- Next, use for the continuous phase of the whole system vector addition of the velocities and scalar addition of pressures. Evaluation of these additions leads to formulas like in (4.1.5). The evaluation of boundary conditions leads to $k_j = k$ for all j's and all phase patterns. The evaluation also implies that the product of Bessel functions and a Fourier expansion with respect to thread $j \neq J$, should be expressed as a product of functions with respect to thread J. To this end, we use Graf's addition theorem and the relations (4.2.1) and (4.2.3). To find a finite set of equations for the unknowns we apply the method of moments to obtain (4.1.28). But now, the components of the matrix $\mathbf{H}$ in (4.1.19) are $\mathbf{H}_{ij}$, given in Appendix B.4, and $\mathbf{H}_{00} \equiv \mathbf{H}_0$. From this point, the analysis is similar to the case of equally spaced threads in a row.

To illustrate the method, we first consider three threads at the vertices of an equilateral triangle. So, we take in Figure 4.5, $b_{12} = b_{23} = b$ and $\beta_{23} = 2\pi/3$. Fixing b and μ, we calculate the eigensystem $\{q_j, \mathbf{x}_j\}$ of $\mathbf{Q}$. The growth rates $q_{j_{max}} = \max_k \{q_j(b; \mu)\}$ as

functions of b are shown in Figure 4.6 for two values of μ. In view of the symmetry of the system, we see that the growth rate $q_{2_{max}}$ for the pattern $(1,-1,1)^T$ coincides with $q_{3_{max}}$ for the pattern $(1,1,-1)^T$. Since the system has a lot of symmetry, it breaks up in two basic patterns only. In the in-phase pattern all threads break up with the same phase, whereas out-of-phase break-up occurs if one thread has a phase difference with respect to the other two. For $\mu = 0.04$, we find that the system will break up out-of-phase for all b. For $\mu = 4$, we find a critical distance b_{cr} such that the system will break up either in-phase or out-of-phase.

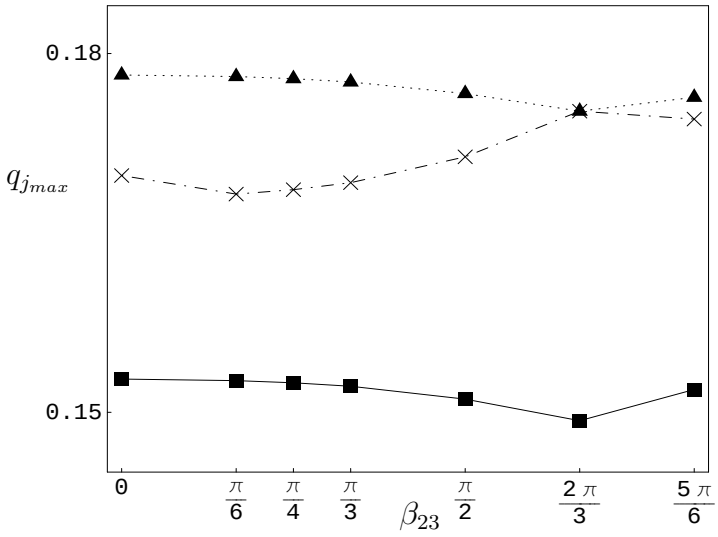

Figure 4.7: *Curves of $q_{j_{max}}$ as functions of β_{23} for $\mu = 0.04$ and $b_{12} = b_{23} = 4$. The patterns corresponding to $j = 1, 2$ and 3 are denoted by box, triangle and cross symbols, respectively.*

We also calculate $q_{j_{max}}$ for non-equilateral triangle configurations by varying the angle β_{23}, keeping b_{12} and b_{23} equal to each other. In Figures 4.7 and 4.8 we plot $q_{j_{max}}$ as functions of β_{23} for two values of μ. For $\mu = 0.04$ and $b_{12} = b_{23} = 4$, we see that the $(1,-1,1)^T$ pattern is dominant for all values of β_{23} (see Figure 4.7). In Figure 4.8(a) for $\mu = 4$, we find that $\beta_{23} = 2\pi/3$ is a critical angle in the sense that for $\beta_{23} < 2\pi/3$ the $(1,1,-1)^T$ pattern is dominant and for $2\pi/3 < \beta_{23} < \pi$ the $(1,-1,1)^T$ pattern. This critical angle depends on the value of b_{12} $(= b_{23})$, e.g. for $\mu = 4$ and $b_{12} = b_{23} = 3$ the pattern $(1,1,1)^T$ is always dominant as shown in Figure 4.8b. In Figures 4.7 and 4.8 we see that the growth rates of the patterns $(1,-1,1)^T$ and $(1,1,-1)^T$ are the same for $\beta_{23} = 2\pi/3$ since then the system has optimal symmetry.

For a system of L threads at random positions, the analysis directly follows from the triangular-thread system. The relations (4.1.5), (4.2.1) and (4.2.3) still hold. Again, there are 2^L phase patterns, which are all essentially different if the configuration does not posses any symmetry. However, for the stability of the system one has to calculate only the stability of L basic phase patterns.

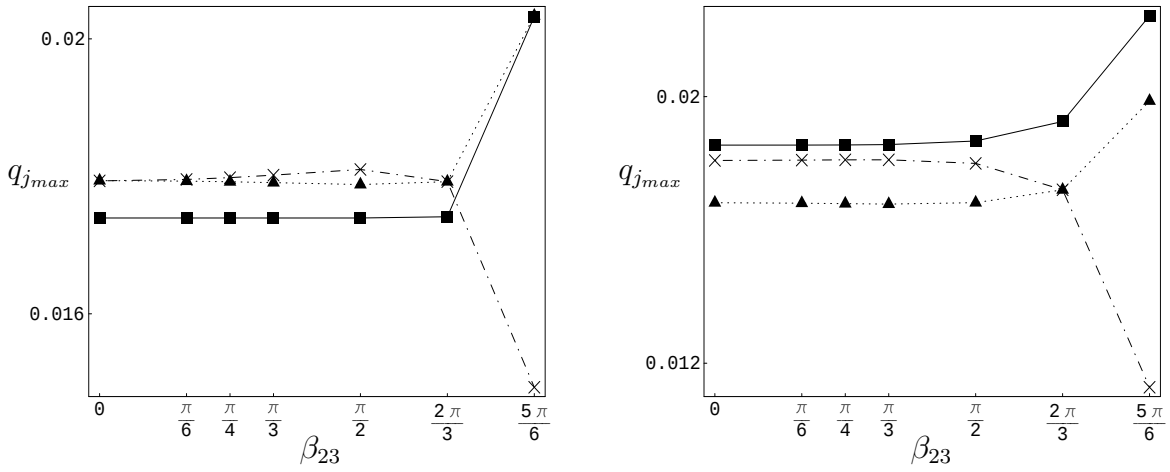

(a) $b_{12} = b_{23} = 4$. (b) $b_{12} = b_{23} = 3$.

Figure 4.8: *Same information as in Figure 4.7, but now for $\mu = 4$, and for two values of the side length.*

4.3 The special case $\mu = 1$ for a set of threads on a row

If threads and surrounding fluid have equal viscosities, $\eta^d = \eta^c = \eta$, so $\mu = 1$, the stability of the system can be established analytically. We shall work out the method in some detail for an arbitrary number of threads on a row. Following the ideas of Stone & Brenner (1996) for the one-thread system, we first focus on the jump S in the normal stress across the interface. For thread j, this jump is given by (compare with (2.3.32))

$$S_j = \frac{\sigma}{a} \sum_{m=0}^{\infty} (1 - (k_j a)^2 - m^2) \varepsilon_{j,m}(t) \cos m\phi_i \cos(k_j z - \alpha_j), \tag{4.3.1}$$

where σ is the surface tension. The idea is to include the jump as a discrete hoop force into the momentum equation:

$$\text{grad } p_j = \eta \text{ div } (\text{grad } \mathbf{v}_j)^T + \mathbf{e}_r \delta(r_j - a) S_j \ . \tag{4.3.2}$$

Here, $\delta(r_j - a)$ is the delta-function and $\mathbf{e}_r$ is the unit vector in the radial direction. Using (2.2.4), expansions like in (4.1.3) and the scaling:

$$S_j = \frac{\sigma}{a} S_j^*, \tag{4.3.3}$$

we obtain equations for the components of (4.3.2) and eventually we arrive at an extension of (2.2.6), reading

$$0 = \frac{1}{r_j}\frac{\partial\left[r_j u_{j,m}\right]}{\partial r_j} + \frac{m}{r_j}v_{j,m} + k_j w_{j,m}, \tag{4.3.4a}$$

$$\frac{\partial p_{j,m}}{\partial r_j} = \frac{1}{r_j}\frac{\partial}{\partial r_j}\left[r_j\frac{\partial u_{j,m}}{\partial r_j}\right] - \frac{m^2+1+(k_j r_j)^2}{r_j^2}u_{j,m} - \frac{2m}{r_j^2}v_{j,m} + \delta(r_j-1)(1-k_j^2-m^2)\varepsilon_{j,m}, \tag{4.3.4b}$$

$$-\frac{m}{r_j}p_{j,m} = \frac{1}{r_j}\frac{\partial}{\partial r_j}\left[r_j\frac{\partial v_{j,m}}{\partial r_j}\right] - \frac{m^2+1+(k_j r_j)^2}{r_j^2}v_{j,m} - \frac{2m}{r_j^2}u_{j,m}, \tag{4.3.4c}$$

$$-k_j p_{j,m} = \frac{1}{r_j}\frac{\partial}{\partial r_j}\left[r_j\frac{\partial w_{j,m}}{\partial r_j}\right] - \frac{m^2+(k_j r_j)^2}{r_j^2}w_{j,m}. \tag{4.3.4d}$$

Combining (4.3.4b) and (4.3.4c), we obtain

$$\frac{\partial p_{j,m}}{\partial r_j} - \frac{m}{r_j}p_{j,m} = \left(\frac{1}{r_j}\frac{\partial}{\partial r_j}\left[r_j\frac{\partial}{\partial r_j}\right] - \frac{(m+1)^2+(k_j r_j)^2}{r_j^2}\right)(u_{j,m}+v_{j,m}) + \delta(r_j-1)(1-k_j^2-m^2)\varepsilon_{j,m}\ , \tag{4.3.5a}$$

$$\frac{\partial p_{j,m}}{\partial r_j} + \frac{m}{r_j}p_{j,m} = \left(\frac{1}{r_j}\frac{\partial}{\partial r_j}\left[r_j\frac{\partial}{\partial r_j}\right] - \frac{(m-1)^2+(k_j r_j)^2}{r_j^2}\right)(u_{j,m}-v_{j,m}) + \delta(r_j-1)(1-k_j^2-m^2)\varepsilon_{j,m}\ . \tag{4.3.5b}$$

These equations together with (4.3.4a) and (4.3.4d) can be solved by means of Hankel transforms. Let us denote these transforms and their inverses by

$$F_{j,n}^m(s) \equiv \int_0^\infty r_j J_m(sr_j) f_{j,n}(r_j)dr_j, \quad f_{j,n}(r_j) \equiv \int_0^\infty s J_m(sr_j)F_{j,n}^m(s)ds. \tag{4.3.6}$$

Here, J_m is the Bessel function of the first kind of order m. Applying the Hankel transform to succesively (4.3.4a), (4.3.5a), (4.3.5b) and (4.3.4d), we obtain a system of linear equations in the variables $(U_{j,m}^{m+1}+V_{j,m}^{m+1})$, $(U_{j,m}^{m-1}-V_{j,m}^{m-1})$, $W_{j,m}^m$ and $P_{j,m}^m$:

$$0 = \frac{s}{2}[(U_{j,m}^{m+1}+V_{j,m}^{m+1}) - (U_{j,m}^{m-1}-V_{j,m}^{m-1})] + k_j W_{j,m}^m, \tag{4.3.7a}$$

$$sP_{j,m}^m = (s^2+k_j^2)(U_{j,m}^{m+1}+V_{j,m}^{m+1}) - (1-k_j^2-m^2)J_{m+1}(s)\varepsilon_{j,m}, \tag{4.3.7b}$$

$$-sP_{j,m}^m = (s^2+k_j^2)(U_{j,m}^{m-1}-V_{j,m}^{m-1}) - (1-k_j^2-m^2)J_{m-1}(s)\varepsilon_{j,m}, \tag{4.3.7c}$$

$$k_j P_{j,m}^m = (s^2+k_j^2)W_{j,m}^m. \tag{4.3.7d}$$

Solving these linear equations and taking the inverse Hankel transform, we find for the m-th mode of the radial and azimuthal velocities

$$u_{j,m} = \frac{(1-k_j^2-m^2)\varepsilon_{j,m}}{4}\left[\int_0^\infty \frac{s^3+2k_j^2 s}{(s^2+k_j^2)^2}\Big(J_{m+1}(s)J_{m+1}(sr_j)+J_{m-1}(s)J_{m-1}(sr_j)\Big)ds\right.$$
$$\left. + \int_0^\infty \frac{s^3}{(s^2+k_j^2)^2}\Big(J_{m-1}(s)J_{m+1}(sr_j)+J_{m+1}(s)J_{m-1}(sr_j)\Big)ds\right], \qquad (4.3.8a)$$

$$v_{j,m} = \frac{(1-k_j^2-m^2)\varepsilon_{j,m}}{4}\left[\int_0^\infty \frac{s^3+2k_j^2 s}{(s^2+k_j^2)^2}\Big(J_{m+1}(s)J_{m+1}(sr_j)-J_{m-1}(s)J_{m-1}(sr_j)\Big)ds\right.$$
$$\left. + \int_0^\infty \frac{s^3}{(s^2+k_j^2)^2}\Big(J_{m-1}(s)J_{m+1}(sr_j)-J_{m+1}(s)J_{m-1}(sr_j)\Big)ds\right]. \qquad (4.3.8b)$$

Application of formula 13.53(6) in Watson (1966) (an example of these evaluations is given in Appendix C.2) leads to, for $r_j > 1$,

$$u_{j,m} = \frac{(1-k_j^2-m^2)}{4}\varepsilon_{j,m}\left[\frac{1}{2k_j}\frac{d}{dk_j}\left[k_j^2\Big(I_{m+1}(k_j)K_{m+1}(k_jr_j)+I_{m-1}(k_j)K_{m-1}(k_jr_j)\Big)\right]\right.$$
$$-k_j\frac{d}{dk_j}\Big[I_{m+1}(k_j)K_{m+1}(k_jr_j)+I_{m-1}(k_j)K_{m-1}(k_jr_j)\Big]$$
$$\left.-\frac{1}{2k_j}\frac{d}{dk_j}\Big[k_j^2\Big(I_{m-1}(k_j)K_{m+1}(k_jr_j)+I_{m+1}(k_j)K_{m-1}(k_jr_j)\Big)\Big]\right], \qquad (4.3.9a)$$

$$v_{j,m} = \frac{(1-k_j^2-m^2)}{4}\varepsilon_{j,m}\left[\frac{1}{2k_j}\frac{d}{dk_j}\left[k_j^2\Big(I_{m+1}(k_j)K_{m+1}(k_jr_j)-I_{m-1}(k_j)K_{m-1}(k_jr_j)\Big)\right]\right.$$
$$-k_j\frac{d}{dk_j}\Big[I_{m+1}(k_j)K_{m+1}(k_jr_j)-I_{m-1}(k_j)K_{m-1}(k_jr_j)\Big]$$
$$\left.-\frac{1}{2k_j}\frac{d}{dk_j}\Big[k_j^2\Big(I_{m-1}(k_j)K_{m+1}(k_jr_j)-I_{m+1}(k_j)K_{m-1}(k_jr_j)\Big)\Big]\right]. \qquad (4.3.9b)$$

Here, I_m and K_m are the modified Bessel functions. As a check on these intermediate results, we consider the $m = 0$ mode. The result is the zero-order Fourier mode of the radial velocity, given by

$$u_j(r_j,z) = k_j^2(1-k_j^2)\left(\int_0^\infty \frac{sJ_1(s)J_1(sr_j)}{(s^2+k_j^2)^2}ds\right)\varepsilon_{j,0}(t)\cos(k_jz-\alpha_j). \qquad (4.3.10)$$

Rescaling to the full dimensions and taking $\alpha_j = 0$, we find that (4.3.10) is in agreement with the work of Stone & Brenner (1996) for the axisymmetric breakup of a single liquid thread.

Next, consider L threads on a row, equally spaced with distances b. We shall restrict the discussion to the zero-mode solution, which implies $v_j = 0$. The radial velocity for the whole system is represented by (4.1.5b), with thread J as frame of reference. Hereafter, we omit the superscript c in (4.1.5b) since the fluids have equal viscosities. At the interface of thread J, substitution of (4.3.9a) for $m = 0$ into (4.1.5b) and application of Graf's addition theorem yield

$$u_{(J)} = A_{0,0}(k_J)\varepsilon_{J,0}(t)\cos k_J z + \sum_{j\neq J}\left(\sum_{n=-\infty}^{\infty} A_{n,j-J}(k_j,b)\cos n\phi_J\right)\varepsilon_{j,0}(t)\cos(k_j z - \alpha_j), \tag{4.3.11}$$

where

$$A_{0,0}(k_J) = -\frac{k_J(1-k_J^2)}{2}\frac{d}{dk_J}\Big[I_1(k_J)K_1(k_J)\Big], \tag{4.3.12}$$

and

$$A_{n,j-J}(k_j,b) = \frac{k_j(1-k_j^2)}{2}\frac{d}{dk}\Big[I_1(k_j)K_n(|j-J|k_j b)I_{n-1}(k_J)\Big]. \tag{4.3.13}$$

Note that $A_{n,j-J} = A_{n,J-j}$. On the other hand, according to (4.1.2) for $m = 0$ the interfacial velocity is given by

$$u_{(J)} = \dot{\varepsilon}_{J,0}(t)\cos k_J z. \tag{4.3.14}$$

Here, the overdot represents the derivative with respect to time t. Combining (4.3.11)) and (4.3.14), we obtain

$$(A_{0,0}(k_j)\varepsilon_{J,0}(t) - \dot{\varepsilon}_{J,0}(t))\cos k_J z + \sum_{j\neq J}\left(\sum_{n=-\infty}^{\infty} A_{n,j-J}(k_j,b)\cos n\phi_J\right)\varepsilon_{j,0}(t)\cos(k_j z - \alpha_j) = 0. \tag{4.3.15}$$

Condition (4.3.15) is only satisfied for all z if $k_j = k$ for all j. Moreover, α_j only takes the values 0 or π. Integration of (4.3.15) over the interval $[0, 2\pi]$ leads to

$$\dot{\varepsilon}_{J,0}(t) = A_{0,0}(k)\varepsilon_{J,0}(t) + \sum_{j\neq J} s_{n,j}A_{0,j-J}(k,b)\varepsilon_{j,0}(t), \tag{4.3.16}$$

with $s_{n,j}$ defined as in (4.1.7). Since we chose $s_{n,J} = 1$, we rewrite (4.3.16) as

$$s_{n,J}\dot{\varepsilon}_{J,0}(t) = \sum_{j=1}^{L} s_{n,j}A_{j-J}\varepsilon_{j,0}(t), \quad \text{with} \quad A_{j-J} \equiv A_{0,j-J}. \tag{4.3.17}$$

Combination of all equations leads to a system of equations

$$\frac{d\mathbf{y}}{dt} = \mathbf{Q}(b,\mu,k)\mathbf{y}, \tag{4.3.18}$$

where

$$\mathbf{Q} = \begin{pmatrix} A_0 & A_1 & A_2 & \cdots & A_{L-2} & A_{L-1} \\ A_1 & A_0 & A_1 & \cdots & \cdots & A_{L-2} \\ \vdots & \vdots & \vdots & \vdots & \vdots & \vdots \\ \vdots & \vdots & \vdots & \vdots & \vdots & \vdots \\ A_{L-2} & \cdots & \cdots & A_1 & A_0 & A_1 \\ A_{L-1} & A_{L-2} & \cdots & A_2 & A_1 & A_0 \end{pmatrix} \text{ and } \mathbf{y} \equiv \begin{pmatrix} s_{n,1}\varepsilon_{1,0}(t) \\ s_{n,2}\varepsilon_{2,0}(t) \\ \vdots \\ s_{n,L}\varepsilon_{L,0}(t) \end{pmatrix}. \quad (4.3.19)$$

The stability of the system is determined by the eigenvalues of $\mathbf{Q}$. For $L = 2$, the eigenvalues are simply given by

$$q^+ = A_0 + A_1, \text{ and } q^- = A_0 - A_1, \quad (4.3.20)$$

with eigenvectors $\mathbf{x}^+ = (1,1)^T$ and $\mathbf{x}^- = (1,-1)^T$, respectively. The $q^+(q^-)$ are the growth rates of in-phase (out-of-phase) perturbations. Evaluating A_0 and A_1, we obtain

$$\begin{aligned} q^{\pm}(k,b) &= (1-k^2)\Bigg[I_1(k)K_1(k) + \frac{k}{2}\Big(I_1(k)K_0(k) - I_0(k)K_1(k)\Big) \\ &\quad \pm I_1(k)\Bigg([kI_0(k) - I_1(k)]K_0(kb) - \frac{kb}{2}I_1(k)K_1(kb)\Bigg)\Bigg]. \end{aligned} \quad (4.3.21)$$

If $b \to \infty$, when the system approaches the single thread case, the second term of (4.3.21) vanishes and we arrive at the result of Stone & Brenner (1996). To determine the stability of the two-threads system, we can easily calculate the growth rate q_{max} by optimizing over k: $q_{max}(b) = \max_k\{q^+(k;b), q^-(k;b)\}$.

For L large enough, we can find an upper bound for q_{max}. In view of the Toeplitz form of matrix (4.3.19), we may exploit the following property (Widom (1965)). Let the 2π-periodic function $h(\theta)$ be given by

$$h(\theta) = A_0 + 2\sum_{n=1}^{L-1} A_n \cos n\theta, \quad (4.3.22)$$

then the eigenvalues of $\mathbf{Q}$ in (4.3.19) are contained in the interval $[M_1, M_2]$ where $M_1 = \min_{0\le\theta\le 2\pi} h(\theta)$, $M_2 = \max_{0\le\theta\le 2\pi} h(\theta)$. Since $h(\theta)$ is bounded from above by

$$h(\theta) < |A_0| + 2\sum_{n=1}^{L-1} |A_n|, \quad (4.3.23)$$

we may take

$$\overline{q}(a,k,b) = |A_0| + 2\sum_{n=1}^{L-1} |A_n| \quad (4.3.24)$$

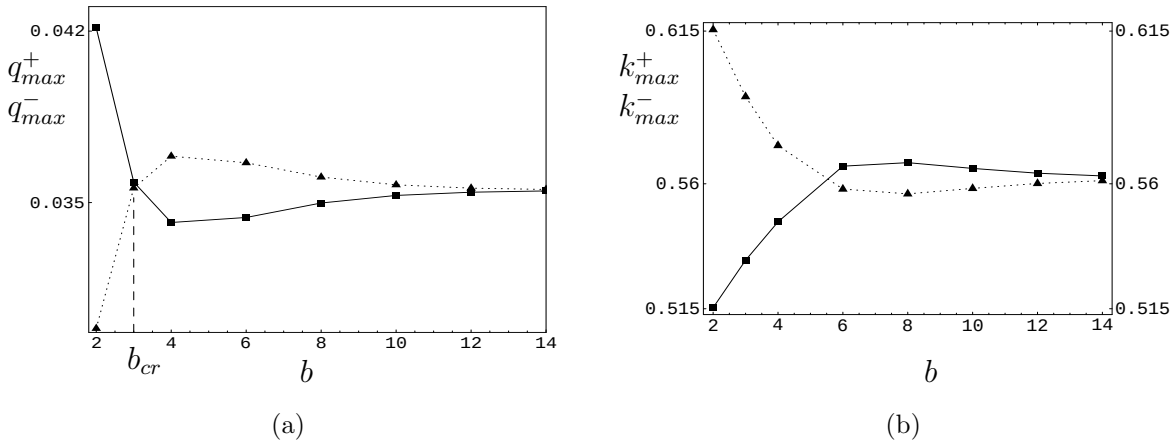

Figure 4.9: *Curves of the growth rates q^+_{max} (box) and q^-_{max} (triangle) and the corresponding wave numbers $k^\pm_{max}$ as functions of b for the two-threads system.*

as an upper bound, for the maximum growth rate q_{max}.

As an illustration, results for $L = 2$ are calculated. For convenience, we define $q^\pm_{max}(b) \equiv \max_k\{q^\pm(k;b)\}$. The functions $q^\pm_{max}(b)$ are plotted in Figure 4.9(a). We see that there exists a critical distance b_{cr} at which the dominant behaviour changes. As extra information we give in Figure 4.9(b) plots of $k^+_{max}(b)$ and $k^-_{max}(b)$, which are defined as those k values for which $q^+(k,b)$ and $q^-(k,b)$ attain their maximum values $q^+_{max}(b)$ and $q^-_{max}(b)$, respectively. The growth rate is given by the envelope of these curves, so by $q_{max}(b) = \max_k\{q^+(k;b), q^-(k;b)\}$ and shown in Figure 4.10. In the latter picture we present results for q_{max} for the cases $L = 2$, $L = 3$ and $L = 10$. We also calculate the values for the upper bound $\overline{q}_{max}$ for $L = 2$ and 10 as shown in Figure 4.11. Comparing the results for $\overline{q}_{max}$ and q_{max} in Figure 4.11, we conclude that the upper bound $\overline{q}_{max}$ is a good approximation for the maximum growth rate q_{max}, especially if $b \geq 3$.

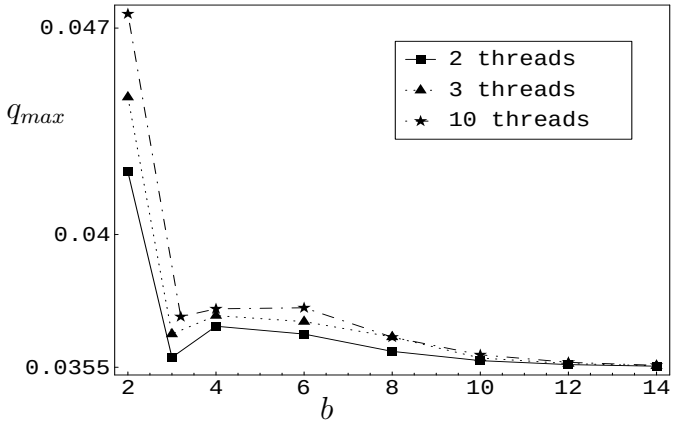

Figure 4.10: *Curves of q_{max} as functions of b for systems with 2, 3 and 10 threads.*

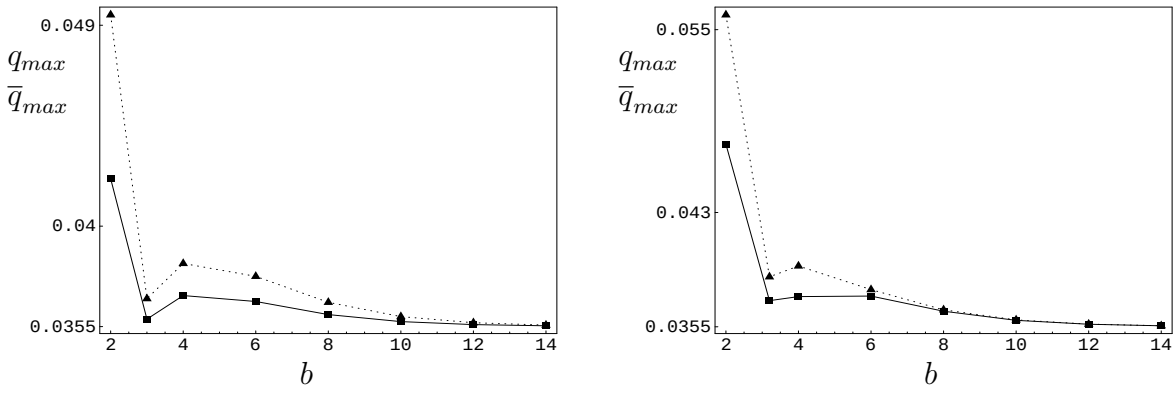

(a) Two threads.

(b) Ten threads.

Figure 4.11: *Comparison of calculated values of q_{max} (box) with the values of the upper bound $\overline{q}_{max}$ (triangle) for two and ten threads.*

4.4 Conclusions

In this chapter, we have shown how the problem of the break-up of an arbitrary number of interacting immersed threads can be tackled. By showing the principles of the theory for a row and a triangular configuration, we could explain how arbitrary configurations have to be treated. The two most general conclusions are as follows. First, all threads break up either in-phase or with a phase difference of π, i.e. out-of-phase, with respect to the other threads. This implies that for a system with L threads, there are in principle 2^L phase patterns for break-up possible. However, since in practice any perturbation will tend to destabilize the system in a random fashion, the phase pattern with the highest growth rate will win and will be observed. In this chapter, we extensively show how the growth rates of phase patterns can be calculated. In principle, this would involve optimization over all possible phase patterns. Our second general conclusion is that the latter is not necessary, but that the optimization involves only the L so-called basic phase patterns. This reduces the amount of work considerably.

By applying the theory to specific cases, we find that in general the ratio of viscosities of threads and solvent is a highly determining factor. If the threads are less viscous than the solvent, the break-up pattern with the threads out-of-phase is the most unstable one. If the threads are more viscous than the solvent, it is found that not one pattern is dominant. Then, it heavily depends on the details of the configuration which pattern will win. The system is found to exhibit a wealth of bifurcations: if a geometrical parameter is slightly varied, the system may suddenly change from one break-up pattern to another. For blending of viscous material this is important information, since out-of-phase patterns are more favourable for obtaining "regular" morphologies than in-phase patterns.

We have also derived an analytical expression to estimate the growth rate for the special case of fluids having equal viscosity. For L threads on a row, we found an

analytical upper bound, and we showed via numerical simulations that this upper bound is a good estimate for the maximum growth rate.

Chapter 5

Stability of one non-Newtonian thread

In this chapter, we consider an infinitely long viscoelastic thread in a tube filled with a Newtonian fluid. We take Jeffreys model as the constitutive relation for the thread. The thread moves due to a constant pressure gradient and does not bend or twist. We investigate the effect of fluid elasticity, confinement and prescribed flow on the stability of the immersed thread. The fluid elasticity of the thread is represented by two parameters: the Deborah number De, i.e. the ratio of the stress relaxation time to the capillary time scale, and the material constant Λ, i.e. the ratio of retardation time to stress relaxation time. The effect of the confinement is represented by the dimensionless length h, i.e. the ratio between the radius of the thread and the radius of the tube. The flow is characterized by the uniform constant pressure-gradient $\mathrm{C_p}$.

5.1 Mathematical formulation and solution methodology

5.1.1 Mathematical formulation

Let us consider a long, neutrally buoyant, linear viscoelastic thread of radius a_1 and zero shear viscosity η_0^d, immersed in a tube of radius a_2 filled with a Newtonian fluid of viscosity η_0^c. We take cylindrical coordinates (r, ϕ, z) with the z-axis along the thread axis. The indices c and d stand for the continuous phase (the surrounding fluid) and the dispersed phase (the thread), respectively. The fluids are assumed to be incompressible. Both phases are assumed to be mutually immiscible, and no external body forces are present. The thread moves due to a constant pressure gradient in longitudinal direction only, but so slowly that the creeping flow approximation (2.1.3) is applicable. The domain of the system is sketched in Figure 5.1.

For the thread, we take as constitutive relation a linear viscoelastic model, the so called Jeffreys model (T indicates the transpose):

$$\left(1+\lambda_1\frac{\partial}{\partial t}\right)\boldsymbol{\tau}^d \;=\; \eta_0^d\left(1+\lambda_2\frac{\partial}{\partial t}\right)\left(\text{grad }\mathbf{v}^d+(\text{grad }\mathbf{v}^d)^T\right). \tag{5.1.1}$$

Here, λ_1 is the stress relaxation time, and λ_2 is the deformation retardation time of

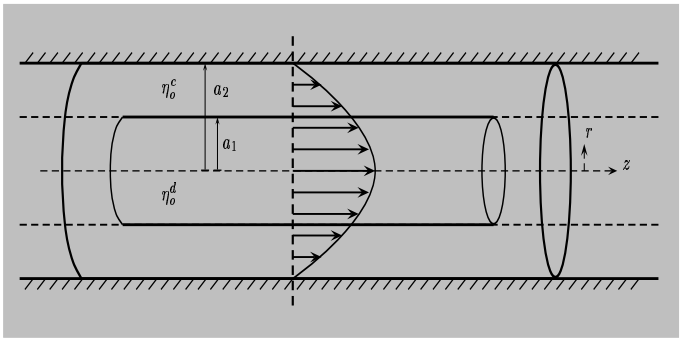

Figure 5.1: *A thread of radius a_1 with viscosity η_0^d in a tube of radius a_2 filled with a fluid with viscosity η_0^c.*

the thread. Note that $\lambda_1 > \lambda_2$ (this is necessary from thermodynamic considerations, since there are no energy sources within the fluid (see Harris (1977))). In the steady unperturbed state, the constitutive equation (5.1.1) reduces to the constitutive equation for a Newtonian fluid. For the surrounding Newtonian fluid, we have

$$\boldsymbol{\tau}^c = \eta_0^c \, [\text{grad } \mathbf{v}^c + (\text{grad } \mathbf{v}^c)^T], \tag{5.1.2}$$

and a similar relation holds for the unperturbed extra stress $\mathbf{\Gamma}^c$ (see (2.1.4).

As unperturbed state, we take the thread to be a perfect cylinder. Its stability is tested by applying a small perturbation. Since the thread does not bend or twist, we apply an axisymmetric perturbation. Thus, the perturbed thread surface is represented by (compare to (2.3.1))

$$R(z,t) = a_1\Big[1 + \epsilon f(z,t)\Big], \quad \text{where} \quad f(z,t) = \Re[\varepsilon_0 e^{ikz+qt}], \tag{5.1.3}$$

with ε_0 the initial amplitude of the perturbation and ϵ a small parameter ($0 < \epsilon \ll 1$). The parameter k represents the wave number of the perturbation, $i = \sqrt{-1}$ is the imaginary unit number, t is the time, and q is the growth rate of the perturbation. The growth rate determines the (linear) stability of the thread. Note that k must be real since the solution is periodic in the z-direction, whereas q can be complex. In the sequel we shall not write the real part symbol '$\Re$' explicitly.

Since we are interested in the dynamics of the perturbed thread, we shall write the solution in the form of (2.1.4). For the axisymmetric case, we take $\mathbf{V} = (U, W)$ as the unperturbed velocity, with U and W the velocity components in radial and axial directions, respectively. Also, $\mathbf{v} = (u, w)$, but now for the perturbed velocity.

As for the boundary conditions: at the wall of the tube we assume the no-slip condition:

$$\mathbf{V} = \mathbf{0} = \mathbf{v}, \quad \text{at } r = a_2. \tag{5.1.4}$$

At the interface, we apply the interfacial conditions derived in Section 2.1.2.

5.1.2 The steady unperturbed solution

The steady unperturbed solution is derived from the solution of the Poiseuille flow. Let $\mathrm{C_p} = dP/dz$ (in Newton/meter^3) be a *constant* pressure gradient for both phases. In the steady state, relation (5.1.1) reduces to the constitutive equation for a Newtonian thread with viscosity η_0^d. So, the general solution of the Poiseuille flow is given by $\mathbf{V} = (0, W(r))$ (a fully developed flow), where

$$W(r) = \frac{1}{4\widehat{\eta}}\mathrm{C_p}r^2 + A\ln\left(\frac{r}{a_2}\right) + B. \tag{5.1.5}$$

Here, $\widehat{\eta} = \eta_0^d$ for the thread and $\widehat{\eta} = \eta_0^c$ for the surrounding fluid. The constants A and B are to be determined from the boundary conditions, and take different values in the two phases. At the origin the solution must remain bounded. At the wall and the interface, we have

$$W(a_2) = 0, \tag{5.1.6a}$$

$$[\![W]\!] = 0, \tag{5.1.6b}$$

$$[\![\Pi_{rz}]\!] = \left[\!\!\left[\widehat{\eta}\frac{\partial W}{\partial r}\right]\!\!\right] = 0\ , \tag{5.1.6c}$$

$$[\![\Pi_{rr}]\!] = [\![-P]\!] = -\frac{\sigma}{a_1}\ . \tag{5.1.6d}$$

Evaluating the boundary conditions, we find for (5.1.5)

$$W = \begin{cases} -\dfrac{a_2^2}{4\eta_0^c}\mathrm{C_p}\left[1 + \dfrac{1-\mu_0}{\mu_0}\left(\dfrac{a_1}{a_2}\right)^2 - \dfrac{1}{\mu_0}\left(\dfrac{r}{a_2}\right)^2\right], & 0 \le r \le a_1, \\ -\dfrac{a_2^2}{4\eta_0^c}\mathrm{C_p}\left[1 - \left(\dfrac{r}{a_2}\right)^2\right], & a_1 \le r \le a_2. \end{cases} \tag{5.1.7}$$

and

$$P = \begin{cases} \mathrm{C_p}z + \dfrac{\sigma}{a_1}, & 0 \le r \le a_1, \\ \mathrm{C_p}z, & a_1 \le r \le a_2. \end{cases} \tag{5.1.8}$$

Here, we have defined

$$\mu_0 = \frac{\eta_0^d}{\eta_0^c}\ , \tag{5.1.9}$$

as the ratio of the zero shear-rate viscosities of both fluids. For convenience, the expressions are brought into dimensionless form. Since we are interested in the influence of the surface tension σ on the stability of the system, we may use it as a scaling factor. So, as units of distance, velocity, and stress components, we take a_1, σ/η_0^c, and σ/a_1, respectively. For instance, we have

$$r = a_1 r^*,\ \mathbf{u} = \frac{\sigma}{\eta_0^c}\mathbf{u}^*,\ \boldsymbol{\tau} = \frac{\sigma}{a_1}\boldsymbol{\tau}^*,\ k = \frac{k^*}{a_1},\ \text{ and }\ t = \frac{a_1\eta_0^c}{\sigma}t^*. \tag{5.1.10}$$

With (5.1.10), the dimensionless pressure gradient ${\mathrm{C_p}}^*$ and the dimensionless growth rate q^* become

$${\mathrm{C_p}}^* = \frac{a_1^2}{\sigma}\mathrm{C_p}, \tag{5.1.11a}$$

$$q^* = \frac{a_1\eta_0^c}{\sigma}q. \tag{5.1.11b}$$

In the sequel, we omit the stars since confusion is not possible. In non-dimensional form we have

$$W = \begin{cases} -\dfrac{\mathrm{C_p}}{4}\left[h^2 + \dfrac{1-\mu_0-r^2}{\mu_0}\right], & 0 \le r \le 1, \\ -\dfrac{\mathrm{C_p}}{4}\left[h^2 - r^2\right], & 1 \le r \le h. \end{cases} \tag{5.1.12}$$

and

$$P = \begin{cases} \mathrm{C_p}z + 1, & 0 \le r \le 1, \\ \mathrm{C_p}z, & 1 \le r \le h. \end{cases} \tag{5.1.13}$$

Here, we have introduced the dimensionless length h by

$$h = \frac{a_2}{a_1}. \tag{5.1.14}$$

The closer h is to 1, the narrower is the gap, i.e. the smaller the distance between the outer surface of the thread and the wall of the tube.

We calculate the derivative of W with respect to r and obtain

$$\frac{\partial W}{\partial r} = \begin{cases} \dfrac{\mathrm{C_p}}{2\mu_0}r, & 0 \le r \le 1, \\ \dfrac{\mathrm{C_p}}{2}r, & 1 \le r \le h. \end{cases} \tag{5.1.15}$$

Note that (5.1.15) has a discontinuity at $r = 1$, except for $\mu_0 = 1$.

5.1.3 The perturbed solution

The perturbed equations are

$$\operatorname{div}\,\mathbf{v} = 0. \tag{5.1.16a}$$

$$\operatorname{grad}\,p = \operatorname{div}\,\boldsymbol{\tau}. \tag{5.1.16b}$$

In dimensionless form, we may write (5.1.1) as

$$\left(1 + \mathrm{De}\frac{\partial}{\partial t}\right)\boldsymbol{\tau}^d = \mu_0\left(1 + \Lambda\mathrm{De}\frac{\partial}{\partial t}\right)\left(\operatorname{grad}\,\mathbf{v}^d + (\operatorname{grad}\,\mathbf{v}^d)^T\right), \tag{5.1.17}$$

with

$$\mathrm{De} = \frac{\lambda_1 \sigma}{a_1 \eta_0^c}, \quad \Lambda = \frac{\lambda_2}{\lambda_1}. \tag{5.1.18}$$

Here, the Deborah number De expresses the ratio of the rheological time scale, i.e. the stress relaxation time λ_1, and the capillary time scale $a_1\eta_0^c/\sigma$. The constant Λ is the ratio of deformation retardation λ_2 and stress relaxation time λ_1. So, these numbers express the contribution of the fluid elasticity to the system. For $\Lambda = 0$, (5.1.17) is the constitutive relation of the Maxwell model, and for $\Lambda = 1$, it is the relation of a Newtonian fluid.

We propose as general expressions for the solution in the dispersed phase

$$p^d = p_0^d(r)e^{ikz+qt}, \tag{5.1.19a}$$

$$u^d = u_0^d(r)e^{ikz+qt}, \tag{5.1.19b}$$

$$w^d = -iw_0^d(r)e^{ikz+qt}, \tag{5.1.19c}$$

$$\boldsymbol{\tau}^d = \boldsymbol{\tau}_0^d(r)e^{ikz+qt}, \tag{5.1.19d}$$

$$\dot{\boldsymbol{\gamma}}^d = \dot{\boldsymbol{\gamma}}_0^d(r)e^{ikz+qt}. \tag{5.1.19e}$$

The rate of strain tensor $\dot{\boldsymbol{\gamma}}^d$ is defined as

$$\dot{\boldsymbol{\gamma}}^d = \text{grad } \mathbf{v}^d + (\text{grad } \mathbf{v}^d)^T. \tag{5.1.20}$$

The factor $-i$ in (5.1.19c) is added for later convenience. Substitution of (5.1.19d) and (5.1.19e) into (5.1.17) yields, after rearranging,

$$\boldsymbol{\tau}_0^d(r) = \eta(q)\dot{\boldsymbol{\gamma}}_0^d(r), \text{ with } \eta(q) = \mu_0 \frac{1 + q\Lambda\mathrm{De}}{1 + q\mathrm{De}}. \tag{5.1.21}$$

Substitution of (5.1.19) and (5.1.21) into (5.1.16) yields the following equations:

$$0 = \frac{1}{r}\frac{\partial \left[ru_0^d\right]}{\partial r} + kw_0^d, \tag{5.1.22a}$$

$$\frac{\partial p_0^d}{\partial r} = \eta(q)\left[\frac{1}{r}\frac{\partial}{\partial r}\left[r\frac{\partial u_0^d}{\partial r}\right] - \frac{1 + (kr)^2}{r^2}u_0^d\right], \tag{5.1.22b}$$

$$-kp_0^d = \eta(q)\left[\frac{1}{r}\frac{\partial}{\partial r}\left[r\frac{\partial w_0^d}{\partial r}\right] - k^2 w_0^d\right]. \tag{5.1.22c}$$

Expressions (5.1.19) and (5.1.22) also hold for the continuous phase with d being replaced by c and $\eta(q)$ by 1. To solve (5.1.22), we use the same analysis as used in Section 2.2.1.

The solution for the dispersed phase ($r < 1$) reads

$$p_0^d(r) = 2\eta(q)A_0 I_0(kr), \tag{5.1.23a}$$

$$u_0^d(r) = A_0 r I_0(kr) - \left[B_0 + \frac{2}{k}A_0\right] I_1(kr), \tag{5.1.23b}$$

$$w_0^d(r) = -A_0 r I_1(kr) + B_0 I_0(kr), \tag{5.1.23c}$$

and for the continuous phase ($1 < r < h$),

$$p_0^c(r) = 2[D_0 K_0(kr) + F_0 I_0(kr)], \tag{5.1.24a}$$

$$u_0^c(r) = D_0 r K_0(kr) + \left[E_0 + \frac{2}{k}D_0\right] K_1(kr) + F_0 r I_0(kr) - \left[G_0 + \frac{2}{k}F_0\right] I_1(kr), \tag{5.1.24b}$$

$$w_0^c(r) = D_0 r K_1(kr) + E_0 K_0(kr) - F_0 r I_1(kr) + G_0 I_0(kr). \tag{5.1.24c}$$

Coefficients A_0, B_0, etc., are to be determined from the boundary conditions at the interface and at the wall. Analogous to Section 2.1.2, we derive four interfacial conditions:

$$[\![u_0]\!] = 0, \tag{5.1.25a}$$

$$[\![w_0]\!] = i\mathrm{C_p}\frac{\mu_0 - 1}{2\mu_0}\varepsilon_0, \tag{5.1.25b}$$

$$\left[\!\!\left[\widehat{\eta}\left(ku_0 - \frac{\partial w_0}{\partial r}\right)\right]\!\!\right] = 0, \tag{5.1.25c}$$

$$\left[\!\!\left[-p_0 + 2\widehat{\eta}\frac{\partial u_0}{\partial r}\right]\!\!\right] = (1 - k^2)\varepsilon_0, \tag{5.1.25d}$$

together with two no-slip boundary conditions

$$u_0^c(h, t) = 0, \tag{5.1.26a}$$

$$w_0^c(h, t) = 0. \tag{5.1.26b}$$

Here, $\widehat{\eta} = \eta(q)$ for the dispersed phase, and $\widehat{\eta} = 1$ for the continuous phase. By use of (5.1.3), (5.1.12) and (5.1.19b), the kinematic condition (2.1.19) leads to

$$u_0^d = \left[q - ik\frac{\mathrm{C_p}}{4}(h^2 - 1)\right]\varepsilon_0, \quad \text{or} \quad \varepsilon_0 = \frac{u_0^d}{q - ik\dfrac{\mathrm{C_p}}{4}(h^2 - 1)}\ . \tag{5.1.27}$$

From (5.1.25), (5.1.26) and (5.1.27) we can determine an equation for the growth rate q. Since q is a complex quantity, this equation will also be complex.

5.2 Stability analysis

Substituting (5.1.23) and (5.1.24) into (5.1.25) and (5.1.26), we obtain the linear system

$$\mathbf{M}\mathbf{z} = \mathbf{e}, \tag{5.2.1}$$

where $\mathbf{M}$ is a 6 by 6 matrix, $\mathbf{z} = (A_0, B_0, D_0, E_0, F_0, G_0)$ and

$$\mathbf{e} = (0, i\mathrm{C_p}(\mu_0 - 1)\varepsilon_0/2\mu_0, 0, (1-k^2)\varepsilon_0, 0, 0)^T. \tag{5.2.2}$$

The expression for $\mathbf{M}$ is given in Appendix B.5. Note that $\mathbf{M}$ is a complex matrix, since $\mathbf{M}$ depends on q.

According to Cramer's rule, the solution of (5.2.1) is given by

$$[\mathbf{z}]_j \equiv z_j = \left[i\frac{(-1)^{2+j}\mathrm{C_p}(\mu_0 - 1)}{2\mu_0}|\mathbf{M}^{2,j}| + (-1)^{4+j}(1-k^2)|\mathbf{M}^{4,j}| \right] \frac{\varepsilon_0(t)}{|\mathbf{M}|}, \tag{5.2.3}$$

where $|\cdot|$ denotes the determinant and $\mathbf{M}^{i,j}$ is the 5×5 sub-matrix of $\mathbf{M}$ that can be found by omitting the i-th row and the j-th column of $\mathbf{M}$. From (5.1.23b), (5.1.27) and (5.2.3) we obtain an implicit equation for q, after rearranging,

$$q = F_1(k, \eta(q), h) + i\ \mathrm{C_p}\ F_2(k, \eta(q), h)\ , \tag{5.2.4}$$

with $\eta(q) = \mu_0(1 + q\Lambda\mathrm{De})/(1 + q\mathrm{De})$, and F_1 and F_2 the complex valued functions,

$$\begin{aligned} F_1 &= \frac{(k^2-1)}{|\mathbf{M}|}\left[\left(I_0(k) - \frac{2}{k} I_1(k) \right) |\mathbf{M}^{4,1}| + I_1(k)|\mathbf{M}^{4,2}| \right], \\ F_2 &= \left[\frac{1-\mu_0}{2\mu_0|\mathbf{M}|} \left[\left(I_0(k) - \frac{2}{k} I_1(k) \right) |\mathbf{M}^{2,1}| + I_1(k)|\mathbf{M}^{2,2}| \right] + \frac{k}{4}(h^2 - 1) \right]. \end{aligned} \tag{5.2.5}$$

As is clear from (5.2.4), $\mathrm{C_p}$ contributes to both the real and the imaginary part of q. The real part of q is responsible for stability ($\Re[q] < 0$) or instability ($\Re[q] > 0$), whereas the imaginary part $\Im[q]$ represents an oscillatory behaviour. In case the thread is Newtonian, that is for $\Lambda = 1$, (5.2.4) becomes

$$q = F_1(k, \mu_0, h) + i\ \mathrm{C_p}\ F_2(k, \mu_0, h)\ . \tag{5.2.6}$$

Since now F_1 and F_2 are real, $\mathrm{C_p}$ only contributes to the imaginary part of q.

Detailed calculations will be presented in the next section.

5.2.1 Effect of fluid elasticity

To specifically study the effect of fluid elasticity, we here take $\mathrm{C_p} = 0$ (no prescribed flow), and $h \gg 1$ (no confinement). Since we are interested in the real part of q, we only have to consider the real part of equation (5.2.4). Figure 5.2(a) shows curves of q ($\equiv \Re[q]$) versus k for various values of μ_0 for viscoelastic threads with $\Lambda = 0$ (Maxwell fluid in a Newtonian matrix), and for $\mathrm{De} = 10$. We observe that the values of q decrease

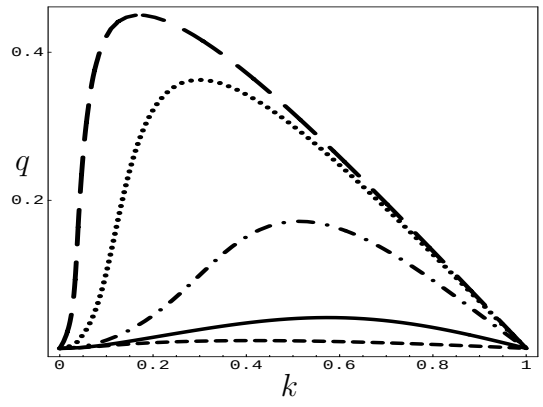

(a) Growth rate q as a function of k for the Maxwell model ($\Lambda = 0, \mathrm{De} = 10$).

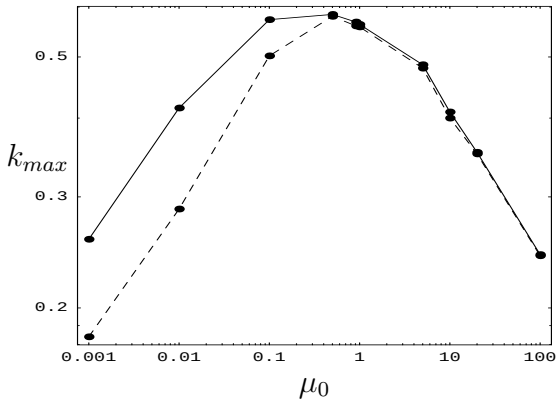

(b) The wave number k_{max} of the fastest growing perturbation as a function of μ for a Newtonian (solid line) and a viscoelastic thread (dashed line).

Figure 5.2: *(a) Curves of q as functions of k for a viscoelastic thread (Maxwell model), for different values of μ_0: $\mu_0 = 10$ (short-dashed curve), $\mu_0 = 1$ (solid curve), $\mu_0 = 0.1$ (dash-dot curve), $\mu_0 = 0.01$ (dotted curve), and $\mu_0 = 0.001$ (long-dashed curve). (b) Comparison of k_{max} for a viscoelastic thread and a Newtonian thread.*

with increasing μ_0. Thus, the more viscous the thread, the more time it takes to break up. If the thread is very viscous, it will remain undeformed for a long time before finally breaking up into droplets of very small size. The analogon of Figure 5.2(a) for a Newtonian thread is Figure 2.2. Figure 5.2(b) shows curves of k_{max} versus μ_0 for a Newtonian and a viscoelastic thread both immersed in a Newtonian matrix. Remind that k_{max} is the wave number related to the fastest growing growth rate q_{max} and therefore determines the drop size. For the viscoelastic thread, q_{max} occurs for smaller values of k than for the Newtonian one. So, the viscoelastic thread will break up in larger droplets (smaller k_{max}) than the comparable Newtonian one.

The effect of fluid elasticity is shown in Figures 5.3 and 5.4, in which q as a function of k is depicted for various values of De (Figure 5.3) or Λ (Figure 5.4). In Figure 5.3, we see that the smaller De, the lower the value of q is. As the instability grows faster for greater values of q, we note that the thread breaks up faster for increasing De, that is when the rheological time scale becomes greater than the capillary time scale (the λ_1-effect contra the $a_1\eta^c/\sigma$-effect). This effect is most manifest for $\mathrm{De} > 1$, and almost diminished to zero for $\mathrm{De} < 1$. Moreover, observing the places of the maxima of q, we see that the value of k_{max} is only very weakly affected by De. The latter implies that De has not much influence on the magnitude of the eventual droplets. In Figure 5.4, we see that the smaller Λ, the greater the value of q is. When Λ decreases, the thread becomes more elastic, i.e. more solid-like. Also here, we see that the value of k_{max} is only very weakly affected by, in this case, Λ, and this thus also holds for the eventual magnitude of the droplets.

To conclude this section, we note that we have found that a viscoelastic thread

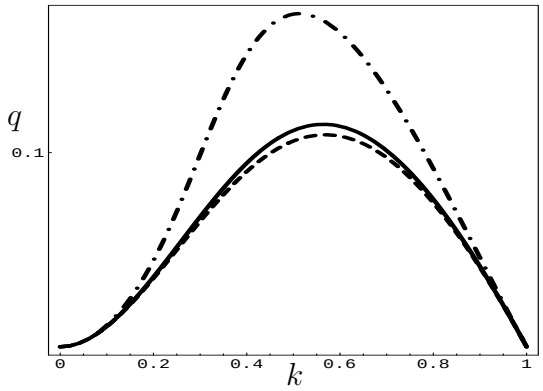

Figure 5.3: *Curves of q as functions of k for viscoelastic threads, for* $\mathrm{De} = 10$ *(dash-dot curve),* $\mathrm{De} = 1$ *(solid) and* $\mathrm{De} = 0.1$ *(dashed). The remaining parameter values are* $\mu_0 = 0.1$, $\Lambda = 0$, $\mathrm{C_p} = 0$ *and* $h \gg 1$.

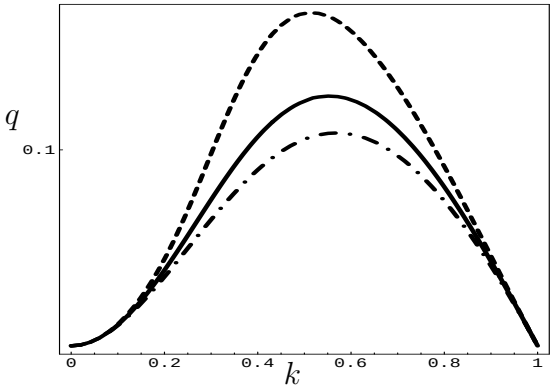

Figure 5.4: *Curves of q as functions of k for viscoelastic threads, for* $\Lambda = 1$ *(dash-dot curve),* $\Lambda = 0.5$ *(solid) and* $\Lambda = 0.01$ *(dashed). The remaining parameter values are* $\mu_0 = 0.1$, $\mathrm{De} = 10$, $\mathrm{C_p} = 0$ *and* $h \gg 1$.

immersed in a Newtonian fluid breaks up faster than a Newtonian one, and that this effect becomes stronger if the elasticity of the viscoelastic thread increases. The value of k where q reaches its maximum is hardly influenced by De and Λ. Hence, the elasticity of the thread has only minor influence on the magnitude of the eventual droplets.

5.2.2 Effect of confinement

In this section, we study the effect of confinement. For this, we consider a case of no prescribed flow, $\mathrm{C_p} = 0$, and a viscoelastic thread with $\Lambda = 0$ (Maxwell model). Figure 5.5 shows the curves of q as functions of k for a confined geometry, first (part (a)), for $h = 2$ and for the same set of values of μ_0 as in Figure (5.2)(a), and, second (part (b)), for a set of three different confinements ($h = 2, 5$, or 20) and for $\mu_0 = 0.1$. Comparing Figure 5.5(a) with Figure 5.2(a), we notice two striking differences: first, the growth rate is drastically smaller (a factor of 10) for the confined thread, and, second, the values of k

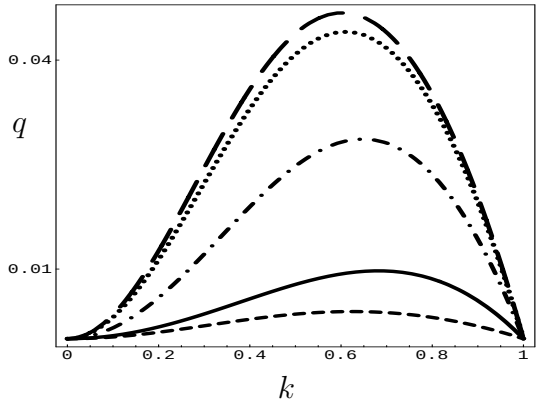

(a) Maxwell model ($\Lambda = 0,\ \mathrm{De} = 10$) with $h = 2$ (confined thread) for different values of μ_0 (see Figure 5.2(a)).

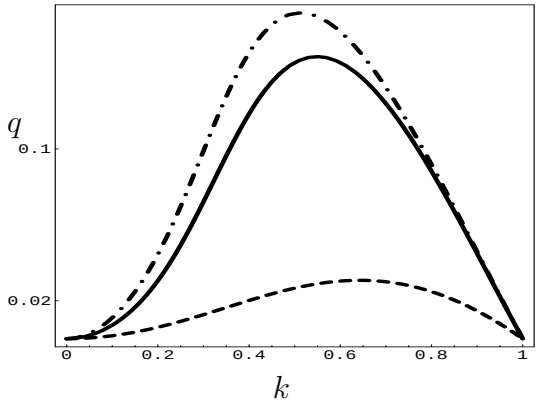

(b) Maxwell model ($\Lambda = 0,\ \mathrm{De} = 10$) for $h = 2$ (dashed curve), $h = 5$ (solid curve), and $h = 20$ (dash-dot curve), for $\mu_0 = 0.1$

Figure 5.5: *Curves of q as functions of k for Maxwell model ($\Lambda = 0,\ \mathrm{De} = 10$) for (a) $h = 2$ and for the same set of values of μ_0 as in Figure 5.2(a), and (b) for several values of h.*

where q is maximal are much less affected by the value of μ_0 for the confined thread than the unconfined thread. Hence, the confinement causes a slower break-up, in which the magnitudes of the droplets are practically insensible of the viscosity ratio μ_0. In Figure 5.5(b), we observe that the growth rate decreases with decreasing h (more confinement), implying that the thread breaks up slower when the degree of confinement is higher (smaller h), which is in accordance with the first conclusion from Figure 5.5(a). Figure 5.6 shows a curve of q_{max} as a function of h for a viscoelastic thread with $\Lambda = 0$, $\mathrm{De} = 10$, $\mu_0 = 0.1$, and $\mathrm{C_p} = 0$. In this Figure, we see that from a certain distance $\overline{h}$ on ($\overline{h} \approx 8$) the value of q_{max} hardly depends on the degree of confinement. Hence, if $h > \overline{h}$, the presence of the tube wall has no longer effect on the thread stability. This implies that

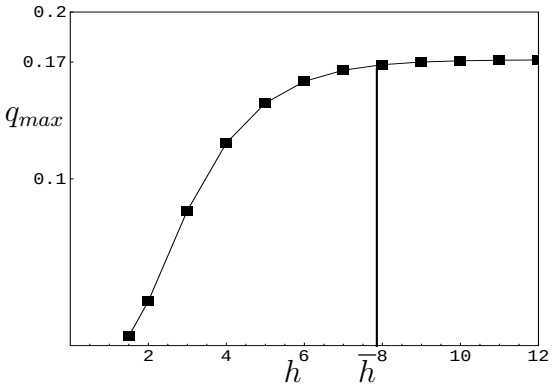

Figure 5.6: *Curve of q_{max} as a function of h for a viscoelastic thread. The remaining parameter values are $\Lambda = 0$, $\mathrm{De} = 10$, $\mu_0 = 0.1$, and $\mathrm{C_p} = 0$.*

$h \gg 1$ effectively means $h > \overline{h} \approx 8$.

5.2.3 Effect of Poiseuille flow

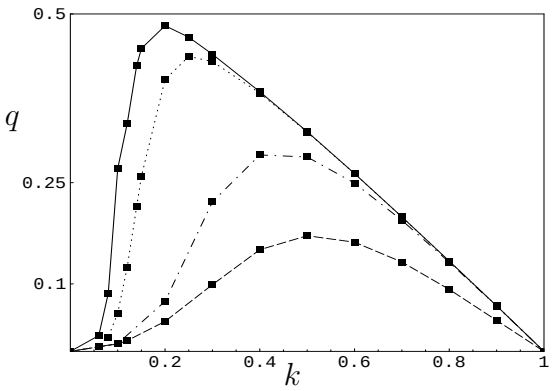

Figure 5.7: *Curves of q as functions of k for viscoelastic threads, for* $\mathrm{C_p} = 0$ *(dashed curve),* $\mathrm{C_p} = 0.02$ *(dash-dot curve),* $\mathrm{C_p} = 0.2$ *(dot curve) and* $\mathrm{C_p} = 0.5$ *(solid curve). The remaining parameter values are* $\Lambda = 0$, $\mathrm{De} = 10$, $\mu_0 = 0.1$, *and* $h \gg 1$.

Finally, we investigate the case $\mathrm{C_p} \neq 0$, that is we consider the effect of the prescribed (Poiseuille) flow on the break-up of the thread. Formula (5.2.4) indicates that in general $\mathrm{C_p}$ contributes to both the real and imaginary parts of q. However, in case of a Newtonian thread (see (5.2.6)), $\mathrm{C_p}$ only contributes to the imaginary part of q. This implies that then the thread is oscillatory unstable, with the growth rate equal to the one within a fluid at rest. In case the thread is viscoelastic, $\mathrm{C_p}$ contributes to both parts of q. In this case, the flow causes the growth rate, i.e. $\Re[q]$, to increase as shown in Figure 5.7, where $q \equiv \Re[q]$ is depicted as a function of k for various values of $\mathrm{C_p}$ (and for $\Lambda = 0$, $\mathrm{De} = 10$, $\mu_0 = 0.1$, and $h \gg 1$). From this we conclude that prescribed (Poiseuille) flow has the effect that a viscoelastic thread will become oscillatory unstable and will break up faster than the one within a fluid at rest.

5.3 Conclusions

In this chapter, we have studied the stability of a viscoelastic (Jeffreys model) thread immersed in a Newtonian fluid occupying a cylindrical tube. The thread is placed concentric in the tube. In the steady state the fluid-thread system flows, driven by a constant uniform pressure gradient, according to a Poiseuille flow (prescribed flow). One after another we have determined the influences of the viscosity ratio μ_0, the degree of confinement h, the prescribed flow ($\mathrm{C_p}$), the Deborah number De, and the material constant Λ on the growth rate q of the break-up process and on the magnitude of the eventual droplets.

Some conclusions that are found here, are:

1. In general, i.e. for $C_p \neq 0$, the growth rate q is a complex number; the (sign of the) real part is responsible for stability or instability (break-up) of the thread; its imaginary part for oscillatory behaviour.

2. The wave number k_{max}, i.e. the wave number related to the fastest growing growth rate, is smaller for a viscoelastic thread than for a Newtonian one, implying that a viscoelastic thread will break up in larger droplets than a Newtonian thread.

3. The rate of break-up of a viscoelastic thread immersed in a Newtonian fluid is influenced by both De and Λ, in so far that the thread breaks up faster for increasing De and decreasing Λ. This also reveals that a viscoelastic thread breaks up faster than a Newtonian one.

4. The magnitude of the eventual droplets is strongly affected by the ratio of viscosities μ_0, but practically unaffected by De, Λ, and h.

5. Confinement (h) does not make the thread stable (no break-up), but it makes the break-up slower, in so far that q decreases with decreasing h.

6. In case of a Newtonian thread, C_p only contributes to the imaginary part of q. This implies that the thread is oscillatory unstable with the growth rate equal to the one within a quiescent fluid.

7. In case of a viscoelastic thread, C_p contributes to both the real and the imaginary part of q. The growth rate, which is equal to $\Re[q]$, is always positive and becomes drastically larger for increasing C_p. This implies that the thread will break up faster than the one within a quiescent fluid. Moreover, the break-up process will show oscillatory behaviour.

Chapter 6

Conclusions and recommendations

In this thesis, we have studied the dynamical behaviour of liquid threads immersed in a fluid as a function of surface tension, viscous forces, presence of a wall (confinement) and prescribed flow. The main goal was to provide a theoretical explanation for the stability or instability of the immersed liquid threads. More specifically, phenomena such as break-up behaviour as observed by Knops (1997) and Elemans et al. (1997) for parallel polymeric liquid threads, and droplet-string formation as reported by Migler (2001) in concentrated polymer blend, were two of the main interests of this thesis. Below we conclude this thesis by extracting the most important findings from the previous chapters and by mentioning some possibilities for directly related future research.

To introduce the reader to techniques and notations, the stability of a single Newtonian thread immersed in another fluid was first addressed. This stability was investigated for two types of driving forces: surface tension only, and surface tension together with shear flow. In case the dynamics was driven by surface tension only, we found that the thread is unstable since the axisymmetric mode of perturbation is always growing. By imposing shear flow, the instability of the thread can be suppressed. In the presence of shear flow, the stability was determined by a so-called capillary number. This number, which depends on the fluid properties, describes the ratio between the applied shear stress and the surface tension. If the applied shear stress is large enough (exceeding a critical capillary number), the thread is stable. We have compared our results with analogous results of Frischknecht (1998). Although we had to make some corrections with respect to the boundary conditions as derived by Frischknecht, we found qualitatively comparable results. Due to these corrections, we found somewhat modified results for the range of the ratio of the viscosities in which no instability will occur. The present results for the stability in the presence of shear flow may shed light on the stability of the narrow string (radius much smaller than the characteristic length of the shear flow) observed by Migler (2001), who proposed that such a string can be stabilized by shear flow.

As an extension of the single-thread case, next the (in)stability of a set of immersed threads under influence of surface tension was investigated: first, the (in)stability of the two-threads system, second, the (in)stability of a finite number of immersed threads. The aim of this part was to model the phenomena observed by Knops (1997) and Elemans et al. (1997). Here, the polymeric fluids were assumed to behave Newtonian. This is

a good approximation since in the experiments reported by Knops (1997) and Elemans et al. (1997) the rate of deformation of the fluids is small. Therefore, the model was governed by the Stokes equations. These equations were solved by means of separation of variables in two, or more, systems of cylindrical coordinates, each one connected to one of the threads. The dependence on the azimuthal direction was written in terms of Fourier expansions. For the two-threads system, the stability of the threads was examined based on both a zero-order and a first-order Fourier expansion. We found, besides the viscosity ratio and the wave number, two new parameters that play an important role in the (in)stability of the threads: the phase difference and the distance between the centers of the threads. The developed theory showed that the threads can break up either in-phase or out-of-phase. The break-up behaviour depends on the viscosity ratio and the distance between the threads. If the threads are more viscous than the matrix phase and close enough to each other, the threads prefer to break up in-phase. Whereas, if the threads are less viscous than the matrix phase, they prefer to break up out-of-phase. These findings agree with the experimental observations reported by Knops (1997) and Elemans et al. (1997). We have also shown that an extension of the zero-order to the first-order Fourier mode leads to minor quantitative corrections in the results. Hence, in practice, a zero-order approximation already suffices.

In case of a finite number of immersed threads, we have presented results for the (in)stability of the threads for two types of configurations: a system of threads on a row, and a system of threads at triangular vertices. For a system with L threads on a row, in principle 2^L phase patterns for break-up are possible. However, we have shown that the growth rate of the system can be calculated by optimizing over only L so-called basic phase patterns, of which the most symmetric patterns are:

- all adjacent threads break up in-phase, i.e. all threads break up identically,
- all adjacent threads break up out-of-phase, i.e. the pattern repeats itself after two threads,

For the triangular configurations, we found that the break-up pattern depends on the type of triangle, i.e. is it an equilateral triangle or a non-equilateral one. In the latter case three patterns are possible, whereas in case of an equilateral triangle, the threads can break up in only two patterns. For the non-equilateral case we found that the break-up pattern also depends on the ratios of the lengths of the sides. In practice, all three patterns may be observed.

For the case of fluids having equal viscosities, we have analytically calculated the growth rate of a set of parallel threads on a row using Hankel transformations. We have derived an analytical expression for the upper bound and we have shown via numerical calculations that this upper bound is a good estimate for the maximum growth rate of the perturbations.

To extend our work to non-Newtonian fluids, we have considered the stability of an infinitely long viscoelastic thread immersed in a tube filled with a Newtonian fluid. As viscoelastic model we used Jeffreys model. The thread was moving in the tube due to a prescribed constant pressure gradient (Poiseuille flow). Here, we have studied by

analytical means the effects of the ratio of (zero-shear rate) viscosities, fluid elasticity, confinement and prescribed flow on the stability of the thread. As for the effect of the ratio of viscosities, we found that the more viscous the thread is, the more time it takes to break up. As for the effect of elasticity, we found that a viscoelastic thread breaks up faster than a Newtonian one, and that the wave number, which is responsible for the break-up, is smaller for a viscoelastic thread than for a Newtonian one. The latter implies that a viscoelastic thread will break up in larger droplets than a Newtonian one. We also observed that the elasticity has not much influence on the magnitude of the eventual droplets. As for the effect of confinement, we observed that the thread breaks up slower when the degree of confinement is higher. We found a critical gap width beyond which the presence of the wall of the tube has no longer an effect on the stability of the thread. The value of this critical gap width determines the critical size of the radius of the thread for deciding whether the thread must be classified as either the wider or the narrower string as introduced by Migler (2001). As for the effect of the Poiseuille flow, we found two noticeable results. First, in case of a Newtonian thread we found that the Poiseuille flow only causes the thread to be oscillatory unstable with the growth rate equal to the one within a fluid at rest. Second, in case of a viscoelastic thread we observed that the Poiseuille flow contributes to both the real and the imaginary part of the growth rate of the perturbation. This implies that the thread will be oscillatory unstable and will break up faster than the one within a fluid at rest.

From the point of view of blending the present results may provide important insights for control of the production process, since characteristic drop formation times, spatial distributions of the droplets and droplets or strings (liquid threads) formation are now known. The present results show how the blending process can be controlled by adjusting the properties of the fluids, the geometry of the system and the type of an imposed flow.

For future research, we would like to recommend the following points:

① In case of two threads, we have considered the break-up when the threads have equal radii. However, in reality the radii of the threads will be different from each other. Hence, the system has less symmetry then. We expect that the ratio of the radii will play a role in the break-up behaviour. The present approach can easily be extended to incorporate this.

② We have investigated the effect of shear flow on the stability of a single thread. The same analysis may be applied to the two-threads system (or the many-threads system). The steady unperturbed state and the kinematic condition will change due to the presence of the shear flow. We expect that the critical shear flow will depend on the distance between the threads.

③ We have studied the effects of confinement and prescribed flow on the stability of a thread placed coaxially in a tube. We expect that the stability will be differently affected by the prescribed flow if we place the thread eccentrically in the tube, because then shear effects will become dominant. These shear effects can stabilize the threads; see Section 2.3.

④ Recent experiments on an immersed drop sheared between plates by Sibillo et al.

(2003) showed that if one of the two phases is a viscoelastic fluid, the drop will elongate and will perform a so-called *Yo-Yo* behaviour. The elongated drop forms two bulbs connected by a string. Above the critical shear, the string does not break up and the elongated drop only rotates like a Yo-Yo (a children's toy). Sibillo et al. has experimentally studied the effect of fluid elasticity on the shear stress. We expect that the Yo-Yo behaviour occurs due to a balance between the shear force, the elasticity force (comes from the elastic fluid), the viscous force, the extensional force (the thread is stretched due to elongated bulbs), and surface tension.

Appendix A

Tensor notation

Here, $p(\mathbf{x})$, $\mathbf{v}(\mathbf{x})$ and $\boldsymbol{\tau}(\mathbf{x})$ represent a scalar, a vector and a 2-tensor field, respectively. Let (x_1, x_2, x_3) be a system of Cartesian coordinates, $(\mathbf{e}_1, \mathbf{e}_2, \mathbf{e}_3)$ be an orthogonal basis in these coordinates, and $(\cdot, \cdot)$ be the dot product. Note that any expression in which an index appears twice is understood to be summed over the range of that index (here $i, j = 1, 2, 3$).

Gradient of a scalar field $p : \mathbb{R}^3 \to \mathbb{R}$. The field $p(\mathbf{x})$ is differentiable with respect to $\mathbf{x}$ in a domain $G \subset \mathbb{R}^3$ if in every $\mathbf{x} \in G$ a linear functional $l(\mathbf{h})$ exists, such that

$$p(\mathbf{x} + \mathbf{h}) = p(\mathbf{x}) + l(\mathbf{h}) + \|\mathbf{h}\| r(\mathbf{x}, \mathbf{h}), \tag{A.0.1}$$

where $r(\mathbf{x}, \mathbf{h}) \to 0$, if $\|\mathbf{h}\| \to 0$; ($\|\mathbf{h}\| = \sqrt{(\mathbf{h}, \mathbf{h})}$, the Euclidean norm). Related to $l(\mathbf{h})$ a vector grad $p(\mathbf{x})$ can be defined by

$$\forall\ \mathbf{h} \in \mathbb{R}^3, \quad l(\mathbf{h}) = (\text{grad } p(\mathbf{x}), \mathbf{h}). \tag{A.0.2}$$

We call grad $p(\mathbf{x})$ the gradient of $p(\mathbf{x})$. By taking $\mathbf{h} = \epsilon\ \mathbf{e}_i$ ($0 < \epsilon \ll 1$) and by using (A.0.1)-(A.0.2), we obtain

$$\begin{aligned} p(\mathbf{x} + \epsilon\ \mathbf{e}_i) &= p(\mathbf{x}) + l(\epsilon\ \mathbf{e}_i) + o(\epsilon) \\ &= p(\mathbf{x}) + \epsilon\ (\text{grad } p(\mathbf{x}), \mathbf{e}_i) + o(\epsilon). \end{aligned} \tag{A.0.3}$$

Let us consider p as $p(x_1, x_2, x_3)$ and write $\mathbf{x} = (x_1, x_2, x_3)$. We know that the derivative of p with respect to x_i is equal to

$$\epsilon\ \frac{\partial p}{\partial x_i} = p(\mathbf{x} + \epsilon\ \mathbf{e}_i) - p(\mathbf{x}) + o(\epsilon). \tag{A.0.4}$$

Comparison of (A.0.3) with (A.0.4) yields

$$(\text{grad } p(\mathbf{x}), \mathbf{e}_i) = \frac{\partial p}{\partial x_i}. \tag{A.0.5}$$

Gradient of a vector field $\mathbf{v} : \mathbb{R}^3 \to \mathbb{R}^3$. The field $\mathbf{v}(\mathbf{x})$ is differentiable, if for every $\mathbf{x} \in G$ a linear mapping $\mathbf{L} : \mathbb{R}^3 \to \mathbb{R}^3$ exists, which is independent of $\mathbf{h}$, and which is such that

$$\mathbf{v}(\mathbf{x}+\mathbf{h}) = \mathbf{v}(\mathbf{x}) + \mathbf{L}(\mathbf{h}) + \|\mathbf{h}\| r(\mathbf{x},\mathbf{h}), \tag{A.0.6}$$

where $r(\mathbf{x},\mathbf{h}) \to 0$, if $\|\mathbf{h}\| \to 0$. Taking $\mathbf{h} = \epsilon\ \mathbf{e}_j$, applying the dot product of this equation with $\mathbf{e}_i$, and neglecting the terms of $o(\epsilon)$, we obtain, after rearranging,

$$(\mathbf{e}_i, \mathbf{v}(\mathbf{x}+\epsilon\ \mathbf{e}_j) - \mathbf{v}(\mathbf{x})) = \epsilon\ (\mathbf{e}_i, \mathbf{L}(\mathbf{e}_j)). \tag{A.0.7}$$

In (A.0.7), we have applied the property of linear mapping $\mathbf{L}$, that is $\mathbf{L}(\epsilon\ \mathbf{e}_j) = \epsilon\ \mathbf{L}(\mathbf{e}_j)$. From the left-hand side of (A.0.7), we obtain

$$(\mathbf{e}_i, \mathbf{v}(\mathbf{x}+\epsilon\ \mathbf{e}_j) - \mathbf{v}(\mathbf{x})) = (\mathbf{e}_i, \epsilon\ \frac{\partial \mathbf{v}}{\partial x_j}) = \epsilon\ \frac{\partial}{\partial x_j}(\mathbf{e}_i, \mathbf{v}) = \epsilon\ \frac{\partial v_i}{\partial x_j}. \tag{A.0.8}$$

Comparison of (A.0.7) with (A.0.8) results in, in terms of components,

$$L_{ij} = \frac{\partial v_i}{\partial x_j}\ . \tag{A.0.9}$$

From (A.0.7) and (A.0.8), we find

$$\frac{\partial}{\partial x_j}(\mathbf{e}_i, \mathbf{v}) = (\text{grad}\ (\mathbf{e}_i, \mathbf{v}), \mathbf{e}_j) = (\mathbf{L}^T \mathbf{e}_i, \mathbf{e}_j). \tag{A.0.10}$$

In (A.0.10) we have applied the adjoint mapping of $\mathbf{L}$. Let us denote $\mathbf{L} \equiv \text{grad}\ \mathbf{v}$. From the preceding results we conclude that we can define grad $\mathbf{v}$ as the linear mapping defined by

$$\forall\ \mathbf{a} \in \mathbb{R}^3, \quad (\text{grad}\ \mathbf{v})^T \mathbf{a} = \text{grad}\ (\mathbf{a}, \mathbf{v}(\mathbf{x})). \tag{A.0.11}$$

Divergence of a vector field $\mathbf{v} : \mathbb{R}^3 \to \mathbb{R}^3$. The divergence of a vector field $\mathbf{v}(\mathbf{x})$, denoted by div $\mathbf{v}(\mathbf{x})$, is defined as

$$\text{div}\ \mathbf{v} = \text{trace}\ (\text{grad}\ \mathbf{v}) = \frac{\partial v_i}{\partial x_i}. \tag{A.0.12}$$

Divergence of a 2-tensor field $\boldsymbol{\tau}(\mathbf{x})$. The divergence of a 2-tensor field $\boldsymbol{\tau}(\mathbf{x})$ is defined by

$$\forall\ \mathbf{a} \in \mathbb{R}^3, \quad \text{div}\ (\boldsymbol{\tau}(\mathbf{x})\mathbf{a}) = (\mathbf{a}, \text{div}\ \boldsymbol{\tau}(\mathbf{x})). \tag{A.0.13}$$

Written out in components, (A.0.13) yields (take $\mathbf{a} = \mathbf{e}_i$)

$$(\text{div}\ \boldsymbol{\tau}(\mathbf{x}))_i = \frac{\partial \tau_{ji}}{\partial x_j}. \tag{A.0.14}$$

Next, we derive (2.2.2). From (2.2.2a) and (A.0.12), we find

$$\text{div}\ \mathbf{v} = \frac{\partial v_i}{\partial x_i} = 0\ . \tag{A.0.15}$$

Using (A.0.14), we obtain

$$\text{div } (\text{grad } \mathbf{v})_i = \frac{\partial (\text{grad } \mathbf{v})_{ji}}{\partial x_j} = \frac{\partial}{\partial x_j}\frac{\partial v_j}{\partial x_i} = \frac{\partial}{\partial x_i}\frac{\partial v_j}{\partial x_j} = 0. \tag{A.0.16}$$

In (A.0.16), we have used (A.0.15). Thus, using (2.1.4)-(2.1.7), and (A.0.16) we find (in a coordinate-free notation)

$$0 = \text{div } \mathbf{v} \ , \tag{A.0.17a}$$

$$\text{grad } p = \widehat{\eta} \ \text{div } (\text{grad } \mathbf{v})^T \ . \tag{A.0.17b}$$

Appendix B

Expressions of the matrices

B.1 Expressions for $\mathbf{M}_m$

For $m = 0$:

$$\mathbf{M}_0 = \begin{pmatrix} I_0(k) - \frac{2}{k} I_1(k) & -I_1(k) & -[K_0(k) + \frac{2}{k} K_1(k)] & -K_1(k) \\ -I_1(k) & I_0(k) & -K_1(k) & -K_0(k) \\ \mu k I_1'(k) & -\mu k I_1(k) & k K_1'(k) & -k K_1(k) \\ 2\mu \left[k I_1(k) - 2 I_1'(k) \right] & -2\mu k I_1'(k) & -2 \left[2 K_1'(k) - k K_1(k) \right] & -2k K_1'(k) \end{pmatrix}$$

For $m = \pm 1, \pm 2, \cdots$:

$$\mathbf{M}_m = \begin{pmatrix} I_m(k) - \frac{m+2}{k} I_{m+1}(k) & -I_{m+1}(k) \\ -\frac{m+2}{k} I_{m+1}(k) & -I_{m+1}(k) \\ -I_{m+1}(k) & I_m(k) \\ \mu \left[m I_m(k) - \frac{(m+1)(m+2)}{k} I_{m+1}(k) + (m+2) I_{m+1}'(k) \right] & \mu \left[k I_{m+1}'(k) - (m+1) I_{m+1}(k) \right] \\ \mu [k I_m(k) - (m+1) I_{m+1}(k) + k I_{m+1}'(k)] & -\mu k [I_{m+1}(k) + I_m'(k)] \\ 2\mu \left[k I_m'(k) - (m+2) I_{m+1}'(k) \right] & -2\mu k I_{m+1}'(k) \end{pmatrix}$$

$$\begin{pmatrix} I_m(k) & -\left[K_m(k) + \frac{m+2}{k} K_{m+1}(k) \right] \\ -\frac{k}{m} I_{m+1}(k) - I_m(k) & -\frac{m+2}{k} K_{m+1}(k) \\ 0 & -K_{m+1}(k) \\ \mu \left[(m-2) I_m(k) - \frac{k}{m} I_{m+1}(k) + k I_m'(k) + \frac{k^2}{m} I_{m+1}'(k) \right] & -\left[m K_m(k) + \frac{(m+1)(m+2)}{k} K_{m+1}(k) - (m+2) K_{m+1}'(k) \right] \\ \mu k I_m(k) & -[k K_m(k) + (m+1) K_{m+1}(k) - k K_{m+1}'(k)] \\ 2\mu [k I_m'(k) - I_m(k)] & -2 \left[k K_m'(k) + (m+2) K_{m+1}'(k) \right] \end{pmatrix}$$

$$\begin{pmatrix} -K_{m+1}(k) & -K_m(k) \\ -K_{m+1}(k) & -\left[\frac{k}{m}K_{m+1}(k) - K_m(k)\right] \\ -K_m(k) & 0 \\ -\left[-kK'_{m+1}(k) + (m+1)K_{m+1}(k)\right] & -\left[(m-2)K_m(k) + \frac{k}{m}K_{m+1}(k) + kK'_m(k) - \frac{k^2}{m}K'_{m+1}(k)\right] \\ -k[K_{m+1}(k) - K'_m(k)] & -kK_m(k) \\ -2kK'_{m+1}(k) & -2[kK'_m(k) - K_m(k)] \end{pmatrix}$$

For the special case $k = 0$, for $m \geq 2$:

$$\mathbf{M}_{m;k=0} = \begin{pmatrix} 1 & \frac{m}{2(m+1)} & -1 & -\frac{m}{2(m-1)} \\ -1 & -\frac{m+2}{2(m+1)} & -1 & -\frac{m-2}{2(m-1)} \\ 2\mu(m-1) & m\mu & -2(m+1) & -m \\ 2\mu(m-1) & \mu(m-2) & 2(m+1) & m+2 \end{pmatrix}$$

B.2 Expressions for $\mathbf{M}_0$ and Q, for the thread in shear flow

For $m = 0$:

$$\mathbf{M}_0 = \begin{pmatrix} I_0(k) - \frac{2}{k}I_1(k) & -I_1(k) & 0 & -[K_0(k) + \frac{2}{k}K_1(k)] & -K_1(k) & 0 \\ 0 & 0 & I_1(k) & 0 & 0 & -K_1(k) \\ -I_1(k) & I_0(k) & 0 & -K_1(k) & -K_0(k) & 0 \\ 0 & 0 & \mu(I_1(k) - kI'_1(k)) & 0 & 0 & -K_1(k) + kK'_1(k) \\ \mu k I'_1(k) & -\mu k I_1(k) & 0 & kK'_1(k) & -kK_1(k) & 0 \\ 2\mu\left[kI_1(k) - 2I'_1(k)\right] & -2\mu k I'_1(k) & 0 & -2\left[2K'_1(k) - kK_1(k)\right] & -2kK'_1(k) & 0 \end{pmatrix}$$

For $m = \pm 1, \pm 2, \cdots$, the matrices are similar to those in Appendix B.1.

The coefficients of polynomial in (2.3.30):

$$a_1 = -(q_{11} + q_{22} + q_{33}),$$

$$a_2 = q_{11}q_{22} + q_{11}q_{33} + q_{22}q_{33} - (q_{12}q_{21} + q_{23}q_{32}),$$

$$a_3 = q_{11}q_{23}q_{32} + q_{33}q_{12}q_{21} - q_{11}q_{22}q_{33}.$$

The elements of the matrix $\mathbf{Q}$ in (2.3.29):

$$
\begin{aligned}
q_{11} &= \frac{k^2}{|\mathbf{M}_{-1}|}\left[\left(I_1(k)-\frac{1}{k}I_0(k)\right)|\mathbf{M}_{-1}^{6,1}|+I_0(k)|\mathbf{M}_{-1}^{6,2}|+I_1(k)|\mathbf{M}_{-1}^{6,3}|\right],\\
q_{12} &= -\frac{\mathrm{Ca}}{|\mathbf{M}_{-1}|}\frac{\mu-1}{\mu+1}\left[\left(I_1(k)-\frac{1}{k}I_0(k)\right)\left(|\mathbf{M}_{-1}^{3,1}|+|\mathbf{M}_{-1}^{5,1}|\right)\right.\\
&\qquad\left.+I_0(k)\left(|\mathbf{M}_{-1}^{3,2}|+|\mathbf{M}_{-1}^{5,2}|\right)+I_1(k)\left(|\mathbf{M}_{-1}^{3,3}|+|\mathbf{M}_{-1}^{5,3}|\right)\right]\\
&\quad-\frac{k\mathrm{Ca}}{|\mathbf{M}_{-1}|}\frac{\mu-1}{\mu+1}\left[\left(I_1(k)-\frac{1}{k}I_0(k)\right)|\mathbf{M}_{-1}^{4,1}|+I_0(k)|\mathbf{M}_{-1}^{4,2}|+I_1(k)|\mathbf{M}_{-1}^{4,3}|\right]\\
&\quad+\frac{k\mathrm{Ca}}{\mu+1},\\
q_{21} &= \frac{\mathrm{Ca}}{|\mathbf{M}_0|}\frac{\mu-1}{\mu+1}\left[\left(I_0(k)-\frac{2}{k}I_1(k)\right)|\mathbf{M}_0^{3,1}|+I_1(k)|\mathbf{M}_0^{3,2}|\right]\\
&\quad-\frac{k\mathrm{Ca}}{|\mathbf{M}_0|}\frac{\mu-1}{\mu+1}\left[\left(I_0(k)-\frac{2}{k}I_1(k)\right)|\mathbf{M}_0^{4,1}|+I_1(k)|\mathbf{M}_0^{4,2}|\right]-\frac{k\mathrm{Ca}}{\mu+1},\\
q_{22} &= \frac{k^2-1}{|\mathbf{M}_0|}\left[\left(I_0(k)-\frac{2}{k}I_1(k)\right)|\mathbf{M}_0^{6,1}|+I_1(k)|\mathbf{M}_0^{6,2}|\right],\\
q_{23} &= -\frac{\mathrm{Ca}}{|\mathbf{M}_0|}\frac{\mu-1}{\mu+1}\left[\left(I_0(k)-\frac{2}{k}I_1(k)\right)|\mathbf{M}_0^{3,1}|+I_1(k)|\mathbf{M}_0^{3,2}|\right]\\
&\quad-\frac{k\mathrm{Ca}}{|\mathbf{M}_0|}\frac{\mu-1}{\mu+1}\left[\left(I_0(k)-\frac{2}{k}I_1(k)\right)|\mathbf{M}_0^{4,1}|+I_1(k)|\mathbf{M}_0^{4,2}|\right]+\frac{k\mathrm{Ca}}{\mu+1},\\
q_{32} &= \frac{\mathrm{Ca}}{|\mathbf{M}_1|}\frac{\mu-1}{\mu+1}\left[\left(I_1(k)-\frac{3}{k}I_2(k)\right)\left(|\mathbf{M}_1^{3,1}|+|\mathbf{M}_1^{5,1}|\right)\right.\\
&\qquad\left.+I_2(k)\left(|\mathbf{M}_1^{3,2}|+|\mathbf{M}_1^{5,2}|\right)+I_1(k)\left(|\mathbf{M}_1^{3,3}|-|\mathbf{M}_1^{5,3}|\right)\right]\\
&\quad-\frac{k\mathrm{Ca}}{|\mathbf{M}_1|}\frac{\mu-1}{\mu+1}\left[\left(I_1(k)-\frac{1}{k}I_0(k)\right)|\mathbf{M}_1^{4,1}|+I_0(k)|\mathbf{M}_1^{4,2}|+I_1(k)|\mathbf{M}_1^{4,3}|\right]\\
&\quad-\frac{k\mathrm{Ca}}{\mu+1},\\
q_{33} &= \frac{k^2}{|\mathbf{M}_1|}\left[\left(I_1(k)-\frac{3}{k}I_2(k)\right)|\mathbf{M}_1^{6,1}|+I_2(k)|\mathbf{M}_1^{6,2}|+I_1(k)|\mathbf{M}_1^{6,3}|\right].
\end{aligned}
$$

B.3 Expressions for $\mathbf{H}_0$ and $\mathbf{H}_1$

Explicit expressions for the block matrices $\mathbf{H}_0$ and $\mathbf{H}_j$, $i,j=1,2,\cdots$. For $M=0$ case:

$$
\mathbf{H}_0=\begin{pmatrix}
kI_0(k)-2I_1(k) & -kI_1(k) & -(kK_0(k)+2K_1(k)) & -kK_1(k)\\
-kI_1(k) & kI_0(k) & -kK_1(k) & -kK_0(k)\\
-2\mu kI_1'(k) & 2\mu kI_1(k) & -2kK_1'(k) & 2kK_1(k)\\
2\mu(kI_1(k)-2I_1'(k)) & -2\mu kI_1'(k) & -2(2K_1'(k)-kK_1(k)) & -2kK_1'(k)
\end{pmatrix}
$$

$$
\mathbf{H}_1=\begin{pmatrix}
0 & 0 & (kbK_1(kb)I_1(k)-kK_0(kb)I_0(k)+2K_0(kb)I_1(k)) & kK_0(kb)I_1(k)\\
0 & 0 & -(kbK_1(kb)I_0(k)-kK_0(kb)I_1(k)) & -kK_0(kb)I_0(k)\\
0 & 0 & -(2kbK_1(kb)I_1(k)-2kK_0(kb)I_0(k)+2K_0(kb)I_1(k)) & -2kK_0(kb)I_1(k)\\
0 & 0 & -2(kK_0(kb)I_1(k)-kbK_1(kb)I_1'(k)-2K_0(kb)I_1'(k)) & 2kK_0(kb)I_1'(k)
\end{pmatrix}
$$

For $M = 1$, the matrix $\mathbf{H}$ is given below. For each table, the first and the second columns indicate the vector $\mathbf{z}_{n,i}$ and a specific row of the matrix $\mathbf{H}$, respectively. Here, $y = kb$ and $A_{i,j}^{(n)} \equiv A_{ij}$, etc..

Entries from the boundary condition $[\![u]\!] = 0$, yielding the first ($[\![u_0]\!]$) and the second ($[\![u_1]\!]$) row of $\mathbf{H}$.

	$[\![u_0]\!]$
A_{10}	$kI_0(k) - 2I_1(k)$
B_{10}	$-kI_1(k)$
D_{10}	$-[kK_0(k) + 2K_1(k)]$
E_{10}	$-kK_1(k)$
A_{11}	0
B_{11}	0
C_{11}	0
D_{11}	0
E_{11}	0
F_{11}	0
A_{20}	0
B_{20}	0
D_{20}	$yK_1(y)I_1(k) - kK_0(y)I_0(k) + 2K_0(y)I_1(k)$
E_{20}	$kK_0(y)I_1(k)$
A_{21}	0
B_{21}	0
C_{21}	0
D_{21}	$\frac{y}{2}\left[K_0(y) + K_2(y)\right]I_1(k) - kK_1(y)I_0(k) + 3K_1(y)I_1(k)$
E_{21}	$kK_1(y)I_1(k)$
F_{21}	0

$[\![u_1]\!]$	
A_{10}	0
B_{10}	0
D_{10}	0
E_{10}	0
A_{11}	$kI_1(k) - 3I_2(k)$
B_{11}	$-kI_2(k)$
C_{11}	$kI_1(k)$
D_{11}	$-[kK_1(k) + 3K_2(k)]$
E_{11}	$-kK_2(k)$
F_{11}	$-kK_1(k)$
A_{20}	0
B_{20}	0
D_{20}	$y[K_0(y)I_0(k) + K_2(y)I_2(k)] - 2kK_1(y)I_1(k) + 2[K_1(y)I_0(k) + K_1(y)I_2(k)]$
E_{20}	$kK_1(y)[I_0(k) + I_2(k)]$
A_{21}	0
B_{21}	0
C_{21}	0
D_{21}	$[yK_1(y) + 3K_2(y)]I_0(k) - k[K_0(y) + K_2(y)]I_1(k)$ $+\left[3K_0(y) + \frac{y}{2}\left[K_1(y) + K_3(y) \right] \right] I_2(k)$
E_{21}	$k[K_2(y)I_0(k) + K_0(y)I_2(k)]$
F_{21}	$\frac{k^2}{2}\left[K_2(y) - K_0(y) \right]\left[I_0(k) - I_2(k) \right]$

Entries from the boundary condition $[\![w]\!] = 0$, yielding the third ($[\![w_0]\!]$) and the fourth ($[\![w_1]\!]$) row of $\mathbf{H}$.

	$[\![w_0]\!]$
A_{10}	$-kI_1(k)$
B_{10}	$kI_0(k)$
D_{10}	$-kK_1(k)$
E_{10}	$-kK_0(k)$
A_{11}	0
B_{11}	0
C_{11}	0
D_{11}	0
E_{11}	0
F_{11}	0
A_{20}	0
B_{20}	0
D_{20}	$-yK_1(y)I_0(k) + kK_0(y)I_1(k)$
E_{20}	$-kK_0(y)I_0(k)$
A_{21}	0
B_{21}	0
C_{21}	0
D_{21}	$-yK_2(y)I_0(k) + kK_1(y)I_1(k)$
E_{21}	$-kK_1(y)I_0(k)$
F_{21}	0

	$[\![w_1]\!]$
A_{10}	0
B_{10}	0
D_{10}	0
E_{10}	0
A_{11}	$-kI_2(k)$
B_{11}	$kI_1(k)$
C_{11}	0
D_{11}	$-kK_2(k)$
E_{11}	$-kK_1(k)$
F_{11}	0
A_{20}	0
B_{20}	0
D_{20}	$-y[K_0(y)+K_2(y)]I_1(k)+kK_1(y)[I_0(k)+I_2(k)]$
E_{20}	$-2kK_1(y)I_1(k)$
A_{21}	0
B_{21}	0
C_{21}	0
D_{21}	$-y[K_1(y)+K_3(y)]I_1(k)+k[K_0(y)I_2(k)+K_2(y)I_0(k)]$
E_{21}	$-k[K_0(y)I_1(k)+K_2(y)I_1(k)]$
F_{21}	0

Entries from the boundary condition $[\![\pi_{rz}]\!] = 0$, yielding the fifth ($[\![\pi_{rz,0}]\!]$) and the sixth ($[\![\pi_{rz,1}]\!]$) row of $\mathbf{H}$.

	$[\![\pi_{rz,0}]\!]$
A_{10}	$2\mu[-kI_0(k) + I_1(k)]$
B_{10}	$2\mu kI_1(k)$
D_{10}	$2[kK_0(k) + K_1(k)]$
E_{10}	$2kK_1(k)$
A_{11}	0
B_{11}	0
C_{11}	0
D_{11}	0
E_{11}	0
F_{11}	0
A_{20}	0
B_{20}	0
D_{20}	$2[kK_0(y)I_0(k) - K_0(y)I_1(k) - yK_1(y)I_1(k)]$
E_{20}	$-2kK_0(y)I_1(k)$
A_{21}	0
B_{21}	0
C_{21}	0
D_{21}	$-2yK_0(y)I_1(k) - 6K_1(y)I_1 + 2kK_1(y)I_0(k)$
E_{21}	$-2kK_1(y)I_1(k)$
F_{21}	0

$[\![\pi_{rz,1}]\!]$	
A_{10}	0
B_{10}	0
D_{10}	0
E_{10}	0
A_{11}	$2\mu[-kI_1(k)+2[I_0(k)-\frac{2I_1(k)}{k}]]$
B_{11}	$\mu k[-\frac{I_1(k)}{k}+2[I_0(k)-\frac{I_1(k)}{k}]]$
C_{11}	$-\mu kI_1(k)$
D_{11}	$2[\,kK_1(k)+2[K_0(k)+\frac{2K_1(k)}{k}]]$
E_{11}	$k[\,\frac{K_1(k)}{k}+2[K_0(k)+\frac{K_1(k)}{k}]]$
F_{11}	$kK_1(k)$
A_{20}	0
B_{20}	0
D_{20}	$4[\,(\frac{k^2+1}{k})K_1(y)I_1(k)-[yK_0(y)+2K_1(y)][I_0(k)-\frac{I_1(k)}{k}]]$
E_{20}	$-4kK_1(y)[I_0(k)-\frac{I_1(k)}{k}]$
A_{21}	0
B_{21}	0
C_{21}	0
D_{21}	$4\,[(\frac{k^2+1}{k})K_0(y)I_1(k)+\frac{k}{y}K_1(y)I_1(k)-[\frac{4}{y}K_1(y)+3K_0(y)+yK_1(y)]$ $[I_0(k)-\frac{I_1(k)}{k}]]$
E_{21}	$-2k[\,\frac{1}{y}K_1(y)I_0+[2K_0(y)+\frac{1}{y}K_1(y)][I_0(k)-\frac{I_1(k)}{k}]]$
F_{21}	$-\frac{k^2}{2}[K_2(y)-K_0(y)][I_0(k)-I_2(k)]$

Entries from the boundary condition $[\![\pi_{rr}]\!] = ((1-k^2)\varepsilon_{1,0} - k^2\varepsilon_{1,1}\cos\phi_1)\cos kz$. yielding the seventh ($[\![\pi_{rr,0}]\!]$) and the eighth ($[\![\pi_{rr,1}]\!]$) row of $\mathbf{H}$.

$[\![\pi_{rr,0}]\!]$	
A_{10}	$2\mu[\,kI_1(k) - 2[I_0(k) - \frac{I_1(k)}{k}]\,]$
B_{10}	$-2\mu k[I_0(k) - \frac{I_1(k)}{k}]$
D_{10}	$2[\,kK_1(k) + 2[K_0(k) + \frac{K_1(k)}{k}]\,]$
E_{10}	$2k[K_0(k) + \frac{K_1(k)}{k}]$
A_{11}	0
B_{11}	0
C_{11}	0
D_{11}	0
E_{11}	0
F_{11}	0
A_{20}	0
B_{20}	0
D_{20}	$2[-kK_0(y)I_1(k) + [yK_1(y) + 2K_0(y)][I_0(k) - \frac{I_1(k)}{k}]]$
E_{20}	$2kK_0(y)[I_0(k) - \frac{I_1(k)}{k}]$
A_{21}	0
B_{21}	0
C_{21}	0
D_{21}	$2[\,-kK_1(y)I_1(k) + [yK_0(y) + 4K_1(y)][I_0(k) - \frac{I_1(k)}{k}]\,]$
E_{21}	$2kK_1(y)[I_0(k) - \frac{I_1(k)}{k}]$
F_{21}	0

$[\![\pi_{rr_{,1}}]\!]$	
A_{10}	0
B_{10}	0
D_{10}	0
E_{10}	0
A_{11}	$2\mu[\,k[I_0(k)-\frac{I_1(k)}{k}]-3[I_1(k)-\frac{2I_2(k)}{k}]\,]$
B_{11}	$-2k\mu[I_1(k)-\dfrac{2I_2(k)}{k}]$
C_{11}	$2k\mu[I_0(k)-\frac{2I_1(k)}{k}]$
D_{11}	$2[\,k[K_0(k)+\frac{K_1(k)}{k}]+3[K_1(k)+\frac{2K_2(k)}{k}]\,]$
E_{11}	$2k[K_1(k)+\frac{2K_2(k)}{k}]$
F_{11}	$2k[K_0(k)+\frac{2K_1(k)}{k}]$
A_{20}	0
B_{20}	0
D_{20}	$2\Big[[yK_0(y)+2K_1(y)]I_1(k)+[yK_2(y)+2K_1(y)][I_1(k)-\frac{2I_2(k)}{k}]$ $-2kK_1(y)[I_0(k)-\dfrac{I_1(k)}{k}]\Big]$
E_{20}	$2k\Big[K_1(y)I_1(k)+K_1(y)[I_1(k)-\dfrac{2I_2(k)}{k}]\Big]$
A_{21}	0
B_{21}	0
C_{21}	0
D_{21}	$\Big[2yK_1(y)I_1(k)-2k[K_0(y)+K_2(y)][I_0(k)-\dfrac{I_1(k)}{k}]$ $+[6K_0(y)+yK_1(y)+yK_3(y)][I_1(k)-\dfrac{2I_2(k)}{k}]\Big]$
E_{21}	$2k\Big[K_0(y)[I_1(k)-\dfrac{2I_2(k)}{k}]+K_2(y)I_1(k)\Big]$
F_{21}	$\dfrac{4k}{y}K_1(y)I_2(k)$

Entries from the boundary condition $[\![v]\!] = 0$, yielding the ninth ($[\![v_1]\!]$) row of $\mathbf{H}$.

	$[\![v_1]\!]$
A_{10}	0
B_{10}	0
D_{10}	0
E_{10}	0
A_{11}	$-3I_2(k)$
B_{11}	$-kI_2(k)$
C_{11}	$-k^2[I_2(k) + \frac{I_1(k)}{k}]$
D_{11}	$-3K_2(k)$
E_{11}	$-kK_2(k)$
F_{11}	$-k^2[K_2(x) - \frac{K_1(x)}{x}]$
A_{20}	0
B_{20}	0
D_{20}	$-y[K_0(y)I_0(x) - K_2(y)I_2(x)] - 2K_1(y)[I_0(x) - I_2(x)]$
E_{20}	$-kK_1(y)[I_0(x) - I_2(x)]$
A_{21}	0
B_{21}	0
C_{21}	0
D_{21}	$-\frac{y}{2}[\,2K_1(y)I_0(k) - [K_1(y) + K_3(y)]I_2(x)\,] + 3[K_0(y)I_2(x) - K_2(y)I_0(x)]$
E_{21}	$k[K_0(y)I_2(x) - K_2(y)I_0(x)]$
F_{21}	$\frac{k^2}{2}[K_0(y) - K_2(y)][I_0(x) + I_2(x)]$

Entries from the boundary condition $[\![\pi_{r\phi}]\!] = 0$,yielding the tenth ($[\![\pi_{r\phi_{,1}}]\!]$) row of $\mathbf{H}$.

	$[\![\pi_{r\phi_{,1}}]\!]$
A_{10}	0
B_{10}	0
D_{10}	0
E_{10}	0
A_{11}	$-4\mu[I_1(k) + \frac{6I_1(k)}{k^2} - \frac{3I_0(k)}{k}]$
B_{11}	$k\mu[\frac{4I_2(k)}{k} - I_1(k)]$
C_{11}	$-\mu k^2[I_1(k) + \frac{4I_1(k)}{k^2} - \frac{2I_0(k)}{k}]$
D_{11}	$4[K_1(k) + \frac{6K_1(k)}{k^2} + \frac{3K_0(k)}{k}]$
E_{11}	$k[\frac{4K_2(k)}{k} + K_1(k)]$
F_{11}	$k^2[K_1(k) + \frac{4K_1(k)}{k^2} + \frac{2K_0(k)}{k}]$
A_{20}	0
B_{20}	0
D_{20}	$4[\,K_1(y)I_1(k) + \frac{yK_0(y)+4K_1(y)}{k}[\frac{2I_1(k)}{k} - I_0(k)]\,]$
E_{20}	$4K_1(y)[\frac{2I_1(k)}{k} - I_0(k)]$
A_{21}	0
B_{21}	0
C_{21}	0
D_{21}	$4[\,K_0(y)I_1(k) + \frac{1}{k}[5K_0(y) + yK_1(y) + \frac{4K_1(y)}{y}][\frac{2I_1(k)}{k} - I_0(k)]\,]$
E_{21}	$2[\,2K_0(y)[\frac{2I_1(k)}{k} - I_0(k)] - \frac{k}{y}K_1(y)I_1(k)\,]$
F_{21}	$-\frac{2k^2}{y}K_1(y)[\,I_1(k) + \frac{2}{k}[\frac{2I_1(k)}{k} - I_0(k)]\,]$

B.4 Expressions for $\mathbf{H}_j$ and $\mathbf{H}_{ij}$

For $j = 0$, the matrix is similar to those in B.3. For $j \neq 0$:

$$\mathbf{H}_j = \begin{pmatrix} 0 & 0 & (jkbK_1(jkb)I_1(k) - kK_0(jkb)I_0(k) + 2K_0(jkb)I_1(k)) & kK_0(jkb)I_1(k) \\ 0 & 0 & -(jkbK_1(jkb)I_0(k) - kK_0(jkb)I_1(k)) & -kK_0(jkb)I_0(k) \\ 0 & 0 & -(2jkbK_1(jkb)I_1(k) - 2kK_0(jkb)I_0(k) + 2K_0(jkb)I_1(k)) & -2kK_0(jkb)I_1(k) \\ 0 & 0 & -2(kK_0(jkb)I_1(k) - jkbK_1(jkb)I_1'(k) - 2K_0(jkb)I_1'(k)) & 2kK_0(jkb)I_1'(k) \end{pmatrix}$$

For $i \neq j$ and $i, j > 0$:

$$\mathbf{H}_{ij} = \begin{pmatrix} 0 & 0 & (kb_{ij}K_1(kb_{ij})I_1(k) - kK_0(kb_{ij})I_0(k) + 2K_0(kb_{ij})I_1(k)) & kK_0(kb_{ij})I_1(k) \\ 0 & 0 & -(kb_{ij}K_1(kb_{ij})I_0(k) - kK_0(kb_{ij})I_1(k)) & -kK_0(kb_{ij})I_0(k) \\ 0 & 0 & -(2kb_{ij}K_1(kb_{ij})I_1(k) - 2kK_0(kb_{ij})I_0(k) + 2K_0(kb_{ij})I_1(k)) & -2kK_0(kb_{ij})I_1(k) \\ 0 & 0 & -2(kK_0(kb_{ij})I_1(k) - kb_{ij}K_1(kb_{ij})I_1'(k) - 2K_0(kb_{ij})I_1'(k)) & 2kK_0(kb_{ij})I_1'(k) \end{pmatrix}$$

Note that $\mathbf{H}_{00} \equiv \mathbf{H}_0$.

B.5 Expressions for M

$$\mathbf{M} = \begin{pmatrix} kI_0(k) - 2I_1(k) & -kI_1(k) & -[kK_0(k) + 2K_1(k)] & -kK_1(k) & -[kI_0(k) - 2I_1(k)] & kI_1(k) \\ -I_1(k) & I_0(k) & -K_1(k) & -K_0(k) & I_1(k) & -I_0(k) \\ \eta(q)kI_1'(k) & -\eta(q)kI_1(k) & kK_1'(k) & -kK_1(k) & -kI_1'(k) & kI_1(k) \\ 2\eta(q)\left[kI_1(k) - 2I_1'(k)\right] & -2\eta(q)kI_1'(k) & -2\left[2K_1'(k) - kK_1(k)\right] & -2kK_1'(k) & -2\left[kI_1(k) - 2I_1'(k)\right] & 2kI_1'(k) \\ 0 & 0 & khK_0(kh) + 2K_1(kh) & kK_1(kh) & khI_0(kh) - 2I_1(kh) & -kI_1(kh) \\ 0 & 0 & hK_1(kh) & K_0(kh) & -hI_1(kh) & I_0(kh) \end{pmatrix}$$

$$\eta(q) = \mu_0 \frac{1 + q\Lambda\mathrm{De}}{1 + q\mathrm{De}}$$

Appendix C

Expressions derived from Graf's addition theorem

C.1 Graf's addition theorem for the triangular configuration

Let us consider Figure 4.5. As an illustration, we evaluate the product of Bessel function and a Fourier expansion of (r_3, ϕ_3) in terms of (r_1, ϕ_1) at point P_1 ($r_1 = 1$). For simplicity, take $k_j = k$ for all j and introduce $\Phi_l = \phi_l - \beta_{13}$ for $l = 1, 3$. The addition theorem states that for $r_1 = 1 < b_{13}$,

$$\begin{aligned} K_m(kr_3)\cos m(\pi - \Phi_3) &= \sum_{n=-\infty}^{\infty} K_{m+n}(kb_{13})I_n(k)\cos n\Phi_1 \\ &= (-1)^m K_m(kr_3)\cos m\Phi_3. \end{aligned} \tag{C.1.1}$$

The relation also holds with cos replaced by sin and $(-1)^m$ by $(-1)^{m+1}$. Using (4.2.3) and (C.1.1) we find for $m \geq 0$,

$$\begin{aligned} r_3 K_m(kr_3)\cos m\Phi_3\cos(\Phi_1 - \Phi_3) &= (-1)^m \sum_{n=-\infty}^{\infty}\Big[K_{m+n}(kb_{13})I_n(k) - \frac{1}{2}b_{13}\Big(K_{m+n-1}(kb_{13})I_{n-1}(k) \\ &\qquad + K_{m+n+1}(kb_{13})I_{n+1}(k)\Big)\Big]\cos n\Phi_1. \\ K_{m+1}(kr_3)\cos((m+1)\Phi_3 - \Phi_1) &= (-1)^{m+1}\sum_{n=-\infty}^{\infty} K_{m+n}(kb_{13})I_{n-1}(k)\cos n\Phi_1. \\ K_{m-1}(kr_3)\cos((m-1)\Phi_3 + \Phi_1) &= (-1)^{m-1}\sum_{n=-\infty}^{\infty} K_{m+n}(kb_{13})I_{n+1}(k)\cos n\Phi_1. \\ r_3 K_{m+1}(kr_3)\cos m\Phi_3 &= (-1)^{m+1}\sum_{n=-\infty}^{\infty}\Big[K_{m+n}(kb_{13})I_{n-1}(k) - b_{13}K_{m+n+1}(kb_{13})I_n(k)\Big]\cos n\Phi_1. \end{aligned} \tag{C.1.2}$$

C.2 Evaluations of integral in (4.3.8) and $A_{n,j-J}$

As for the evaluation of the expressions in (4.3.8), we only work out the $m = 0$ case, since the other cases follow analogously. From formula 13.53(6) in Watson (1966), we have for n odd,

$$\cos\left(\frac{n+1}{2}\pi\right)\int_0^{\infty}\frac{s^n J_1(s)J_1(sr_j)}{s^2 + k_j^2}ds = -k_j^{n-1}I_1(k_j)K_1(k_j r_j), \tag{C.2.1}$$

provided that $r_j \geq 1$. Differentiating both sides of (C.2.1) with respect to k_j, we obtain

$$\cos\left(\frac{n+1}{2}\pi\right)\int_0^\infty \frac{s^n J_1(s)J_1(sr_j)}{(s^2+k_j^2)^2}ds = \frac{1}{2k_j}\frac{d}{dk_j}\Big[k_j^{n-1}I_1(k_j)K_1(k_jr_j)\Big]. \tag{C.2.2}$$

To calculate $A_{n,j-J}$, we proceed as follows:

$$\begin{aligned} u_{j,0}\cos(\phi_J-\phi_j) &= -\frac{k_j(1-k_j^2)}{2}\frac{d}{dk_j}\Big[I_1(k_j)K_1(k_jr_j)\cos(\phi_J-\phi_j)\Big] \\ &= \frac{k_j(1-k_j^2)}{2}\frac{d}{dk_j}\Big[\sum_{n=-\infty}^{\infty} I_1(k_j)K_n(|j-J|k_jb)I_{n-1}(k_Jr_J)\cos n\phi_J\Big] \\ &= \sum_{n=-\infty}^{\infty}\left(\frac{k_j(1-k_j^2)}{2}\frac{d}{dk}\Big[I_1(k_j)K_n(|j-J|k_jb)I_{n-1}(k_Jr_J)\Big]\right)\cos n\phi_J. \end{aligned} \tag{C.2.3}$$

Summation follows from the first formula of (C.1.2) The interchange of the order of summation and differentiation is allowed thanks to the uniform convergence of the series. From (C.2.3), since calculations are carried out at $r_J = 1$ we define

$$A_{n,j-J} = \frac{k_j(1-k_j^2)}{2}\frac{d}{dk_j}\Big[I_1(k_j)K_n(|j-J|kb)I_{n-1}(k_J)\Big]. \tag{C.2.4}$$

References

[Bousfield et al. (1986)] Bousfield, D. W., Keunings, R., Marrucci, G., & Denn, M. M. 1986 Nonlinear analysis of the surface tension driven breakup of viscoelastic filaments. *J. Non-Newtonian Fluid Mech.* **21**, 79.

[Brenn et al. (2000)] Brenn, G., Liu, Z. & Durst, F. 2000 Linear analysis of the temporal instability of axisymmetrical non-Newtonian liquid jets. *Int. J. Multiphase flow.* **26**, 1621.

[Chandrasekhar (1961)] Chandrasekhar, S. 1961 *Hydrodynamic and hydromagnetic stability.* Dover.

[Chin & Han (1979)] Chin, H. B. & Han, C. D. 1979 Studies on droplet deformation and breakup. I. Droplet deformation in extensional flow. *J. Rheology* **23**, 557.

[Chin & Han (1980)] Chin, H. B. & Han, C. D. 1980 Studies on droplet deformation and breakup. II. Breakup of a droplet in nonuniform shear flow. *J. Rheology* **24**, 1.

[Christanti & Walker (2001)] Christanti, Y. & Walker, L. M. 2001 Surface tension driven jet break up of strain-hardening polymer solutions. *J. Non-Newtonian Fluid Mech.* **100**, 9.

[Eggers (1993)] Eggers, J. 1993 Universal pinching of 3D axisymmetric free-surface flow. *Phys. Rev. Lett.* **71**, 3458.

[Eggers (1995)] Eggers, J. 1995 Theory of drop formation. *Phys. Fluids* **7**, 941.

[Eggers (1997)] Eggers, J. 1997 Nonlinear dynamics and breakup of free surfaces flows. *Rev. Mod. Phys.* **3**, 865.

[Elemans et al. (1997)] Elemans, P. H. M., van Wunnik, J. M. & van Dam, R. A. 1997 Development of morphology in blends of immiscible polymers. *AIChE J.* **43**, 1649.

[Frischknecht (1998)] Frischknecht, A. 1998 Stability of cylindrical domains in phase-separating binary fluids in shear flow. *Phys. Rev. E* **58**, 3495.

[Greco (2002)] Greco, F. 2002 Drop deformation for non-Newtonian fluids in slow flows. *J. Non-Newtonian Fluid Mech.* **107**, 111.

[Guido et al. (2000)] Guido, S., Minale, M. & Maffettone, P. L. 2000 3D shape of a Newtonian drop in a Newtonian liquid under transient shear flows. *Proc. XIIIth International Congress on Rheology* **2**, 42. Cambridge, UK.

[Hagedorn et al. (2003)] Hagedorn, J. G., Martys, N. S. & Douglas, J. F. 2003 Breakup of a fluid thread in a confined geometry: Droplet-Plug transition, perturbation sensitivity and kinetic stabilization with confinement. *preprint, private communication.*

[Harrington (1993)] Harrington, R. F. 1993 *Field computation by moment methods.* IEEE Press.

[Harris (1977)] Harris, J. 1977 *Rheology and non-Newtonian flow.* Longman.

[Hashimoto et al. (1995)] Hashimoto, T., Matsuzaka, K., Moses ,E. & Onuki, A. 1995 String phase in phase-separating fluids under shear flow. *Phys. Rev. Lett.* **74**, 126.

[Khakhar & Ottino (1987)] Khakhar, D. V. & Ottino, J. M. 1987 Breakup of liquid threads in linear flows. *Int. J. Multiphase Flow* **13**, 71.

[Kinoshita et al. (1994)] Kinoshita, C. M., Teng, H. & Masutani, S. M. 1994 A study of the instability of liquid jets and comparison with Tomotika's analysis. *Int. J. Multiphase Flow* **20**, 523.

[Knops (1997)] Knops, Y. M. M. 1997 Morphology development in polymer blends: The hydrodynamic interaction between disintegrating threads. *Final Report of the postgraduate programme Mathematics for Industry, SAI*, Eindhoven University of Technology.

[Knops et al. (2001)] Knops, Y. M. M., Slot, J. J. M., Elemans, P. H. M. & Bulters, M. J. H. 2001 Simultaneous breakup of multiple viscous threads surrounded by viscous liquid. *AIChE J.* **47**, 1740.

[Li & Fontelos (2003)] Li, J. & Fontelos, M. A. 2003 Drop dynamics on the beads-on-string structure of viscoelastic jets: A numerical study. *Phys. Fluids* **15**, 922.

[Meister & Scheele (1967)] Meister, B. J. & Scheele, G. F. 1967 Generalized solution of the Tomotika stability analysis for a cylindrical jet. *AIChE J.* **13**, 682.

[Merkin (1997)] Merkin, D. R. 1997 *Introduction to the theory of stability.* Springer.

[Migler (2001)] Migler, K. B. 2001 String formation in sheared polymer blends: Coalescence, breakup, and finite size effect. *Phys. Rev. Lett.* **86**, 1023.

[Mikami et al. (1975)] Mikami, T., Cox, R. G. & Mason, S. G. 1975 Breakup of extending liquid threads. *Int. J. Multiphase Flow* **2**, 113.

[Navot (1999)] Navot, Y. 1999 Critical behavior of drop breakup in axisymmetric viscous flow. *Phys. Fluids* **11**, 990.

[Palierne & Lequeux (1991)] Palierne, J. F. & Lequeux, F. 1992 Sausage instability of a thread in a matrix; linear theory for viscoelastic fluids and interface. *J. Non-Newtonian Fluid Mech.* **40**, 289.

[Papageorgiou (1995)] Papageorgiou, D. T. 1995 On the breakup of viscous liquid threads. *Phys. Fluids* **7**, 1529.

[Pathak & Migler (2003)] Pathak, J. A. & Migler, K. M. 2003 Droplet-string deformation and stability during microconfined shear flow. *preprint Langmuir.*

[Plateau (1849)] Plateau, J. 1849 *Acad. Sci. Bruxelles Mem* **23**, 5.

[Rallison (1984)] Rallison, J. M. 1984 The deformation of small viscous drops and bubbles in shear flows. *Ann. Rev. Fluid. Mech.* **16**, 45.

[Rayleigh (1878)] Rayleigh, Lord. 1878 On the instability of jets. *Proc. Lond. Math. Soc.* **10**, 4.

[Rayleigh (1892)] Rayleigh, Lord. 1892 On the instability of a cylinder of viscous liquid under the capillary force. *Phil. Mag.* **34**, 145.

[Savart (1833)] Savart, F. 1833 *Annal. Chim* **53**, 337.

[Sibillo et al. (2003)] Sibillo, V., Simeone, M. & Guido, S. 2003 Drop breakup in shear flow with non-Newtonian fluids. *Proc. 1st Annual European Rheology Conference*, 51. Guimarães, Portugal.

[Son et al. (2003)] Son, Y., Martys, N. S., Hagedorn, J. G. & Migler, K. B. 2003 Suppression of capillary instability of a polymeric thread via parallel plate confinement. *Macromolecules* **36**, 5825.

[Stone (1994)] Stone, H. A. 1994 Dynamics of drop deformation and breakup in viscous fluids. *Annu. Rev. Fluid Mech.* **26**, 65.

[Stone & Brenner (1996)] Stone, H. A. & Brenner, M. P. 1996 Note on the capillary thread instability for fluids of equal viscosities. *J. Fluid Mech.* **318**, 373.

[Taylor (1934)] Taylor, G. I. 1934 The formation of emulsions in definable fields of flow. *Proc. Roy. Soc.* **A146**, 501.

[Tomotika (1935)] Tomotika, S. 1935 On the instability of a cylindrical thread of a viscous liquid surrounded by another viscous fluid. *Proc. Roy. Soc. A* **150**, 322.

[Tomotika (1936)] Tomotika, S. 1936 Breaking up of a drop of viscous liquid immersed in another viscous fluid which is extending at a uniform rate. *Proc. Roy. Soc. A* **153**, 302.

[Watson (1966)] WATSON, G.N. 1966 *A treatise on the theory of Bessel functions, 2nd edition*. Cambridge University Press.

[Weber (1931)] WEBER, C. 1931 On the instability of a liquid jet. *Z. Angew. Math. Phys.* **11**, 136.

[Widom (1965)] WIDOM, H. 1965 *Toeplitz matrices, MAA Studies in Mathematics Vol. 3: Studies in real and complex analysis* (Editor: Hirschman, I.I.,Jr.) Prentice-Hall.

Nomenclature

The following is a list of notations used in the thesis. Vectors and matrices are denoted by small and capital Roman bold typeface, respectively. Tensors are denoted by bold Greek letters. In addition, some symbols are defined locally within the text.

Roman symbols

a	:	Initial radius of the thread
$b, b_{12},\ etc.$	:	Distance between threads
$\mathbf{e}_r, \mathbf{e}_\phi, \mathbf{e}_z$	:	Unit vectors in radial, azimuthal and axial direction
$\mathbf{g},\ \mathrm{g}_i$	:	Stress vector/Hydrodynamic force
h	:	Ratio of the inner and the outer cylinders
i	:	Imaginary unit number
I_n, K_n	:	Modified Bessel functions of order n
$\mathbf{I}$	:	Identity matrix
k	:	Wave number
$\mathbf{L}(\equiv (\nabla \mathbf{v})^T),\ L_{ij}$	:	Velocity gradient tensor
$\mathbf{n},\ \mathrm{n}_i$	:	Normal vector
p	:	Perturbed pressure
P	:	Unperturbed pressure
q	:	Growth rate of the amplitude
r	:	Radial coordinate
$\mathbf{s},\ s_i$	:	Phase pattern
t	:	Time variable
u, v, w	:	Radial, azimuthal, and axial velocities
$\mathbf{u}$	:	Velocity
$\mathbf{v} = (u, v, w)$	:	Perturbed velocity vector
$\mathbf{V} = (U, V, W)$	:	Unperturbed velocity vector
z	:	Axial coordinate

Dimensionless numbers

Ca	:	Capillary number
$\mathrm{C_p}$	:	Constant pressure gradient
De	:	Deborah number

Greek symbols

α	:	Phase difference
$\dot{\boldsymbol{\gamma}},\ \dot{\gamma}_{ij}$	:	Rate of strain tensor
Γ_0	:	Constant shear stress
$\boldsymbol{\Gamma},\ \Gamma_{ij}$	:	Unperturbed extra stress tensor
$\boldsymbol{\delta}$	:	Identity tensor
$0 < \epsilon \ll 1$	:	Perturbation parameter
ε_n	:	Perturbation amplitude of order n
η_o	:	Zero shear viscosity / Newtonian viscosity
λ_1	:	Stress relaxation time
λ_2	:	Deformation retardation time
$\Lambda = \lambda_2/\lambda_1$		
μ	:	Ratio of zero shear viscosity
$\boldsymbol{\pi},\ \pi_{ij}$	:	Perturbed total stress tensor
$\boldsymbol{\Pi},\ \Pi_{ij}$	:	Unperturbed total stress tensor
σ	:	Surface tension
$\boldsymbol{\tau}$	:	Total stress tensor
$\boldsymbol{\tau},\ \tau_{ij}$	:	Perturbed extra stress tensor
ϕ	:	Azimuthal coordinate

Subscripts

cr	:	Critical value
max	:	Maximum value

Superscripts

c	:	Continuous phase
d	:	Dispersed phase
$*$	:	Dimensionless version
T	:	Transpose

Summary

In a polymer blending process, relatively big drops of one material are immersed into a shear flow of a second material. Due to the shear stresses, long threads are formed. At some moment a thread may become so thin that the interfacial stress (surface tension) becomes important. The effect of the interfacial stress is a tendency to attain the drop-shape. Initiated by random perturbations, surface waves may develop along the thread. Driven by surface tension, these waves may grow or attenuate in amplitude, depending on the stability of the system. In an unstable state, the thread will eventually break up into an array of small spherical droplets.

The main interest of this thesis is to consider two unexpected phenomena observed in experiments: first, in-phase and out-of-phase break-up as reported by Knops (1997) and Elemans et al. (1997) for parallel polymeric liquid threads, and second, a stable string (thread) in droplet-string formation as reported by Migler (2001) in a concentrated polymer blend. The experiments reported by Knops (1997) and Elemans et al. (1997) reveal that the interactions between the threads are of essential relevance for the way they break up. The experiments on shear between plates reported by Migler (2001) reveal that if the size of the string becomes comparable to the gap width, the wall effect (confinement) suppresses the instability of the string.

In this thesis, the origin of the phenomena described above and the dependence on the geometrical and rheological parameters is studied by analytical means. The dynamical behaviour of liquid threads immersed in a fluid is considered in relation to surface tension, viscous forces, presence of a wall and external flow. In most of this work the fluids are assumed to be incompressible, Newtonian, and so viscous that the creeping flow approximation is applicable. So, the system is governed by the equation of continuity and the Stokes equations. The thread surface is perturbed by a small random perturbation and it is studied how this evolves in time. The governing equations are solved by means of separation of variables. In this, the dependence on the azimuthal directions is written in the form of (complex) Fourier expansions. Substitution of the general solution into the boundary conditions yields an infinite set of linear equations for the unknown coefficients of the expansion. This set is solved using the method of moments. From this the so-called *growth rate* is calculated, which is a measure for the growth (or decay) of the perturbations. A positive growth rate indicates that the system is unstable, a negative one that it is stable.

First, the stability of a single Newtonian thread immersed in an unconfined region is considered. The stability is studied for two types of driving forces: pure surface tension, and surface tension together with shear flow. Under influence of surface tension only, the thread turns out to be unstable. Under influence of both surface tension and shear flow, the instability is suppressed provided that the applied shear is large enough.

Next, as an extension of the single-thread case, the (in)stability of a set of immersed threads under influence of surface tension is considered: first, the two-threads system, and, second, the many-threads system. Here, the equations are formulated in two, or more, systems of cylindrical coordinates, each one connected to one of the threads. For the two-threads system, the stability is examined based on a zero-order and a first-order Fourier expansion; the improvement due to a higher-order expansion turned out to be rather small. It is found that the thread can break up either in-phase or out-of-phase. The break-up behaviour depends on the ratio of the viscosities and the distance between the centers of the threads. These findings are in full agreement with the experimental results reported by Knops (1997) and Elemans et al. (1997).

For the many-threads system, the stability is investigated for two types of configuration: a system of L threads on a row, and a system of threads at triangular vertices. For a system with L threads on a row, the growth rate of the perturbations can be calculated by optimizing over only L so-called *basic phase patterns*. For the triangular configurations the break-up pattern depends on the type of triangle, i.e. an equilateral triangle or an non-equilateral one.

For fluids with equal viscosities, the growth rate of a set of parallel threads on a row is calculated using Hankel transformations. An expression for the upper bound of the growth rate is derived. This upper bound turns out to be sharp estimate for the maximum growth rate of the perturbations.

Finally, the study is extended to non-Newtonian fluids. The stability of a viscoelastic thread immersed in a tube filled with a Newtonian fluid is considered. As constitutive relation for the thread Jeffreys model is applied. The thread is moving in the tube due to a prescribed constant pressure gradient (Poiseuille flow). The effects of the ratio of viscosities, fluid elasticity, confinement and prescribed flow, on the stability of the immersed thread are studied. The more viscous a thread is, the more time it takes to break up. However, a viscoelastic thread breaks up faster and in larger droplets than a Newtonian one with the same viscosity. The elasticity has not much influence on the magnitude of the eventual droplets, and the thread breaks up slower when the degree of confinement is higher. A critical gap width beyond which the presence of the wall of the tube has no longer an effect on the stability of the thread is found. In case of a Newtonian thread, the Poiseuille flow causes the thread to be oscillatory unstable with the growth rate equal to the one within a fluid at rest, whereas, in case of a viscoelastic thread, the Poiseuille flow contributes to both the real and the imaginary part of the growth rate of the perturbation. It is found that a viscoelastic thread immersed in a Poiseuille flow will break up faster than one within a fluid at rest. So, in short, Poiseuille flow destabilizes the thread but shear flow stabilizes it.

From the point of view of blending the present results may provide important insights for the control of the production process. For example, they yield insights into characteristic drop formation times, spatial distributions of the droplets and droplets or strings (liquid threads) formation. The present results show how the blending process can be controlled by adjusting the properties of the fluids, the geometrical properties of the system and the type of an imposed flow.

Samenvatting

Bij het mengen van vloeistoffen voegt men vaak druppels van het ene materiaal toe aan een afschuifstroming van het andere. De druppels deformeren dan en vormen draden die steeds langer en dus dunner worden. Als de straal kleiner en kleiner wordt, en dus de kromming van het oppervlak groter en groter, gaat de oppervlaktespanning een steeds belangrijker rol spelen in het dynamisch proces. Onder invloed daarvan heeft de draad de neiging op te breken in kleine druppels. In de praktijk bevinden zich altijd verstoringen op het draadoppervlak. Die kunnen beschreven worden als de superpositie van golven met allerlei golflengten. In een instabiele situatie groeien deze in amplitude. De golf waarvan de amplitude het snelst groeit bepaalt hoe de draad uiteindelijk opbreekt en hoe groot de resulterende druppeltjes zijn. De groeisnelheid van deze speciale verstoring wordt de 'groeifactor' genoemd.

Dit proefschrift richt zich vooral op de verklaring van twee onverwachte fenomenen die zijn waargenomen in experimenten. Ten eerste het feit dat naburige parallelle draden alleen in-fase of uit-fase opbreken zoals gerapporteerd door Knops (1997) en Elemans et al. (1997). Dit wijst erop dat naburige draden een sterke interactie hebben tijdens het opbreken. Ten tweede het verschijnsel dat draden niet opbreken als ze zich bevinden in een relatief nauwe geometrie zoals waargenomen door Migler (2001). Kennelijk heeft de nabijheid van een wand sterke invloed op het opbreken.

De bovengenoemde effecten en de invloed van de geometrische en reologische parameters daarop worden in dit proefschrift bestudeerd via analytische methoden. Het dynamische gedrag van de vloeistofdraden kan voor kleine verstoringen van het oppervlak geheel analytisch worden beschreven, waarbij de invloed van de oppervlaktespanning, de visceuse krachten, de aanwezigheid van een stroming en de nabijheid van een wand in rekening worden gebracht. De betrokken vloeistoffen worden incompressibel verondersteld en dusdanig visceus dat de dynamica goed wordt beschreven door de Stokesvergelijkingen. Deze worden opgelost door middel van het scheiden van variabelen en het gebruik van (complexe) Fourierreeksen. Substitutie van deze reeksen in de randcondities die gelden op het draadoppervlak leidt tot een oneindig aantal lineaire vergelijkingen voor de onbekende coefficienten. Dit stelsel wordt opgelost met behulp van een 'momenten methode'. De aldus gevonden oplossingen leiden tot de groeifactor van het systeem.

Allereerst is de situatie van een Newtonse draad in een onbegrensde Newtonse vloeistof bestudeerd. Bij afwezigheid van een stroming en/of een wand blijkt dit systeem altijd instabiel te zijn en zal de draad dus opbreken. Het opleggen van een afschuifstroming rond de draad blijkt de draad te kunnen stabiliseren mits de stroming sterk genoeg is.

Vervolgens is gekeken naar een aantal ondergedompelde draden. Voor twee draden zijn nulde-orde en eerste-orde termen in de Fourierontwikkelingen meegenomen. Het

blijkt dat de resultaten voor de stabiliteit daar vrij ongevoelig voor zijn. Hieruit is geconcludeerd dat het verdere onderzoek zich kan beperken tot nulde-orde Fourierontwikkelingen. Dit impliceert dat in de analyse de draden steeds axisymmetrisch vervormen. Een belangrijke conclusie uit de analyse van het model is dat naburige draden inderdaad alleen maar in-fase of uit-fase kunnen opbreken, precies zoals in metingen is geobserveerd. Welke van de twee mogelijkheden optreedt hangt voor twee draden alleen af van de verhouding van de viscositeiten van de vloeistoffen binnen en buiten de draden en van de afstand tussen de draden.

Voor systemen met meer draden zijn twee configuraties beschouwd: L draden ($L > 2$) op een rij met gelijke tussenafstanden en drie draden in een driehoekige geometrie. Voor het eerste geval zijn er in principe 2^L opbreekpatronen mogelijk. Het patroon met de grootste groeifactor zal na verloop van tijd geobserveerd worden. Voor grote L waarden zouden de berekeningen langdurig zijn indien gemaximaliseerd zou moeten worden over al deze configuraties. In het proefschrift wordt aangetoond dat het voldoende is de groeifactoren van slechts L basispatronen uit te rekenen en daarvan het maximum te nemen. Voor de driehoekige situatie maakt het nogal uit voor het opbreekpatroon of de driehoek gelijkzijdig is of niet.

Speciale aandacht wordt besteed aan de situatie waarin alle vloeistoffen dezelfde viscositeit hebben. In dat geval kunnen Hankeltransformaties worden toegepast en kan de groeifactor bijna geheel analytisch berekend worden. Voor meer dan twee draden is er een bovengrens afgeleid die zeer scherp blijkt te zijn als de draden niet erg dicht bij elkaar liggen. Dit volgt uit vergelijking met numerieke resultaten.

Ook is de invloed onderzocht van mogelijke elasticiteit van de draad. Als viscoelastische constitutieve relatie is daarvoor het model van Jeffreys gebruikt. Reeds bekend was dat de visceuse component van de draden het opbreken vertraagd. Gevonden is dat de elastische component het opbreken versnelt, maar nauwelijks invloed heeft op de grootte van de resulterende druppeltjes.

Tenslotte is een viscoelastische draad in een met een Newtonse vloeistof gevulde buis geplaatst. Daarmee kan het effect van de aanwezigheid van een wand bestudeerd worden. Het blijkt dat het opbreken door de wand niet verhinderd maar wel vertraagd wordt en dat des te meer naarmate de afstand tussen draad en wand kleiner is. De nabijheid van de wand is nauwelijks meer van invloed als de afstand groter is dan een zekere kritische waarde. Deze is in dit proefschrift berekend. Door de vloeistof in de buis te laten stromen is nagegaan welke invloed een Poiseuille-achtig stromingsprofiel rond de draad op het opbreken heeft. Voor een Newtonse draad is het effect van zo'n stroming dat het opbreken oscillaties gaat vertonen: op het oppervlak verschijnen staande golven, maar de snelheid van het opbreken is niet afhankelijk van de stroming. Echter, als de draad ook elastisch is, veroorzaakt dit soort stroming een versneld opbreken.

De resultaten van dit proefschrift kunnen van groot nut zijn bij het besturen van mengprocessen. Voor gegeven parameterwaarden kan berekend worden of de draden opbreken, hoe snel dat gebeurt, hoe groot de druppeltjes zullen zijn en hoe hun ruimtelijke verdeling zal zijn. Dit verschaft de mogelijkheid om te bepalen welke parameterwaarden het gewenste mengresultaat opleveren. Daarmee kunnen kostbare en tijdrovende experimenten uitgespaard worden.

About the author

Agus Yodi Gunawan was born in Sumedang, West Java, Indonesia, on August 2, 1971. After his pre-university education (SMA) at the SMA Negeri 1 Sumedang, from September 1990 until October 1994, he studied mathematics at the Departemen Matematika, Institut Teknologi Bandung (ITB), Indonesia. In June 1995 he became staff member of the Departemen Matematika ITB. From September 1995 until October 1997 he followed the master's program in Mathematics at the same Institute, and graduated with a thesis about "Wave groups in the KdV equation", under supervision of Dr. W.S. Budhi (ITB) and prof.dr. E. van Groesen (University of Twente, The Netherlands). After his master graduation, he carried out a Ph.D. project in the Applied Analysis group at the Department of Mathematics and Computer Science of the Eindhoven University of Technology from February 2000 until January 2004. This project was supported by the QUE-Project of the Departemen Matematika ITB. In this function he worked under the supervision of prof.dr. J. Molenaar and dr.ir. A.A.F. van de Ven. After getting his Ph.D., he will return to ITB as a lecturer. He is married and has got one lovely daughter.